MAGNETO-THERMO-MECHANICAL RESPONSE AND MAGNETO-CALORIC EFFECT IN MAGNETIC SHAPE MEMORY ALLOYS

A Thesis

by

CENGIZ YEGIN

Submitted to the Office of Graduate Studies of
Texas A&M University
in partial fulfillment of the requirements for the degree of

MASTER OF SCIENCE

May 2012

Major Subject: Materials Science and Engineering

MAGNETO-THERMO-MECHANICAL RESPONSE AND MAGNETO-CALORIC EFFECT IN MAGNETIC SHAPE MEMORY ALLOYS

A Thesis

by

CENGIZ YEGIN

Submitted to the Office of Graduate Studies of
Texas A&M University
in partial fulfillment of the requirements for the degree of

MASTER OF SCIENCE

Approved by:

Chair of Committee,	Ibrahim Karaman
Committee Members,	Karl Hartwig
	Miladin Radovic
	Joseph Ross
Intercollegiate Faculty Chair,	Ibrahim Karaman

May 2012

Major Subject: Materials Science and Engineering

ABSTRACT

Magneto-Thermo-Mechanical Response and Magneto-Caloric Effect in Magnetic Shape Memory Alloys. (May 2012)

Cengiz Yegin, B.S., Bogazici University, Turkey

Chair of Advisory Committee: Dr. Ibrahim Karaman

Ni-Co-Mn-In system is a new type of magnetic shape memory alloys (MSMAs) where the first order structural and magnetic phase transitions overlap. These materials can generate large reversible shape changes due to magnetic-field-induced martensitic transformation, and exhibit magneto-caloric effect and magnetoresistance. Ni-Co-Mn-Sn alloys are inexpensive alternatives of the Ni-Co-Mn-In alloys. In both materials, austenite has higher magnetization levels than martensite. Fe-Mn-Ga is another MSMA system, however, whose magnetization trend is opposite to those of the Ni-Co-Mn-X (In-Sn) systems upon phase transformation. The MSMAs have attracted great interest in recent years, and their magnetic and thermo-mechanical properties need to be further investigated.

In the present study, the effects of indium concentration, cooling, and annealing on martensitic transformation and magnetic response of single crystalline Ni-Co-Mn-In alloys were investigated. Increasing indium content reduced the martensitic transformation start (M_s) temperature, while increasing temperature hysteresis and saturation magnetization. Increasing annealing temperature led to an increase in the M_s

temperature whereas annealing at 400°C and 500°C led to the kinetic arrest of austenite. Cooling after solution heat treatment also notably affected the transformation temperatures and magnetization response. While the transformation temperatures increased in the oil quenched samples compared to those in the water quenched samples, these temperatures decreased in furnace cooled samples due to the kinetic arrest. The possible reasons for the kinetic arrest are: atomic order changes, or precipitate formation.

Shape memory and superelastic response, and magnetic field-induced shape recovery behavior of sintered $Ni_{43}Co_7Mn_{39}Sn_{11}$ polycrystalline alloys were also examined. The microstructural analysis showed the existence of small pores, which seem to increase the damage tolerance of the sintered polycrystalline samples. The recoverable transformation strain, irrecoverable strain and transformation temperature hysteresis increased with stress upon cooling under stress. Moreover, magnetic-field-induced strain due to the field-induced phase transformation was confirmed to be 0.6% at 319K. Almost perfect superelastic response was obtained at 343K. A magnetic entropy change of 22 J kg^{-1} K^{-1} were determined at 219K from magneto-caloric effect measurements which were conducted on annealed $Ni_{43}Co_7Mn_{39}Sn_{11}$ ribbons.

Magnetic characteristics and martensitic transformation behavior of polycrystalline Fe-Mn-Ga alloys were also examined. Cast alloys at various compositions were undergone homogenization heat treatments. It was verified by magnetization measurements that the alloys heat treated at 1050°C shows martensitic transformation. The heat treatment time was determined to be 1 day or 1 week depending on the compositions.

DEDICATION

To my parents

ACKNOWLEDGEMENTS

I would like to express my deep gratitude to all who helped me finish my MS study. At first hand, I would like to thank my advisor, Prof. Ibrahim Karaman, who helped me in all stages of the project. His suggestions were very helpful both to complete my thesis and for my future life. This project would not have been finished without his support. I am honored to have the opportunity to work with him. I would like to thank my committee members, Prof. Joseph Ross, Prof. Karl Hartwig and Prof. Miladin Radovic for their suggestions on my research.

I would also like to thank Dr. Wataru Ito for sharing his ideas with me during his visits, and I am thankful to Prof. Yuriy Chumlyakov for his valuable discussions and his guidance to complete my thesis.

Special thanks my fiancé, Ms. Yagmur Ravli, who gave meaning to my life. Her love, understanding, continuous support and motivation played a significant role for completing my work.

Finally, I would like to thank my labmates, Ebubekir Dogan, Murat Kaynak, James Monroe, Ji Ma, Alper Evirgen, Dr. Pinar Karpuz, Brian Franco, Dr. Kadri C. Atli, Dr. Nevin Ozdemir, Erhan Akin, Zhu Ruixian, Ankush Kothalkar, Dr . Alper Cerit, Ceylan Hayrettin and Sonia Razavi for the comfortable and peaceful environment they supported.

TABLE OF CONTENTS

LIST OF FIGURES

LIST OF TABLES

TABLE Page

1. INTRODUCTION

1.1 Background

Magnetic shape memory alloys (MSMAs) have recently been identified as a class of multifunctional materials which can be used in applications such as actuation, sensing, energy harvesting, and magnetic refrigeration. They are capable of generating large amounts of shape change under magnetic fields [1-4]. They also exhibit shape memory effect and superelastic response like conventional shape memory alloys [5]. The Heusler alloy, Ni_2MnGa, is the most popular MSMA in which a magnetic field-induced strain (MFIS) was first observed in 1996 [1] and later a large MFIS - up to 10% - has been reported [3-6]. The mechanism that produces MFIS in Ni_2MnGa single crystals is the rearrangement of martensite variants as a result of the application of an external magnetic field [3]. When the magnetocrystalline anisotropy energy (MAE) of the martesite is larger than the required energy to move the martensite variant boundaries - also called twin boundaries - the variant starts to grow which leads to a macroscopic shape change. Despite producing large strains at relatively high frequencies, the actuation stress levels in Ni_2MnGa single crystals is less than 10MPa [3]. Since MAE is defined in Figure 1-1a is limited with saturation magnetic field, it cannot be increased with further application of magnetic fields. Moreover, the percentage of the MAE that can be utilized depends on the orientation of the magnetic easy and hard axes of martensite variants.

This thesis follows the style of Applied Physics Letters.

The orientation dependence of this mechanism makes it applicable only to single crystals because successful operation of this mechanism is very difficult in polycrystalline materials. Thus, MFIS and actuation stress produced as a result of MAE is limited. Brittleness of Ni_2MnGa alloys in polycrystalline form is also a significant problem that prevents them being used in applications [3-5].

Another mechanism resulting in MFIS is the field-induced martensitic phase transformation (FIPT) where higher actuation stress levels than those in the field-induced rearrangement of martensite variants can be achieved [4]. In FIPT, Zeeman energy (ZE) is responsible for MFIS and output stress. As shown in Figure 1-1b, ZE (1) originates from the difference between the saturation magnetizations (M_{sat}) of two phases which are capable of martensitically transforming into each other and (2) can be increased by the application of magnetic field [4-5]. Also, ZE can be enhanced by increasing the difference between M_{sat} levels of the transforming phases. As opposed to MAE, ZE is not strongly orientation dependent which makes it operational not only for single crystals but also for polycrystalline materials [5]. Therefore, the single crystalline alloys can be replaced with the polycrystalline alternatives to reduce the cost of fabrication.

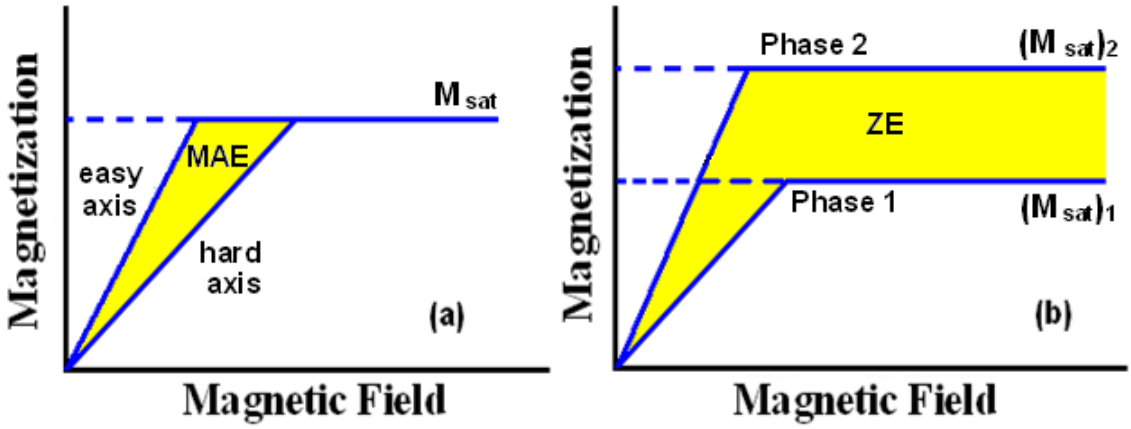

Figure 1-1) (a) MAE for ferromagnetic martensite in Ni_2MnGa which is defined as the area between the magnetization response of easy and hard axes and **(b)** ZE difference between two transforming phases which leads to magnetic field-induced phase transformation.

FIPT in Ni-Mn-Ga alloys was investigated [7] and it was shown that a high level of magnetic field is required to activate the FIPT since both austenite and martensite phases are ferromagnetic, and the saturation magnetization levels are close to each other. However, it has recently been discovered that FIPT is observed in Ni-Mn-X (X=In, Sn, Sb) alloy systems - also called metamagnetic shape memory alloys (MMSMAs) - where there is a huge difference between the saturation magnetizations of ferromagnetic austenite and paramagnetic martensite phases across the phase transformation [8-12]. MMSMAs, produce MFIS with output stresses more than 100MPa [5] and show several interesting properties such as the inverse magnetocaloric effect [10, 13-14], giant magnetoresistance [15-16], and giant magnetothermal conductivity [17]. Addition of Co to Ni-Mn-X ternary alloys is employed to increase Curie temperature, saturation magnetization, and eventually ZE, which is responsible for FIPT [11].

Ni-Co-Mn-X (X=In, Sn) quaternary alloy systems have been shown to exhibit metamagnetic phase transition with high work output levels, nearly perfect superelasticity and shape memory effect [18-20]. However, In is a very expensive element which increases the cost of fabrication of Ni-Co-Mn-In alloys. Thus, it is replaced with Sn to reduce the cost. Moreover, Ni-Co-Mn-In single crystalline alloys are brittle and growth of single crystals requires complicated fabrication techniques [5]. Since production of Ni-Co-Mn-Sn single crystals have not been achieved so far, polycrystalline form of these alloys is employed as alternatives to Ni-Co-Mn-In single crystals. Brittleness is also a significant problem for the polycrystalline alloys which are manufactured by ingot metallurgy due to cubic to tetragonal martensitic transformation [9]. Thus, sintering was performed in polycrystalline Ni-Co-Mn-Sn powders to obtain bulk alloys which are relatively ductile and have higher fracture toughness.

Very recently, Omori et. al [21] introduced a new MMSMA system, Fe-Mn-Ga in both single and polycrystalline forms, where martensitic and magnetic transformation occurs similar to Ni-(Co)-Mn-X alloy systems, but in the reverse direction since the austenite is paramagnetic and martensite is ferromagnetic [21-22]. FIPT [22] and MAE [23] have also been reported in these alloys. In Fe-Mn-Ga alloys, an application of magnetic field increases the martensitic transformation temperatures and so does mechanical stress. Therefore the mechanical stress and the magnetic field can be coupled to reduce the magnetic field requirement for the phase transformation, or vice versa.

MMSMAs have attracted great attention due to their outstanding properties in terms of actuation and sensing. These properties can be illustrated by inverse

magnetocaloric effect where magnetic energy is converted to thermal energy, energy harvesting where magnetic energy is converted to voltage output, and magnetoresistance where resistivity of a conductor or a semiconductor can be controlled by an application of magnetic field. Research on MMSMAs is still in progress and their candidacy to be widely used in actuation mechanisms in the near future is evident.

1.2 Objectives

Metamagnetic shape memory alloys, especially NiCoMnIn alloys, have been proven to be promising multifunctional materials due to high actuation stress and work output. However, a high magnetic field requirement for field induced phase transformation restricts their utility in actuation or sensing applications. In addition, transformation hysteresis that occurs during martensitic phase transformation leads to energy dissipation and decreases the efficiency of conversion of magnetic energy to the mechanical output. Therefore, magnetic shape memory properties of these alloys should be investigated for the feasibility of reducing the required magnetic field levels for actuation and transformation hysteresis for higher efficiency in applications. Magnetic properties of Ni-Co-Mn-In, magnetic and thermo-mechanical properties of Ni-Co-Mn-Sn, and magnetic properties of Fe-Mn-Ga with similar magnetic shape memory characteristics are also investigated to enhance the utility of MMSMAs as high performance actuators with high MFIS levels, magneto-caloric properties, reliability, lower cost, and etc. The purpose of the study is to understand:

a. *The effect of In content, cooling rate, and annealing on magnetic properties of* $Ni_{45}Co_5Mn_{(36+x)}In_{(14-x)}$ *(at %) single crystals:* Research on Ni-Mn-Co-In single crystals have shown that changing In concentration drastically influences the martensitic transformation temperatures [24]. Magnetization measurements of $Ni_{45}Co_5Mn_{(36+x)}In_{(14-x)}$ will be performed to observe these influences on the properties such as saturation magnetization, martensitic transformation temperatures, and Curie temperature. The effect of annealing temperatures and cooling rate on those properties will also be studied.

b. *Magneto-thermo-mechanical properties of bulk polycrystalline* $Ni_{43}Co_7Mn_{39}Sn_{11}$ *alloys:* Although Ni-Co-Mn-Sn alloys seem to be an alternative system to Ni-Co-Mn-In single crystals in terms of lower cost and convenience in fabrication, there is not an extensive work on the magneto-thermo-mechanical coupling of these alloys. Since the fabrication of Ni-Co-Mn-Sn single crystals has not been achieved so far, polycrystalline specimens were examined. Compared to the polycrystalline Ni-Co-Mn-Sn alloys which were manufactured by ingot metallurgy, the ones manufactured by powder metallurgy are relatively more ductile. Sintered polycrystalline specimens will undergo several thermal cycling, superelasticity, and magnetization tests to determine the changes in phase transformation temperatures under stress and magnetic field. Moreover, magnetocaloric effect (MCE) of $Ni_{43}Co_4Mn_{42}Sn_{11}$ in bulk specimens and ribbons will be determined by thermomagnetization and isothermal magnetization tests. The MCE in ribbons will be examined due to their capability of reaching high

saturation magnetization levels under low magnetic field levels with a smooth metamagnetic phase transition.

c. *Magnetization response and martensitic transformation in Fe-Mn-Ga alloys:* This alloy system has recently been introduced and they exhibit a reverse magnetization trend to the Ni-Co-Mn-X (X=In,Sn). Since the applied magnetic field increases the transformation temperatures of alloys in this system similar to the mechanical stress, Magnetic field and stress can be utilized in applications as auxiliary forces. Thus, magnetization response and martensitic transformation behavior of Fe-Mn-Ga alloys must be clearly identified. Upon this objective, Fe-Mn-Ga samples at several atomic percentages will be fabricated, and homogenized at various temperatures and time periods. Following these efforts, magnetic characterization will be performed to obtain the ideal composition and annealing conditions. Also, MCE will be examined by further magnetization measurements.

2. BASIC CONCEPTS

In this section, the basic thermo-mechanical and magnetic properties of NiCoMnX (X=In,Sn) and Fe-Mn-Ga MSMAs will be introduced such as shape memory effect, magnetic field-induced transformation, the magnetocaloric effect and kinetic arrest of martensitic transformation.

2.1 Shape Memory Effect

Shape memory alloys (SMAs) are a class of smart materials which are capable of converting thermal energy to mechanical work, or vice versa. They are advantageous over other smart materials due to high shape recovery stresses of up to 1000 MPa in NiTi [25] and large recoverable strain values. The recoverable strain is generated as a result of the shape memory effect (SME) due to martensitic phase transformation between austenite and martensite - two stable phases of SMAs - in forward and reverse directions. Shape recovery can be induced via conventional and magnetic shape memory effect. The details are in the following;

2.1.1 Conventional Shape Memory Effect and Superelastic Behavior

Figure 2-1 shows the evolution of the conventional SME which takes place as a result of thermoelastic martensitic transformation. There are four characteristic temperatures describing this transformation: Martensite start temperature (M_s), where martensite starts to grow up in austenite; martensite finish temperature (M_f), below which the entire body is martensite; austenite start temperature (A_s), where austenite

starts to grow in martensite; austenite finish temperature (A_f), above which the entire body is austenite (at its original state). Ito. et.al [18] clearly defined all these temperatures on a thermomagnetization curve as shown in the figure on page 27. These temperatures are also determined from thermal cycling tests under mechanical force that is shown in the figure on page 57.

When a single crystal SMA is in the austenite phase and cooled down to a temperature below M_s, martensite variants start to form by twinning as indicated in Figure 2-1 There is no macroscopic shape change during cooling but the mobility of twin boundaries increases. Twinned martensite – also called undeformed martensite - occurred as a consequence of heating turns into detwinned (deformed) martensite by external loading. Twin boundaries move to accommodate the external stress and deformation eventually occurs. Reverse transformation begins when the sample is heated up to a temperature above A_s and the sample completely transforms to austenite when the temperature is greater than A_f. Therefore, the sample goes back to its original, geometrically stable shape.

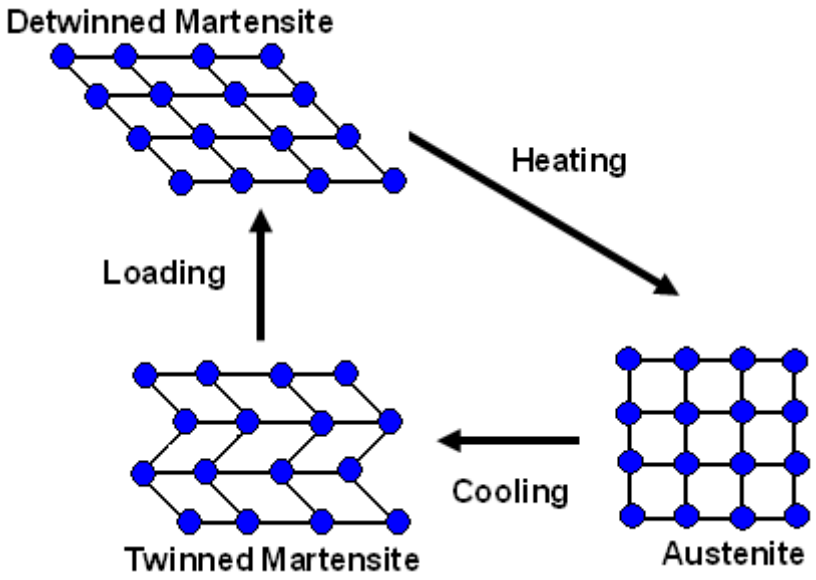

Figure 2-1) Schematic of conventional shape memory effect is shown under heating-cooling and mechanical load.

Figure 2-2 shows the stress vs. strain curve of an SMA whose behavior is dependent on A_s and A_f temperatures. When the operating temperature is above A_f, that is the sample is fully austenite, typical closed-loop superelastic behavior is observed. Once the sample is loaded with stress, it goes into elastic deformation through path 1, shown by the arrow in the figure. When the stress level reaches the critical point for the phase transformation, martensite variants are formed and the sample is in the mixed phase along path 2, and it is fully detwinned martensite on path 3. A similar process takes place during unloading: following path 4 and going down to a stress level for reverse transformation, shown by an open circle, the austenite phase appears in the sample and shape recovery begins (path A), and consequently the original undistorted state is obtained.

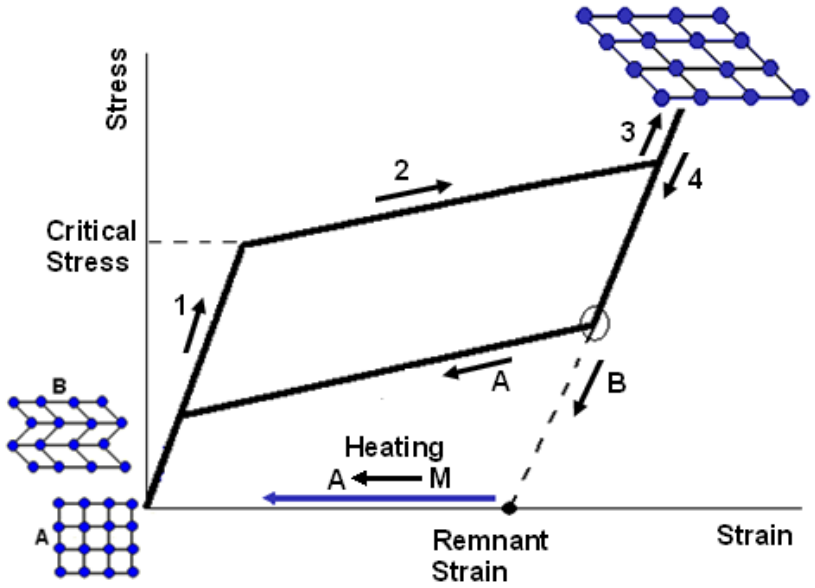

Figure 2-2) Stress-strain curve of an SMA indicating the phase transformation by external loading. Path A shows typical superelastic behavior and path B shows remnant strain as a result of stress.

However, the stress-strain behavior changes when the operating temperature of the experiment is below A_s, that is the sample is not fully austenite and martensite twins exist. As indicated by a dashed line (path B) in Figure 2-2 that the strain (solid circle) is present although the stress is unloaded. The remnant strain can be recovered by heating the sample.

2.1.2 Magnetic Shape Memory Effect

In addition to SME and superelasticity, application of magnetic field can also cause shape recovery in MSMAs. Figure 2-3 depicts the energy domain coupling of three driving forces that induce strain. While strain and shape recovery can be achieved by thermal and mechanical forces, a magnetic field is the third driving force in MSMAs. Any of these two effects can be coupled by keeping the third constant; for instance

magneto-mechanical coupling is obtained under isothermal conditions, or magneto-thermal coupling under zero loading.

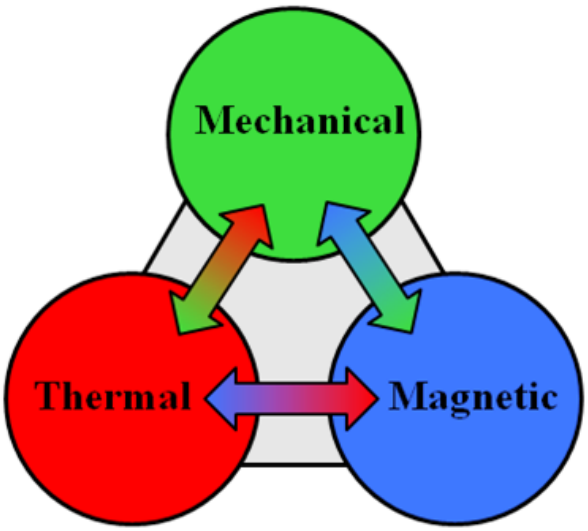

Figure 2-3) Schematic view of energy domain coupling among three driving forces of induced strain in magnetic shape memory alloys.

MFIS in MSMAs was discovered in 1996 [1] and have progressively been studied in terms of notable properties such as magnetic actuation and sensing, energy harvesting, and magnetic refrigeration [2-3, 13-14, 26]. High levels of MFIS - about 10% in Ni_2MnGa single crystals - have been reported on the basis of field-induced reorientation of martensite variants. Reorientation of martensite twins as a result of twin boundary motion is depicted in Figure 2-4a. In this case, an applied magnetic field leads to the motion of twin boundaries; the favorably oriented twins along the direction of magnetic field grow at the expense of the other twins, and eventually the shape of the material changes. The magnetocrystalline anisotropy energy of the material must be

considerably higher than the energy required to move the twin boundaries in order to to induce variant reorientation. Moreover, the requirement of both a magnetic field and an external stress to obtain reversible shape change and low output stress levels in this mechanism [27] is the limitations of its practical usage.

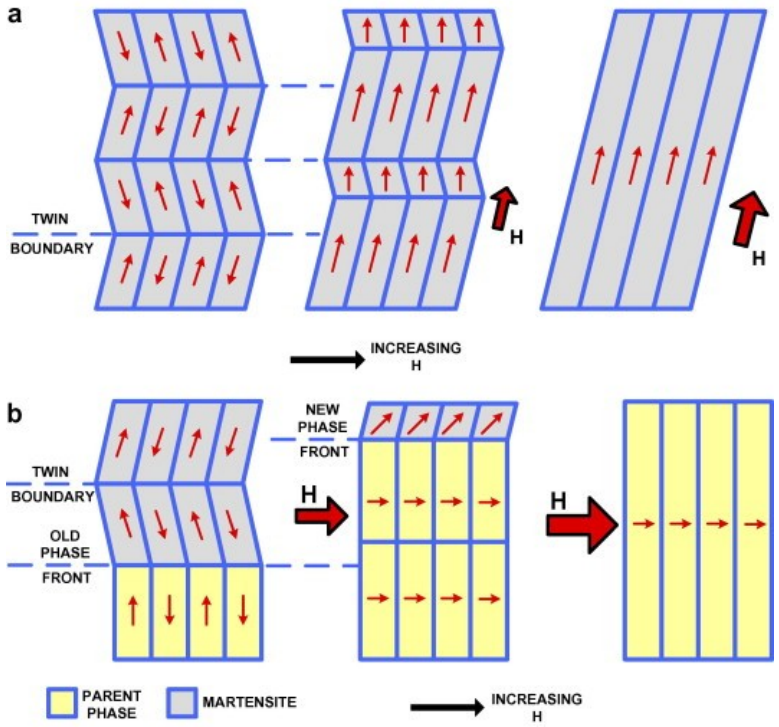

Figure 2-4) (a) Field-induced reorientation of martensite variants and **(b)** field-induced martensitic phase transformation in magnetic shape memory alloys [4].

The other mechanism which results in producing a large MFIS is magnetic-field-induced martensitic transformation [5, 8-12]. It has recently been reported that Ni-Mn-X (X=In,Sn,Sb) Heusler alloys show magnetic field-induced reverse transformation (MFIRT) from martensite to austenite as indicated in Figure 2-4b [4]. It was mentioned in the previous section that Co was a quaternary addition to increase the saturation

magnetization and Curie temperature of these alloys [5, 11]. In this mechanism, application of a magnetic field to the alloy at its martensite phase – at a temperature near A_s – leads a shape recovery. Thus the magnetic field can be replaced by heating in the schematics of conventional shape memory effect in Figure 2-1.

MFIRT is the method for obtaining MFIS and shape recovery with high actuation stress and work output which makes it more advantageous than the field-induced reorientation of martensite variants in practical applications. The output stress can be approximated by the Clasius-Clapeyron relation for the stress induced martensitic transformation [11] in Eq. 2.1 below,

$$\Delta\sigma \approx \frac{\Delta S}{\varepsilon . V_m}\Delta T \approx \frac{\Delta H}{\varepsilon . V_m}\Delta M \qquad (2.1)$$

where V_m is the molar volume of the material, ε is the strain between the martensite and austenite phases, and ΔH and ΔM are the change in the magnetic field and the magnetization across the martensitic transformation, respectively. It is obvious from the relation that the output stress is directly related to the change in magnetization. In Ni-Mn-X (X=In,Sn,Sb) materials, also called metamagnetic shape memory alloys (MMSMAs), huge difference in magnetization between martensite and austenite leads to a large output stress, whereas in the alloy systems, whose driving mechanism for MFIS is field-induced reorientation of martensite variants such as Ni_2MnGa [1, 3], FePd [28, 29], FePt [30], NiFeGa [31], a small difference in the magnetization between martensite

and austenite results in low output stress. As shown in Figure 1-1b, ZE is the energy responsible for the magnetic-field-induced phase transition and can further be increased by increasing the applied field and the difference between the magnetization levels of austenite and martensite [5]. Thus, MFIS and output stress can be enhanced by increasing ZE, which complies with Eq. (2.1) where the actuation stress is a function of the magnetization difference (ΔM) and the magnetic field (ΔH).

The following two sections will discuss the magnetic shape memory properties of Ni-Mn-based MMSMAs and the Fe-Mn-Ga ternary system which has recently been discovered as an example of metamagnetic shape memory behavior.

2.2 Ni-Mn Based Metamagnetic Shape Memory Alloys

Ni-Mn-X (X=In, Sn, Sb) MMSMAs exhibit magnetic shape memory behavior due to FIPT where they are ferromagnetic in austenite and paramagnetic in martensite phase [32-37]. The austenite phase of these Heusler alloys has cubic $L2_1$ or B_2 crystal structures depending on the degree of order (high and low degree of orders, respectively). Cubic structures form into monoclinic or orthorhombic martensite phases across phase transformation [32]. Magnetization behavior of an off-stoichiometric $Ni_{50}Mn_{34}In_{16}$ alloy is shown in Figure 2-5a [12]. When the alloy is at a high temperature and cooled down, it transforms from a paramagnetic austenite (parent) phase to ferromagnetic austenite with a second order phase transition where the Curie temperature is about 260K. Once the sample is further cooled down, first order transition takes place where the martensitic transformation occurs from ferromagnetic austenite to

paramagnetic (of anti-ferromagnetic) martensite. Recent studies show that the martensite is paramagnetic in Ni-Mn-X alloys [32]. The magnetic evolution of each temperature interval is depicted in the upper part of Figure 2-5a. The arrows show the direction of magnetic moment between atoms in a unit cell. Obviously, there is a considerable change in the direction of magnetic moments during martensitic transformation that will quantify the ZE difference between two phases and MFIS.

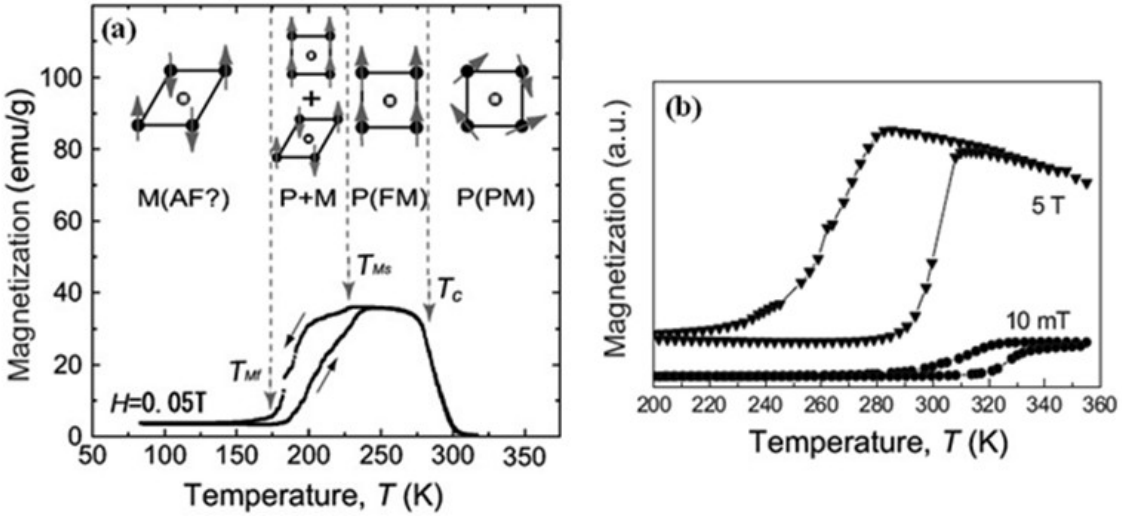

Figure 2-5) (a) Thermomagnetization curve for $Ni_{50}Mn_{34}In_{16}$ sample under the magnetic field of 0.05T [12] and (b) thermomagnetization curves of $Ni_{45.2}Co_{5.1}Mn_{36.7}In_{13}$ ribbons under 0.01T and 5T [38].

Figure 2-5b demonstrates the thermomagnetization curves of $Ni_{45.2}Co_{5.1}Mn_{36.7}In_{13}$ ribbons under the magnetic fields of 0.01T and 5T [38]. When the sample is fully austenite, a 0.01T magnetic field is applied and one cooling-heating cycle is completed. Then 5T is applied and another cycle is completed. Apparently, the martensitic transformation temperatures decrease under higher magnetic fields. The

reason for this decrease is that the applied magnetic field favors austenite because saturation magnetization is higher in these alloys. Additional undercooling is required to obtain the chemical energy to overcome the magnetic energy which opposes phase transformation [5].

In this study, single crystal Ni-Co-Mn-In MMSMAs is one of the main points of interest. It was observed in the experiments that, MT temperatures and magnetization states in transforming phases can easily be controlled by annealing, cooling processes after annealing, and adjustment of In content in addition to the notable properties of these alloys such as the magnetic shape memory effect and perfect superelasticity. The results of the experiments will be discussed in Section 4. However, brittleness, the high cost of indium and the difficulty and complexity of producing single crystals have been an issue with further investigation on Ni-Co-Mn-In. Therefore a cheaper alternative with similar properties, Ni-Co-Mn-Sn in polycrystalline form, was investigated. Ni-Co-Mn-Sn polycrystalline alloys, which were sintered without pressure, also produced magnetic shape memory effect and nearly perfect superelasticity with enhanced ductility.

$Ni_{43}Co_4Mn_{42}Sn_{11}$ annealed ribbons were studied in terms of the magnetocaloric effect (MCE) since they easily go under phase transformation in a very low magnetic field and exhibit high magnetization. Experimental results of bulk specimens with the same composition were compared with those of annealed ribbons. Microstructural observations, results of thermomechanical tests and discussion of magnetic properties of the Ni-Co-Mn-Sn alloys will be included in Section 5.

2.3 Fe-Mn-Ga Metamagnetic Shape Memory Alloys

Fe-Mn-Ga is a new magnetic shape memory alloy system that was first reported in 2009 [21]. These alloys undergo martensitic phase transformation from the paramagnetic cubic $L2_1$ phase to ferromagnetic tetragonal martensite that is the opposite of the Ni-Mn-based MMSMAs in terms of the magnetization states between the austenite and martensite phases. [21-23] This behavior in Fe-Mn-Ga alloys is defined as magnetic-field-induced forward transformation (MFIFT) since an applied magnetic field triggers martensitic transformation in the forward direction from the austenite phase to low temperature martensite phase. Figure 2-6 indicates the magnetization behavior of the $Fe_{43}Mn_{28}Ga_{29}$ polycrystalline alloy as a function of temperature under magnetic fields of 0.05T and 7T [21]. High magnetization is attained in the martensite phase and heating the sample to a temperature above the reverse transformation start temperature leads to a drastic decrease in magnetization. The paramagnetic austenite phase is obtained by further heating. In the magnetization curve (Figure 2-6), the martensitic transformation temperatures increase by 20K under magnetic field of 7T while it has been reported that those temperature decrease about 30K in the single crystal $Ni_{45}Co_5Mn_{36.6}In_{13.4}$ alloys [11]. Omori et. al [21] has not reported MFIS due to MFIFT, but they obtained a strain of about 0.6% in $Fe_{43}Mn_{28}Ga_{29}$ single crystals by applying a magnetic field up to 8T. No reversible length change is reported upon removing the magnetic field. This behavior is defined as magnetostriction and is substantially larger than the magnetostriction of Terfenol-D due to MFIFT [21].

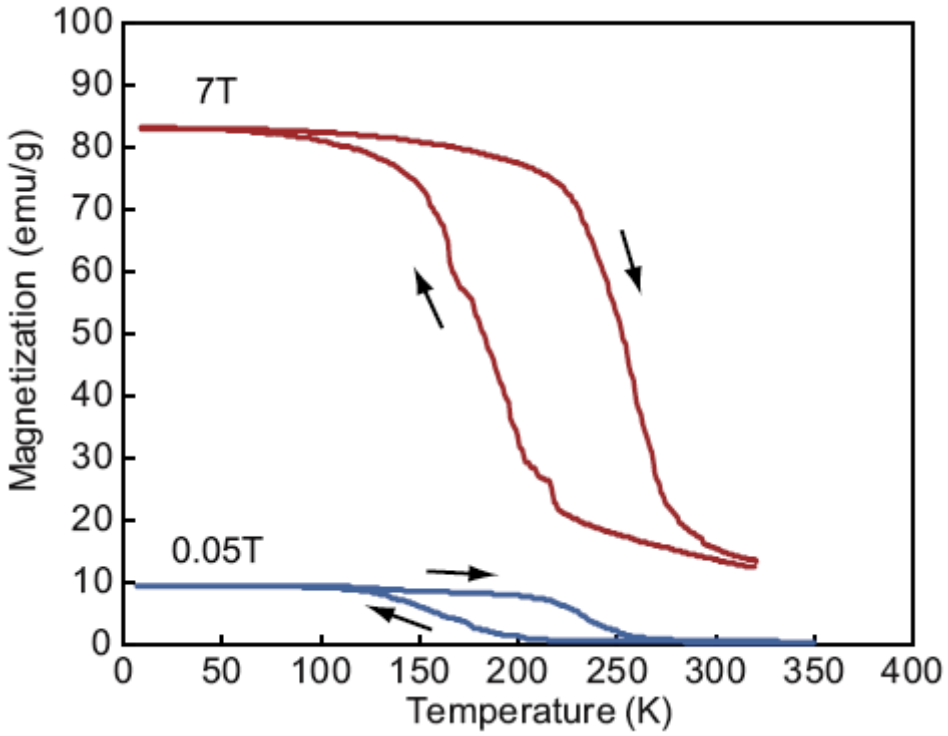

Figure 2-6) Thermomagnetization curves of $Fe_{43}Mn_{28}Ga_{29}$ polycrystalline alloys under 0.05T and 7T magnetic fields [21].

Further research was conducted on the Fe-Mn-Ga alloy system to improve magnetic properties and shape memory strain [22-23]. Nearly stoichiometric Heusler alloys of Fe_2MnGa were fabricated in a wide composition range. Figure 2-7 shows the ternary phase diagram of synthesized Fe-Mn-Ga alloys and the points indicated by circles and solid triangles denote BCC and FCC structured compositions, respectively [22]. The area surrounded by the borderline contains the alloy compositions show MT character and are MSMAs. The $Fe_{50}Mn_{22.5}Ga_{27.5}$ sample which is shown by the star in the area line exhibits ferromagnetism in martensite with a higher saturation magnetization - around 94emu/g under the magnetic field of 5T - than the $Fe_{43}Mn_{28}Ga_{29}$

alloy with a saturation magnetization of about 82 emu/g under 7T (Figure 2-6). High ΔM can be gained by MT from martensite with a higher magnetization to paramagnetic austenite, which in turn helps to achieve MFIFT and a larger magnetocaloric effect. Moreover, large lattice distortion that occurs during MT generates a large shape memory effect in the sample with a strain of 3.6%. It is important to note that this large amount of shape memory strain has not been reported in the other polycrystalline MSMAs [22].

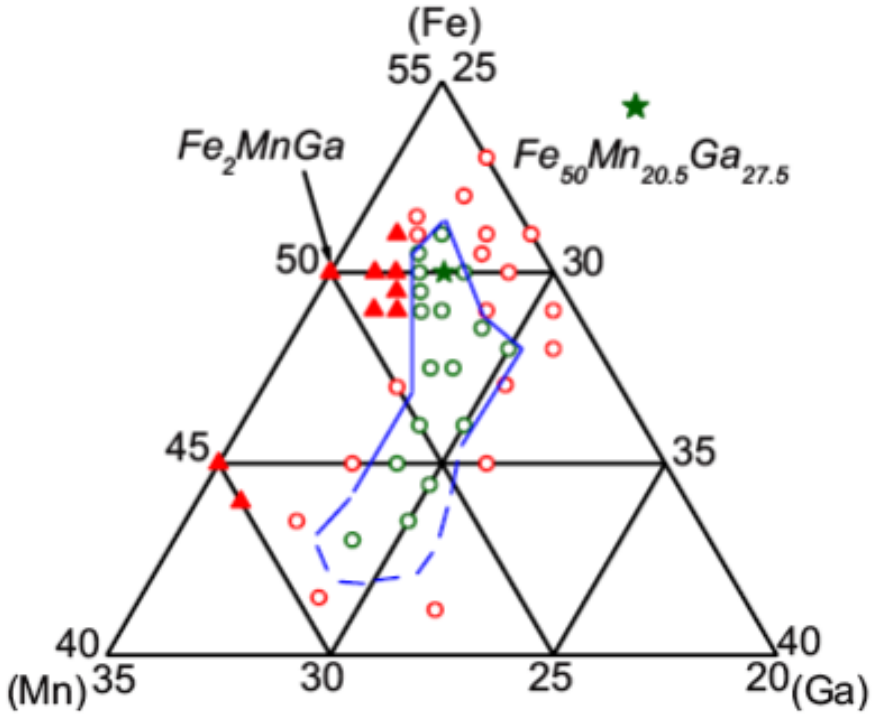

Figure 2-7) Phase diagram of Fe-Mn-Ga alloys. BCC and FCC (▲) structures formed in the composition range. The surrounded area describes the region of MSMAs [22].

Fe-Mn-Ga has recently been discovered as an alternative alloy system to Ni-Mn-based MMSMAs with similar magnetic and shape memory properties. The existence of

magnetic-field-induced phase transformation makes Fe-Mn-Ga alloys available both for single crystal and polycrystalline forms like in Ni-Mn-based alloys. Recalling from Figure 2-6 that increasing magnetic field during cooling-heating cycle shifts MT temperatures to the right, we know that a magnetic field can be utilized as an auxiliary mechanism to mechanical loading since applying stress increases MT temperatures [3-5] in MSMAs. Thus, stress can be employed in applications where a low magnetic field is required. Alloying efforts and a systematic heat treatment study have been made to enhance magneto-thermo-mechanical and magnetocaloric properties which will be discussed in Section 6.

2.4 Magnetocaloric Effect

The magnetocaloric effect (MCE) is defined as the heating or cooling of a magnetic material when a magnetic field is applied. MCE occurs in a magnetic solid as a result of the entropy variation due to the coupling of the magnetic spin system with the magnetic field [39]. An isothermally applied magnetic field generally reduces the entropy of the spin structure due to aligning randomly oriented magnetic moments (spins) to its own direction and converting the disordered system to an ordered one. Figure 2-8 schematically shows the basic process of magnetic field applications to a spin system. The spins return to the disordered state by adiabatic demagnetization due to the thermal energy provided by the phonon bath of the sample that will result in cooling of the system.

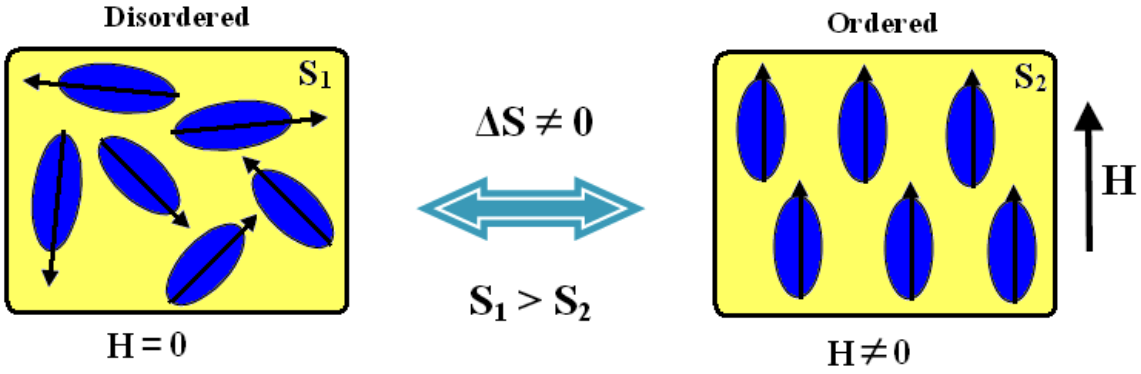

Figure 2-8) Basic process of MCE when magnetic field is applied or removed in a magnetic system in an isothermal process.

Since the discovery of the MCE by Warburg in 1881 on iron samples [40], it has been widely utilized in magnetic materials to reach low temperatures. Continuous research has been conducted on magnetic materials, and a giant MCE in the $Gd_5(Si_xGe_{1-x})_4$ alloy system has been reported by Pecharsky and Gschneidner [41]. Afterwards, several elements and alloys such as $La(Fe_xSi_{1-x})_{13}$ [42], $MnAs_{1-x}Sb_x$ [43] and $MnFeP_{0.45}As_{0.55}$ [44] were reported to be used in magnetic cooling. Research on materials for room-temperature refrigeration in lower magnetic fields has been popular in recent years [41, 44 and 47]. In alloy systems that exhibit MCE, adiabatic demagnetization causes cooling by increasing entropy, whereas in some systems adiabatic magnetization leads to cooling. An inverse MCE is observed in systems such as $Mn_{1.95}Cr_{0.05}Sb$ [48], $MnV_{0.18}Sb$ [49], and $Fe_{49}Rh_{51}$ [50] where applied magnetic field increases the entropy. In such systems, magnetically inhomogeneous states are present near first-order transformation that gives rise to mixed magnetic interactions. It is stated

that applied magnetic field to these systems introduces more spin disorder and eventually increases the entropy.

MSMAs are another interesting group of alloys associated with MCE due to magnetic shape memory effect. Among Ni-Mn-based ferromagnetic Heusler alloys, MCE in Ni-Mn-Ga has been investigated in a broad composition range where these alloys undergo an MT from ferromagnetic austenite to ferromagnetic martensite whose ferromagnetic exchanges are different. First-order martensitic transformation occurs in Ni-Mn-Ga and a large MCE can be obtained at a temperature across MT [51-53]; an inverse MCE has been reported in nearly stoichiometric Ni_2MnGa [52]. Moreover, extensive research has been made on the MCE in Ni-Mn-X (X=In, Sn, Sb) alloys due to large changes in magnetization across MT, and inverse MCE has been reported [35, 54-61]. As discussed earlier in this section, the MCE is related to the entropy change of the system. The field-induced magnetic entropy change (ΔS_M) can be quantified by the Maxwell Relation [10, 57]:

$$\Delta S_M(H,T) = \mu_0 \int_0^H \left(\frac{\partial M}{\partial H} \right)_H dH \tag{2.2}$$

The above equation can be approximated for discreet intervals as follows [57]:

$$\Delta S_M(H,T) \approx \frac{1}{\Delta T} \left[\int_0^H M(T+\Delta T, H) dH - \int_0^H M(T,H) dH \right] \tag{2.3}$$

It is evident from Eq. 2.3 that ΔS_M is directly related to the change in magnetization. Since martensite and austenite are paramagnetic and ferromagnetic respectively, a drastic magnetization change occurs during MT. The same type of MT in the opposite direction takes place in Fe-Mn-Ga alloys which will make all Ni-Mn-X, Ni-Co-Mn-X quaternary, and Fe-Mn-Ga alloy systems ideal materials for MCE study. Figure 2-9a shows the isothermal magnetization curves of $Ni_{43}Co_5Mn_{41}Sn_{11}$ melt-spun ribbons measured near MT temperature on heating [62]. These curves suggest the typical metamagnetic behavior associated with the field-induced reverse phase transformation, since they transform from martensite with low magnetization to austenite with high magnetization upon application of a magnetic field. ΔS_M as a function of temperature, which is calculated based on the Maxwell relation in the field of 10kOe, is depicted in Figure 2-9b. The curve with the square markers represents the magnetic entropy change of the melt-spun ribbons corresponding to the isothermal magnetization curves in Figure 2-9a. Maximum ΔS_M, approximately 10 J kg^{-1} K^{-1}, is found near room temperature. This value is small compared to the other magnetocaloric materials such as $Gd_5Si_2Ge_2$ and $La(Fe,Si)_{13}$ where maximum ΔS_M under the field of 50 kOe is 18 J kg^{-1} K^{-1} at 276K [41] and 30 J kg^{-1} K^{-1} at 184K [63]. However, the MCE from the $Ni_{43}Co_5Mn_{41}Sn_{11}$ melt-spun ribbon was attained in magnetic field and at room temperature which is of importance for practical applications. Other Ni-Mn-based MMSMAs from which high amounts of ΔS_M have been reported can be illustrated as 29 J kg^{-1} K^{-1} in $Ni_{50}Mn_{35.3}In_{14.7}$ [58] and 19 J kg^{-1} K^{-1} in Ni-Mn-Sn [10] both near room temperature and under 50kOe.

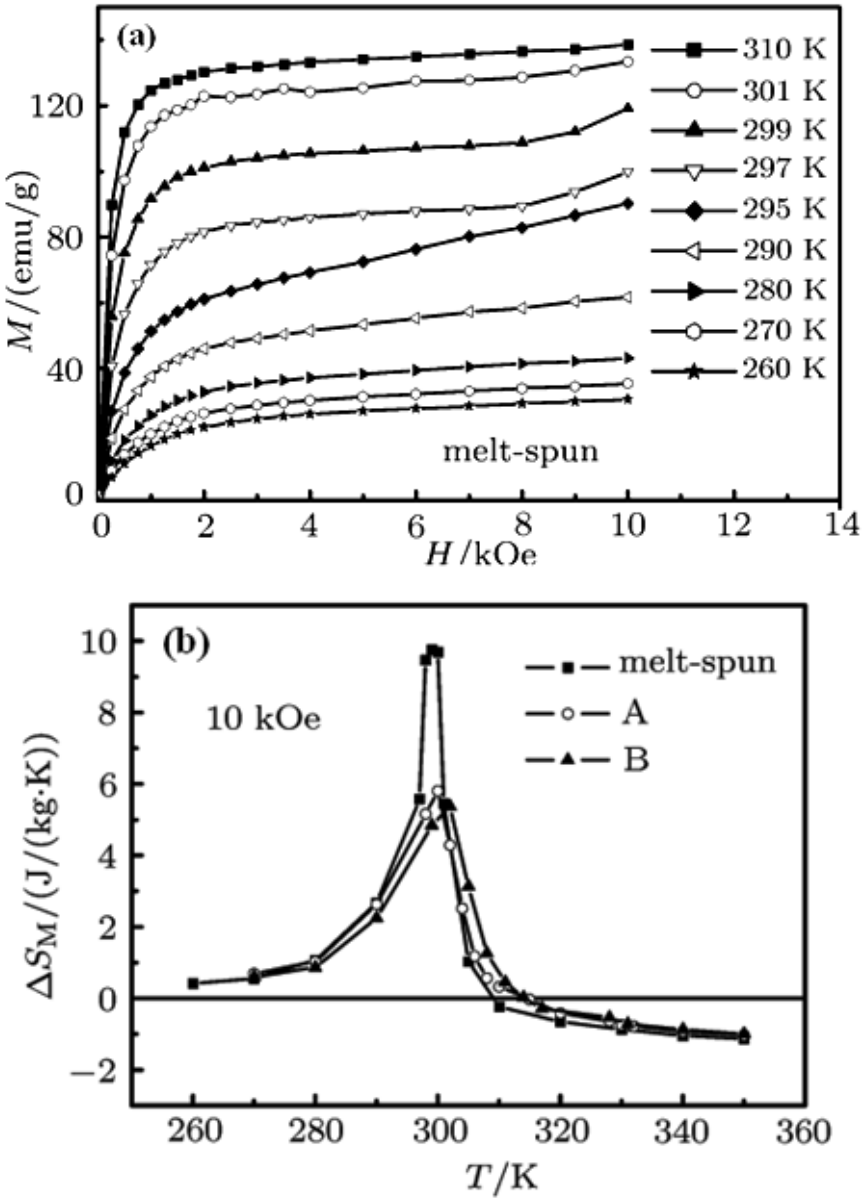

Figure 2-9) (a) Magnetization isotherms for the Ni-Co-Mn-Sn melt-spun ribbons in the field up to 10kOe on heating and **(b)** magnetic entropy change of Ni-Co-Mn-Sn melt-spun ribbons and other samples as a function of temperature [62].

2.5 Kinetic Arrest of Martensitic Transformation

Kinetic arrest (KA) is a phenomenon which is described as interruption of MT at certain temperatures during cooling under a magnetic field. MT does not proceed with further cooling and the austenite phase still remains down to low temperatures [64, 65]. The temperature corresponding to KA is T_{KA}. Along with the research on KA during transition between different magnetization states in materials such as $Ce(Fe_{0.96}Ru_{0.04})_2$ [66], colloidal systems [67, 68], and some theoretical aspects [69], this phenomenon has also been reported in several Ni-Mn-based MSMAs such as NiCoMnAl [64], NiCoMnSn [65], NiCoMnGa [70], NiMnIn [71, 72], and NiCoMnIn [18, 60]. Since KA behavior significantly influences the transformation properties of MMSMAs, its features at low temperatures are still under discussion.

Figure 2-10 demonstrates the thermomagnetization curves of $Ni_{45}Mn_{36.7}Co_5In_{13.3}$ single crystal under field strengths of 0.05T, 3T, 5T and 8T. All measurements start at around 300K and the temperature is scanned between 300K and 4.2K. The cooling-heating curve in the field of 0.05T clearly defines the MT temperatures. As a typical response in MMSMAs, an increasing magnetic field decreases the MT temperatures and the cooling-heating curves shift leftwards. M_f is close to 150K in the curves of 3T and 5T and it is estimated to be around 150K in the 8T curve in which no MT is observed. It is seen in the cooling-heating curve obtained under 5T that although the material undergoes MT, the magnetization level of martensite is still high (around 100 emu g^{-1}). XRD experiments conducted on the material under 5T in Ref.18 verify that the mixture of austenite and martensite phases are existent in the martensite phase region that is the

consequence of interruption for transformation at around 150K on cooling [18]. Therefore, the sample incompletely transforms from its parent phase to the martensite. Further increasing the magnetic field up to 8T completely prevents MT and the sample remains in austenite down to low temperatures which can be elucidated as the "stabilization of parent phase". This unusual behavior is explained by reduction of the entropy difference between the parent and martensite phases to very low levels, even zero [18, 64-65]. Disappearance of the magnetic entropy change is expected to zero the Gibbs energy of the system that triggers MT.

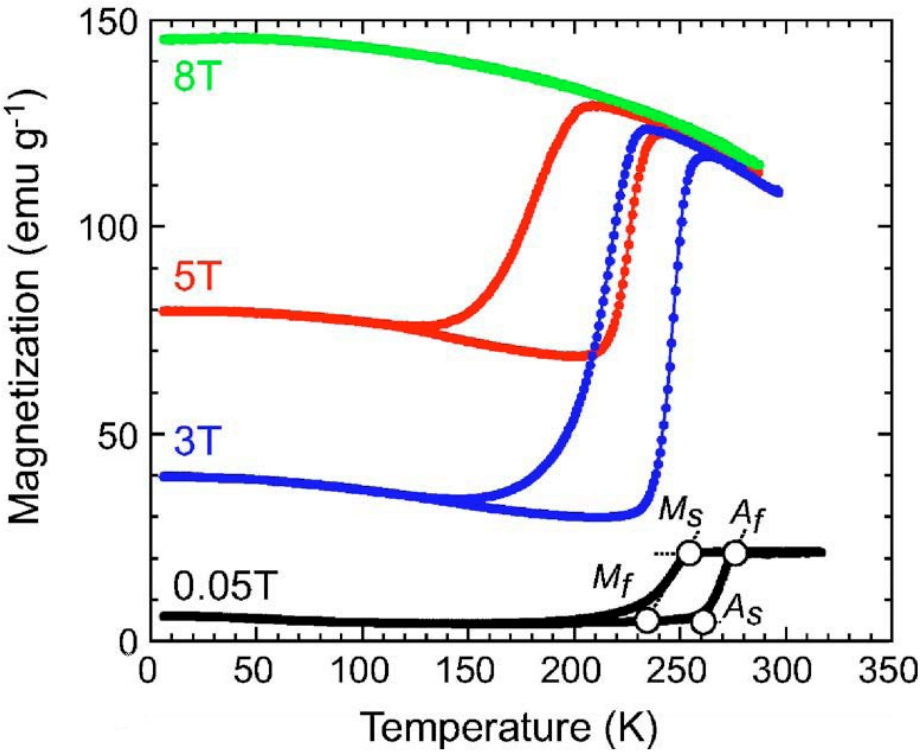

Figure 2-10) Thermomagnetization curves of $Ni_{45}Mn_{36.7}Co_5In_{13.3}$ single crystal under 0.05T, 3T, 5T, and 8T magnetic fields [18].

Figure 2-11 indicates the magnetic field temperature phase diagram of $Ni_{45}Mn_{36.7}Co_5In_{13.3}$ single crystal where H_{Ms} and H_{Af} are the martensitic transformation starting field and the reverse transformation finishing field respectively, and H_0 is the equilibrium magnetic field which is defined as the average of H_{Ms} and H_{Af} [18]. The figure was plotted by the data points extracted from isothermal magnetization and electrical resistivity measurements (Fig. 4a-b in Ref.18). The difference between H_{Ms} and H_{Af} is continuously increasing at decreasing temperature. However, H_0 is increasing from 260K to 150K and stays constant at temperatures lower than 150K. H_0 is entitled as the critical magnetic field which equalizes the Gibbs energies of the parent and martensite phases at a temperature of $T_0 \approx (M_s+A_f)/2$ [63, 64]. The relationship between the critical magnetic field and entropy change can be built via the Calsius-Clapeyron relation in the magnetic phase diagram:

$$\frac{dH_0}{dT} = -\frac{\Delta S}{\Delta M} \tag{2.4}$$

where ΔS and ΔM are the entropy and magnetization differences between austenite and martensite phases, respectively. ΔM determined from the isothermal magnetization curves (Fig 4a in Ref.18) is almost constant for each isotherm that makes ΔS a number proportional to dH_0/dT. Since H_0 is not changing with temperatures below 150K, dH_0/dT is almost zero; that is to say ΔS is almost zero. The driving force (Gibbs energy) of MT with respect to temperature is given below:

$$\Delta G \approx \Delta S.\Delta T \tag{2.5}$$

Since ΔS~0 below 150K, the driving force of MT disappears and phase transformation does not occur at temperatures below 150K. Although KA behavior in MMSMAs mentioned above is explained as the disappearance of entropy change and driving energy change between the parent and the martensite phases, the main reason underlying this phenomenon is still some point of discussion [18].

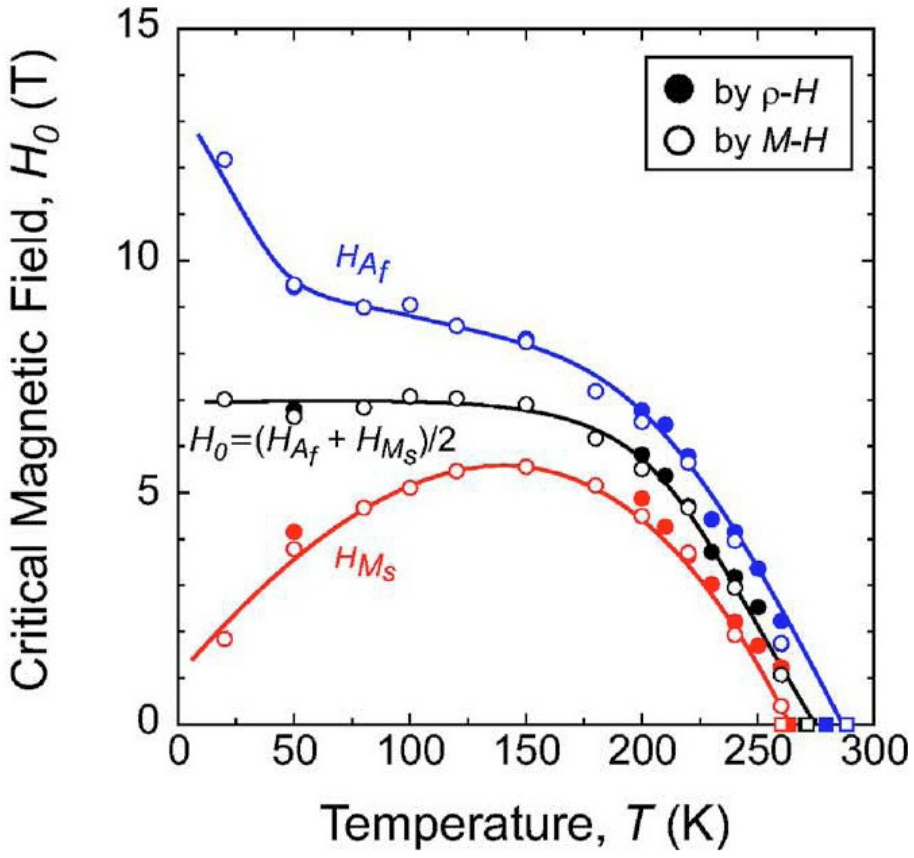

Figure 2-11) Magnetic field temperature phase diagram where H_{Ms}, H_{Af}, and H_0 were extracted from isothermal magnetization and electrical resistivity measurements [18].

3. EXPERIMENTAL PROCEDURES

3.1 Alloy Fabrication, Processing and Microstructural Analysis

$Ni_{45}Mn_{36.5}Co_5In_{13.4}$ (at%) were prepared using vacuum induction melting by Professor Yuriy Chumlyakov. Single crystals were grown using the Bridgman technique in He atmosphere. Then, the crystals were cut into rectangular prism shape samples with dimensions of 4 mm x 4mm x 8mm by using wire electro discharge machining. The long axes of these samples were used as the compression axis. Three rectangular prism samples were homogenized at 900°C for 1 day. One of these samples was quenched in iced water, one of the others was quenched in oil, and the last one was slowly cooled in the furnace. The water quenched sample was sliced into 1mm thick samples, and these slices were annealed from 400°C to 800°C with an increment of 100°C for 3 hours and again water quenched. X-Ray diffraction (XRD) measurements were done to determine the atomic ordering. Data was collected on Bruker D8 powder X-ray diffractometer (fitted with Cu Source, and LynxEYE detector), with a step size of 0.015 degrees and a step time of 0.1 seconds/step.

Bulk polycrystalline $Ni_{43}Co_7Mn_{39}Sn_{11}$ (at %) ingot were melted using high frequency induction, and spherical powders were obtained from this alloy by conventional nitrogen gas atomization under an atmosphere with an argon pressure of 1.5-5MPa. The spherical powders with a diameter of 1-250μm were separated into four groups, and the ones with a diameter of 25μm were selected for sintering. These 25μm-diameter powders were sealed in two different quartz tubes under an argon atmosphere and sintered at 900°C for 2 and 6 days and quenched in iced water. All these operations

were performed by Professor Kainuma group in University of Tohoku, Japan. For mechanical testing, rectangular specimens with dimensions of 3.2 x 2.6 x 5.3mm^3 and 3 x 1.9 x 5.5mm^3 were prepared from the 6-day sintered and 2-day sintered samples respectively. Optical images were obtained using a Keyence model VHX-600 digital microscope.

Bulk $Ni_{43}Co_4Mn_{42}Sn_{11}$ (at %) alloys in polycrystalline form were fabricated by Dr. Jian Liu from Institute for Metallic Materials, Germany, which has research collaboration with our group. The alloys were prepared by induction melting by using pure Ni, Co, Mn and Sn elements. Ribbons were obtained by melt-spinning the induction melted alloys. Bulk and ribbon specimens were annealed at 900°C for 1 day and 2 hours respectively, and subsequently quenched in iced water.

Several polycrystalline Fe-Mn-Ga alloys, except two compositions that were received from external sources, were melted under argon atmosphere by using pure Fe, Mn and Ga metals in an Edmund Bühler GmbH arc melting system. The samples were re-melted three times, and subsequently annealed at different temperatures for various time periods to achieve the desired homogeneity. All the samples were quenched in iced water. For microstructure analysis, backscattered electron (BSE) images were attained by using a Cameca SX50 electron microprobe which is capable of digital imaging with 6 element topographic BSE detector array. Also, matrix and second phase compositions of the alloys were determined by this electron microprobe equipped with 4 wavelength-dispersive X-ray spectrometers, PGT energy-dispersive X-ray system

cathodoluminescence detector. Table6-1 shows the nominal and real matrix compositions of Fe-Mn-Ga alloys.

3.2 Magneto-Thermo-Mechanical Testing

Thermal cycling and superelasticity experiments were performed under compression to determine the magneto-thermo-mechanical behavior of $Ni_{43}Co_7Mn_{39}Sn_{11}$ alloys using a custom-designed magneto-thermo-mechanical setup which consists of an MTS servo-hydraulic test frame and a Lake Shore Model EM4-CS electromagnet attached to the test frame with a capacity of generating uniform magnetic fields up to 1.6 Tesla.

A custom built nonmagnetic Ti-6Al-4V alloy grips were attached to the test frame. A Lake Shore high sensitivity cryogenic transverse Hall probe sensor (resolution: ±0.01 mT within the ±30 T range) was combined within a Lake Shore model 450 gaussmeter for magnetic field measurement and the probe was mounted perpendicular to the compression axis**.** A capacitive displacement sensor (Capacitec, Ayer, MA, USA) was used to measure the displacement and, in turn the strain. Heating and cooling was controlled by an Omega CN8200 series temperature controller for each grip and a K-type thermocouple attached to the sample. Copper tube was wrapped around the grips and liquid nitrogen was flowed though it for cooling and a cryogenic grade on/off solenoid valve connected to temperature controller was utilized to control the flow of liquid nitrogen. Heating was achieved by the heating band wrapped around the tubes. A

nonmagnetic polymer chamber was attached to the system to isolate the experiment from the surroundings and prevent sudden temperature drops.

3.3 Magnetization Measurements and Transformation Temperatures

Magnetic properties of the alloys investigated in this study were determined using a Quantum Design Superconducting Interference Device (SQUID) with a vibrating sample magnetometer (VSM) at a heating-cooling rate of 5K min^{-1}. The samples were cut into very small pieced with the weight on the order of milligrams and tested. Thermomagnetization experiments were conducted to determine the magnetic properties of the samples in austenite and martensite phases. Meanwhile, isothermal magnetization measurements were performed to quantify the magnetocaloric effect and magnetic field-induced strain, if exists. Furthermore, differential scanning calorimetry (DSC) measurements were done to determine the martensitic transformation temperatures at a heating-cooling rate of 10K min^{-1}.

4. EFFECT OF ALLOYING, ANNEALING TEMPERATURE AND COOLING RATE IN Ni-Co-Mn-In SINGLE CRYSTALS

Ni-Co-Mn-In single crystals are investigated in this section due to their enhanced magnetic shape memory properties and perfect superelastic behavior [5]. It was confirmed in the previous research that solution heat treated (or homogenized) $Ni_{45}Co_5Mn_{36.7}In_{13.3}$ [11] and $Ni_{45}Co_5Mn_{36.5}In_{13.5}$ [5] single crystals at 900°C for 1-day exhibit the desired magnetic properties such as metamagnetic shape memory effect, high saturation magnetization and shape recovery. Therefore, it is of great importance to investigate the Ni-Co-Mn-In MMSMAs at various In contents to obtain the ideal alloy composition. Section 4-1 will examine the effect of indium content in N-Co-Mn-In alloys in terms of MT temperatures and saturation magnetization.

4.1 Effect of Indium Content on Martensitic Transformation of Ni-Co-Mn-In Alloys

Figure 4-1 indicates the thermomagnetization curves of $Ni_{45}Co_5Mn_{36.6}In_{13.4}$ (In-13.4 sample) single crystal which was homogenized at 900°C for 1 day and quenched in iced water. These curves are the cooling-heating cycles at the magnetic fields of 0.05T, 1T and 7T that were selected from the results at 0.05T, 1T, 3T, 5Tand 7T. It is clearly shown that metamagnetic phase transition exists from ferromagnetic austenite phase to paramagnetic martensite phase, and MT temperatures decrease by increasing magnetic field since the austenite phase is favored by field application.

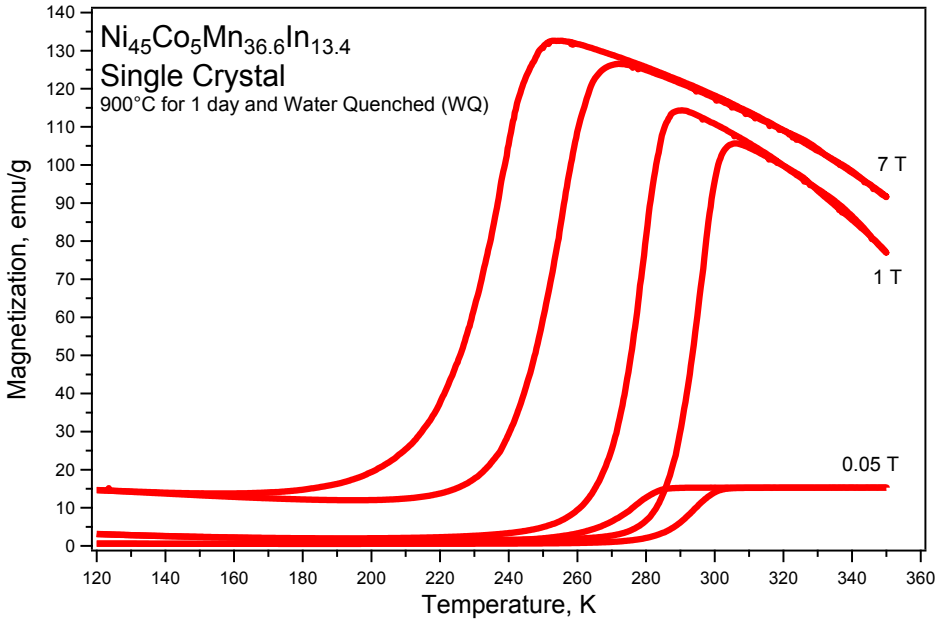

Figure 4-1) Thermomagnetization curves of $Ni_{45}Co_5Mn_{36.6}In_{13.4}$ single crystal which was quenched in water after homogenization at 900°C for 1 day. Magnetization measurements were performed under 0.05T, 1T and 7T.

Thermomagnetization measurements of $Ni_{45}Co_5Mn_{36.8}In_{13.2}$ (In-13.2 sample) polycrstalline alloy is shown in Figure 4-2. Selected magnetic field levels are 0.05T, 3T and 7T for this sample. Orientation independence of MMSMAs let the single crystals to be replaced by the polycrystalline samples, and it is obvious that the polycrystalline sample in Figure 4-2 shows typical metamagnetic shape memory response. In this case, when the sample is loaded with the field of 0.05 T at the austenite phase and cooled down, it transforms from paramagnetic austenite to ferromagnetic austenite at around 362K. This temperature is the Curie temperature (T_c) of the alloy and demonstrated in Figure 4-4 on page 38. Further cooling initiates the martensitic transformation at around 304K. When the magnetic field is increased to higher levels, the thermomagnetization response is similar to that of $Ni_{45}Co_5Mn_{36.6}In_{13.4}$ in Figure 4-1. Figure 4-3 shows the

magnetization response of the single crystal sample with the highest In concentration - 13.5 at% (In-13.5 sample) - across MT. T_c, M_s and A_s temperatures are determined from the cooling-heating curve in the field of 0.05T. While T_c of In-13.5 sample is greater than the T_c of In-13.2 sample, M_s is greater in In-13.2 sample. When the magnetic field was increased to 7T in austenite and the sample was cooled down, it was shown that the In-13.5 sample followed the path which is shown by the arrow in Figure 4-3, and did not completely transform. This incomplete transformation is attributed to the kinetic arrest phenomenon that was discussed in Section 2.5. Further increase in magnetic field may cause the MT to be interrupted and the sample remains in austenite over the whole temperature range. Then, the sample was cooled down to 5K and magnetic field was applied in martensite phase –the point shown by the star in Figure 4-3- to be able to determine the reverse transformation temperatures. Finally, the 7T thermomagnetization curve was obtained.

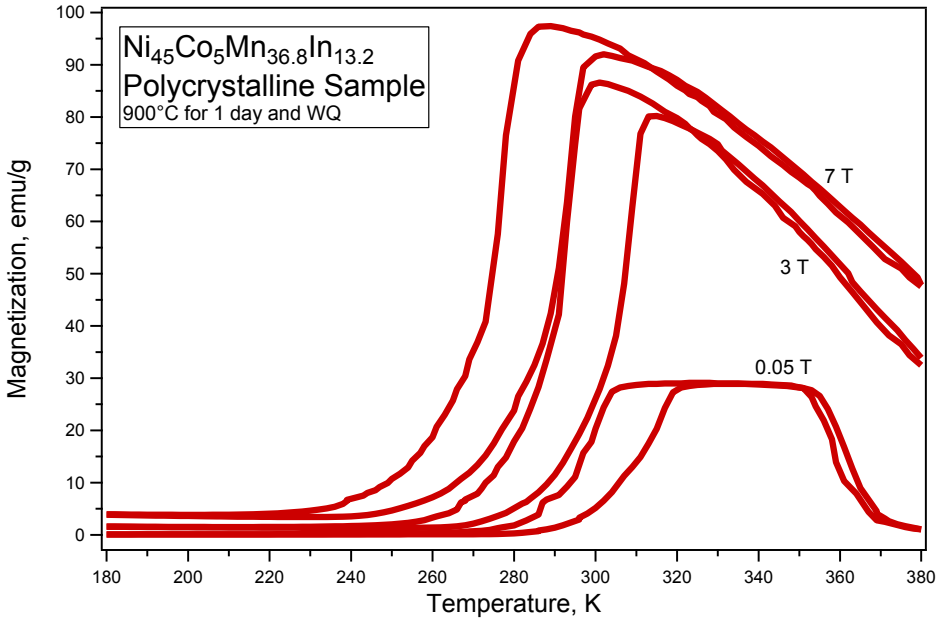

Figure 4-2) Thermomagnetization curves of a polycrystalline $Ni_{45}Co_5Mn_{36.8}In_{13.2}$ alloy which was homogenized at 900°C for 1 day and water quenched. Magnetization measurements were performed under 0.05T, 3T and 7T.

Figure 4-4 depicts the comparison of the thermomagnetization curves in the field of 0.05T that were taken from Figures 4-1, 4-2 and 4-3. T_c of the In-13.2 and In-13.5 samples were determined to be 362K and 373K respectively, where Tc of In-13.4 sample was not detected. The highest saturation magnetization was obtained from the In-13.5 sample whereas the smallest one was shown in the In-13.4 sample. Ms Temperatures of In-13.2 and In-13.4 samples were detected around room temperature. In-13.5 sample has the highest saturation magnetization in both low field and high field magnetization curves. Moreover, temperature hysteresis (T_{hys}) increases by increasing In content, where T_{hys} values obtained under 0.05T are about 15K, 21K and 41K for In-13.2, In-13.4 and In-13.5 samples, respectively.

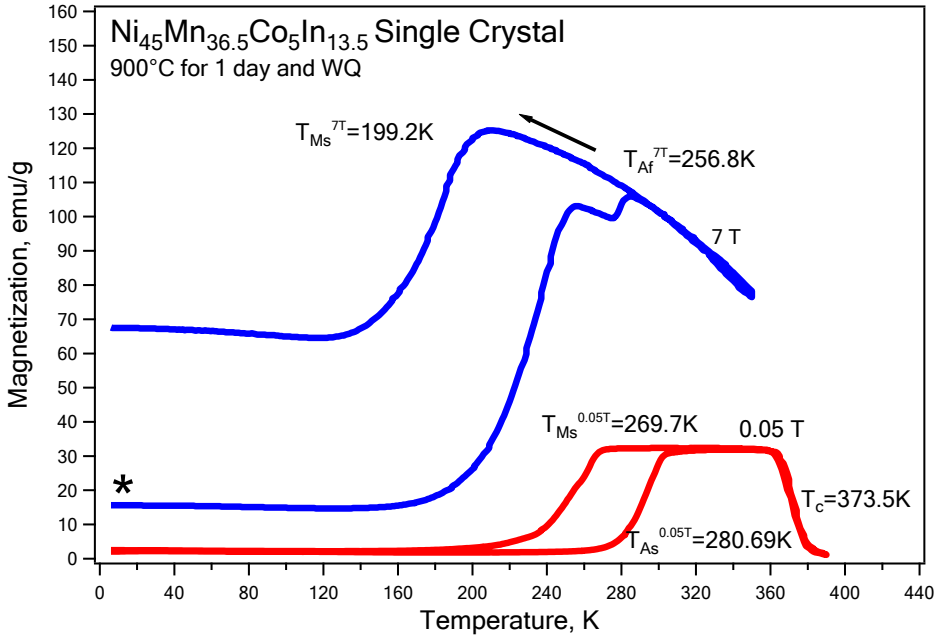

Figure 4-3) Thermomagnetization curves of $Ni_{45}Co_5Mn_{36.5}In_{13.5}$ single crystal which was homogenized at 900°C for 1 day and water quenched. Magnetization measurements were performed under 0.05T and 7T.

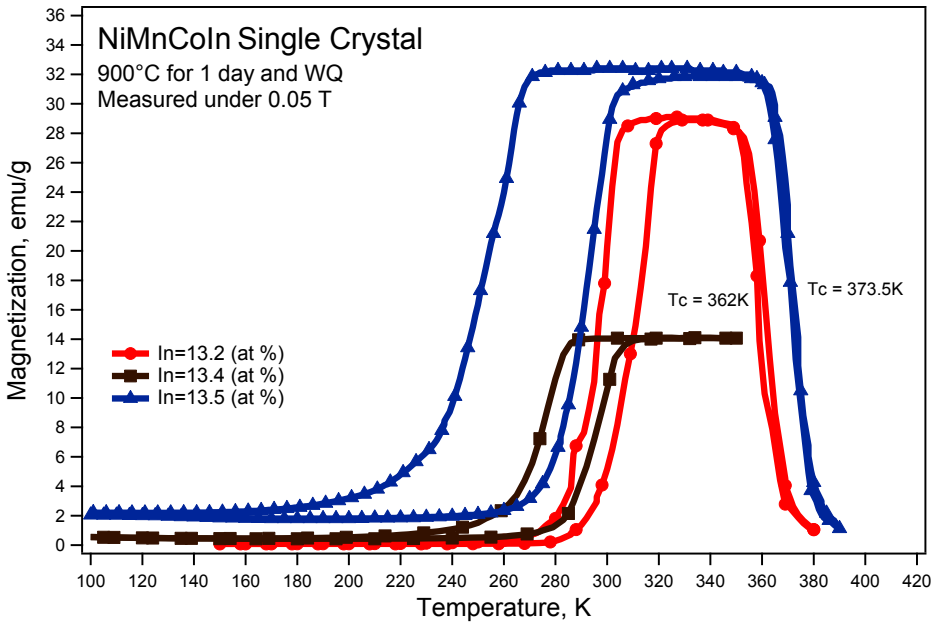

Figure 4-4) Thermomagnetization curves of Ni-Co-Mn-In specimens homogenized at 900°C for 1 day and water quenched at various In concentrations. Measurements were performed under 0.05 T.

In Figure 4-5, thermomagnetization curves obtained from the samples in the field of 7T are compared like in Figure 4-4. It is apparently shown from the figure that increasing In content increases the magnetization levels, while it reduces the MT temperatures. The In-13.4 sample seems to have the highest change in magnetization (ΔM) across the MT. Application of 7T magnetic field hinders the complete transformation from austenite to martensite in In-13.5 sample, meanwhile the other two samples can easily transform to martensite.

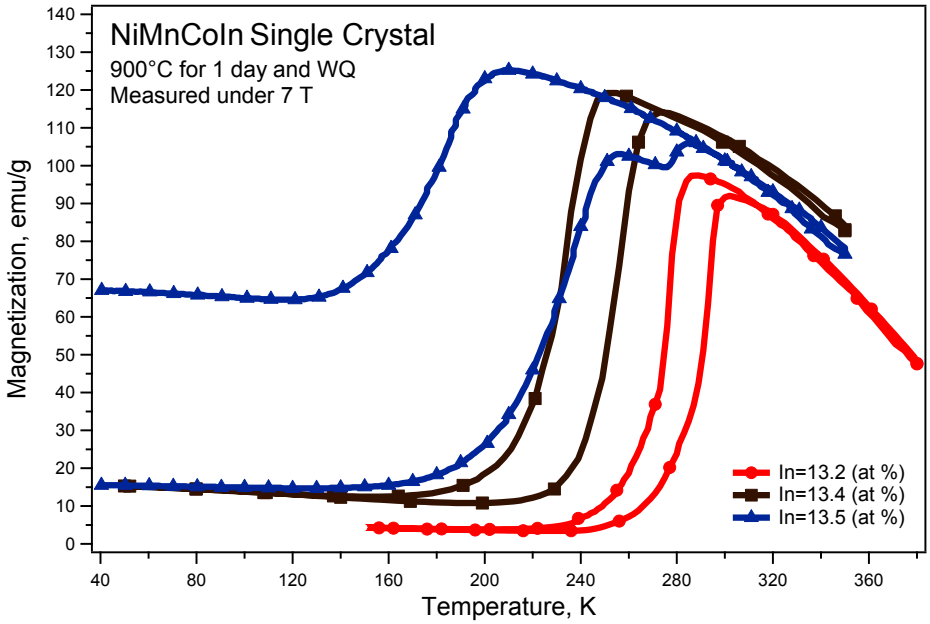

Figure 4-5) Thermomagnetization curves of Ni-Co-Mn-In specimens homogenized at 900°C for 1 day and water quenched at various In concentrations. Measurements were performed under 7 T.

Figure 4-6 depicts the M_s Temperatures of the samples in the magnetic fields of 0.05T and 7T as a function of In content, where the M_s values were extracted from Figures 4-4 and 4-5. Increasing In concentration reduces M_s. There is a sharper decrease

in the Ms temperatures under 7T magnetic field than that of 0.05T which is shown by the blue curve. MT hardly occurs in the In-13.5 sample due to KA behavior. The M_s temperatures obtained under 0.05T for In-13.2, In-13.4 and In-13.5 samples are 304K, 283K and 270K, respectively. These values are lower than the M_s values obtained from the Ni-Co-Mn-In single crystals that was heat treated at 900C for 37 days [24] where the corresponding M_s values are around 320K, 300K and 280K.

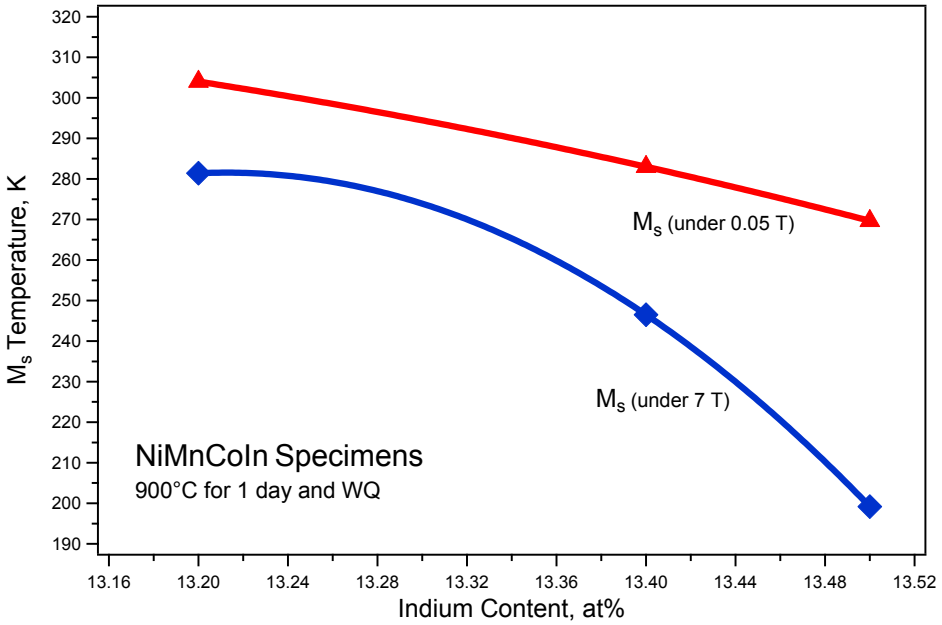

Figure 4-6) Ms Temperatures of Ni-Co-Mn-In specimens as a function of In content under 0.05 T and 7 T.

Ni-Co-Mn-In alloys were investigated at various different In concentrations. In-13.4 sample was selected for further investigation due to the most convenient metamagnetic transition behavior among the three samples with its (1) highest ΔM (2)

considerably low T_{hys}. Effect of annealing on the homogenized $Ni_{45}Co_5Mn_{36.6}In_{13.4}$ single crystal alloy will be discussed next.

4.2 Effect of Cooling Rate on Martensitic Transformation of $Ni_{45}Co_5Mn_{36.6}In_{13.4}$ Single Crystals

Homogenization of three $Ni_{45}Co_5Mn_{36.6}In_{13.4}$ single crystal alloys at 900°C for 1 day was followed by quenching one of them in iced water, quenching one of the others in oil, and cooling the last one in the homogenization furnace with an average cooling rate of 100K/hour. Thermomagnetization curves of the water quenched (WQ) sample in the fields of 0.05T, 1T and 7T was already shown in Figure 4-1. Thermomagnetization curves of the oil quenched (OQ) and furnace cooled (FC) samples in the same magnetic field strengths as the WQ sample are displayed in the Figures 4-7 and 4-8, respectively. MT temperatures of WQ and OQ samples for each magnetic field can be determined since they exhibit the expected metamagnetic phase transition. However, the FC sample did not undergo MT under 7T which is associated with the KA behavior suppressing it's` transformation to the martensite phase.

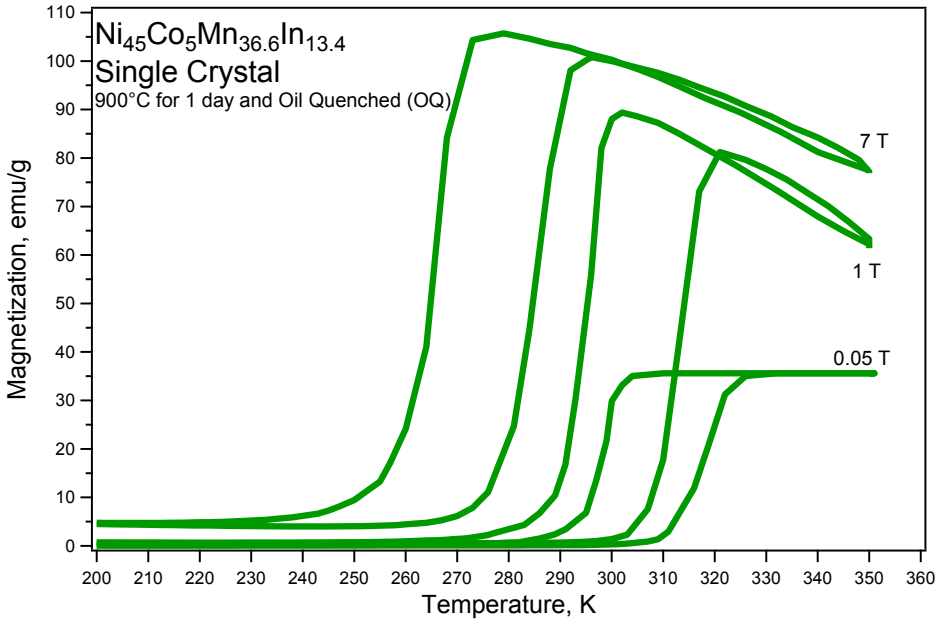

Figure 4-7) Thermomagnetization curves of $Ni_{45}Co_5Mn_{36.6}In_{13.4}$ single crystal which was quenched in oil after homogenization at 900°C for 1 day. Magnetization measurements were performed under 0.05T, 1T and 7T.

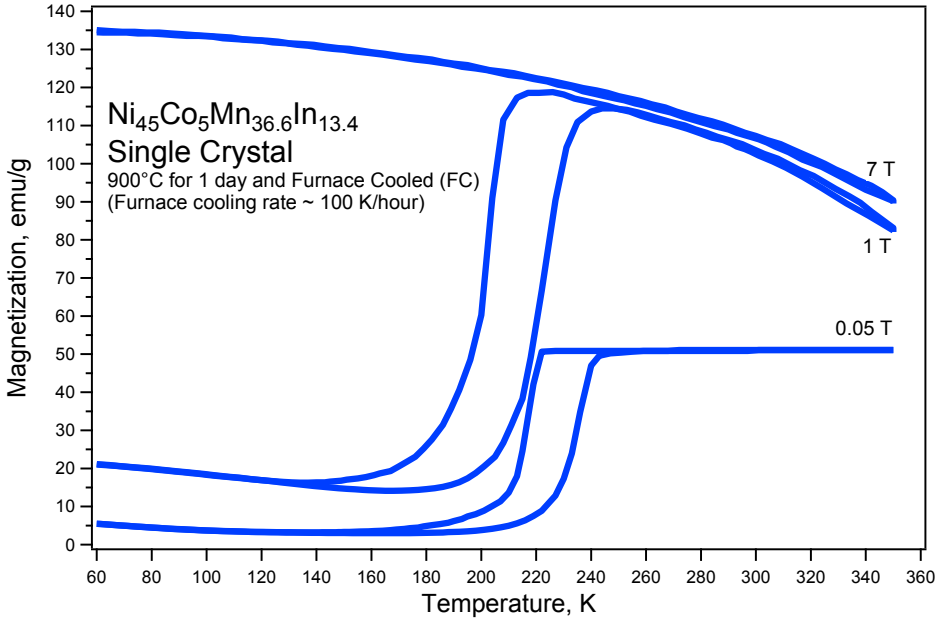

Figure 4-8) Thermomagnetization curves of $Ni_{45}Co_5Mn_{36.6}In_{13.4}$ single crystal which was furnace cooled after homogenization at 900°C for 1 day. Magnetization measurements were performed under 0.05T, 1T and 7T.

FC sample was again tested by a full magnetization-temperature scan in the fields of 0.05T, 1T, 3T, 5T, and 7T, to specify the transformation behavior in the intermediate field strengths. As indicated in Figure 4-9, second attempt measurement of the FC sample led to a less sharp MT in the fields of 0.05T and 1T than those in the first attempt. This might be due to changes in the spin structure of the material that further improves the suppression of MT. The details of this behavior are still under discussion. The thermomagnetization curve under 3T in Figure 4-9 shows that the sample hardly transforms and it is a mixture of two phases at low temperatures in which the major volume is still austenite. 5T magnetic field completely suppresses the transformation like the magnetic field of 7T.

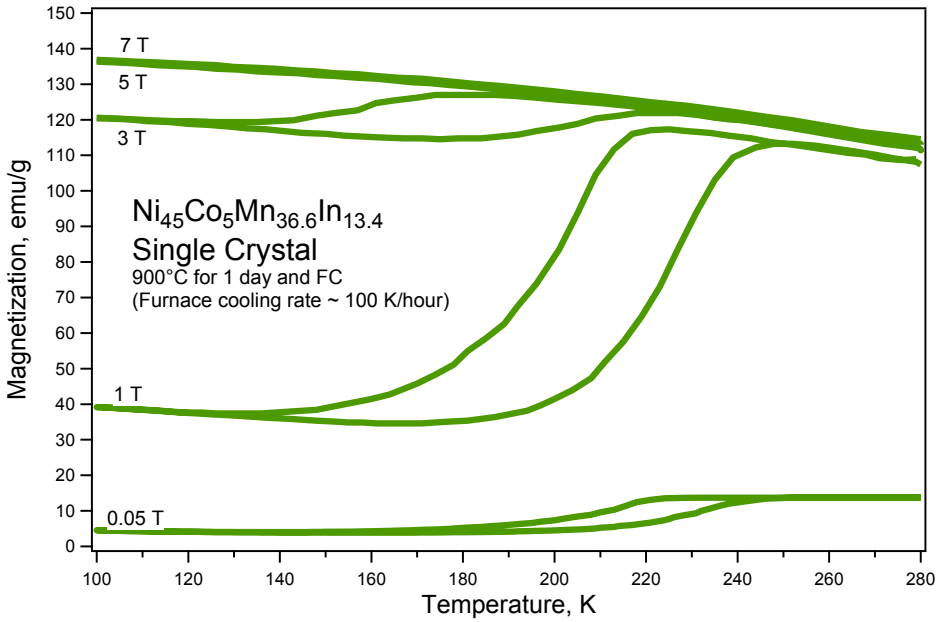

Figure 4-9) Thermomagnetization curves of $Ni_{45}Co_5Mn_{36.6}In_{13.4}$ single crystal which was furnace cooled after homogenization at 900°C for 1 day. Magnetization measurements were performed under 0.05T, 1T, 3T, 5T and 7T.

Magnetic field dependence of the M_s Temperatures of the OQ, WQ and FC samples are shown in Figure 4-10, which the data points were extracted from the thermomagnetization curves. dM_s/dH for each sample was determined from the slopes of the linear fits. The WQ and OQ samples have similar dM_s/dH values, -5.5K/T and -5.3K/T respectively. On the other hand, the slope of the FC sample is fairly larger than the other the slopes of the other samples. dM_s/dH of about -14.5K/T which was attained from the FC sample is also larger than those of the single crystal $Ni_{45}Co_5Mn_{36.5}In_{13.5}$ alloy with -12.6K/T [5], and the annealed $Ni_{45}Co_5Mn_{36.6}In_{13.4}$ single crystal at 500°C (A-5) with -9.9K/T. It is revealed from this value that the application of 1T field reduces M_s about 15K. The large values of dM_s/dH may allow us to control the MT over a wide temperature range by applying even low magnetic field strengths.

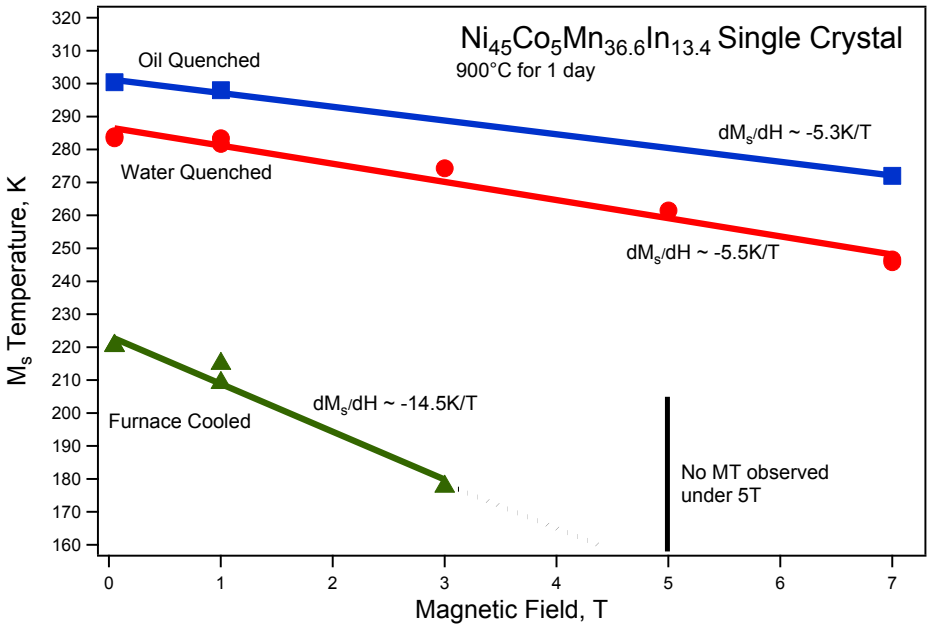

Figure 4-10) Ms Temperatures of water quenched, oil quenched and furnace cooled specimens of $Ni_{45}Co_5Mn_{36.6}In_{13.4}$ single crystals as a function of magnetic field. The data points were extracted from the thermomagnetization curves.

It has been verified as a consequence of numerous experimental efforts on Ni-Co-Mn-In single crystal alloys, particularly the composition of $Ni_{45}Co_5Mn_{36.6}In_{13.4}$ that the magnetic properties of this alloy system such as MT temperatures, M_{sat} and T_c can extensively be controlled by annealing, varying In concentration, and cooling rate.

4.3 Effect of Annealing Temperature on Martensitic Transformation of $Ni_{45}Co_5Mn_{36.6}In_{13.4}$ Single Crystals

Several $Ni_{45}Co_5Mn_{36.6}In_{13.4}$ single crystals that were homogenized at 900°C for 1 day followed by water quenching are subjected to post-annealing at temperatures of 400°C, 500°C, 600°C, 700°C and 800°C. The samples are denoted by A-4, A-5, A-6 A-7 and A-8 as the leftmost digit of their annealing temperatures. Also, the solution heat treated sample at 900°C is denoted by A-9. Annealing time was determined to be 3 hours by numerous trials throughout the research where Chen et. al [73] used 3 hours of annealing as well, at different annealing temperatures. Figures 4-11 and 4-12 show the selected thermomagnetization curves of the $Ni_{45}Co_5Mn_{36.6}In_{13.4}$ single crystals obtained from the samples A-5 and A-7, respectively. It was not observed any metamagnetic shape memory behavior in the sample A-4, while the others showed the characteristic behavior of MMSMAs. Once Figure 4-11 and 4-12 are compared in terms of magnetization behavior, it is shown that MT occurs in the fields of 0.05T and 1T in the samples A-5 and A-7 as expected. However, the sample A-5 in Figure 4-11 does not completely transform to martensite in the field of 7T and austenite-martensite mixture remains at low temperatures, which is attributed to the KA behavior. Further magnetic

field could be applied o determine whether the MT is thoroughly interrupted and the sample is in austenite in the full temperature range. Nevertheless, it was not achieved because the instrument used for magnetization measurements – SQUID – was restricted to apply a maximum magnetic field of 7 T. KA behavior was not observed in the samples A-6, A-7, A-8 and A-9 (Figure 4-1) upon application of high magnetic fields.

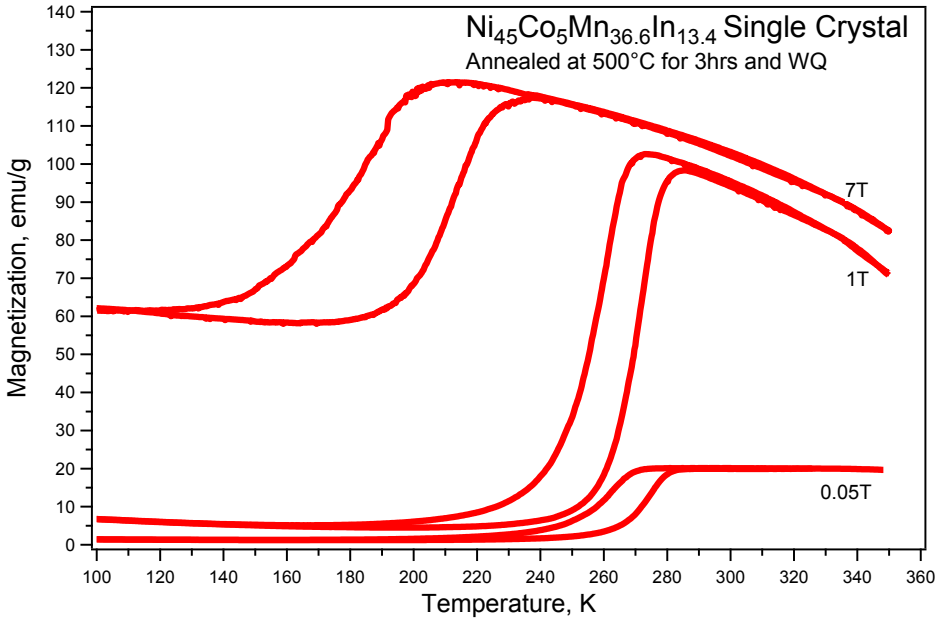

Figure 4-11) Thermomagnetization curves of $Ni_{45}Co_5Mn_{36.6}In_{13.4}$ single crystal annealed at 500°C. Measurements under 0.05T, 1T and 7T are indicated.

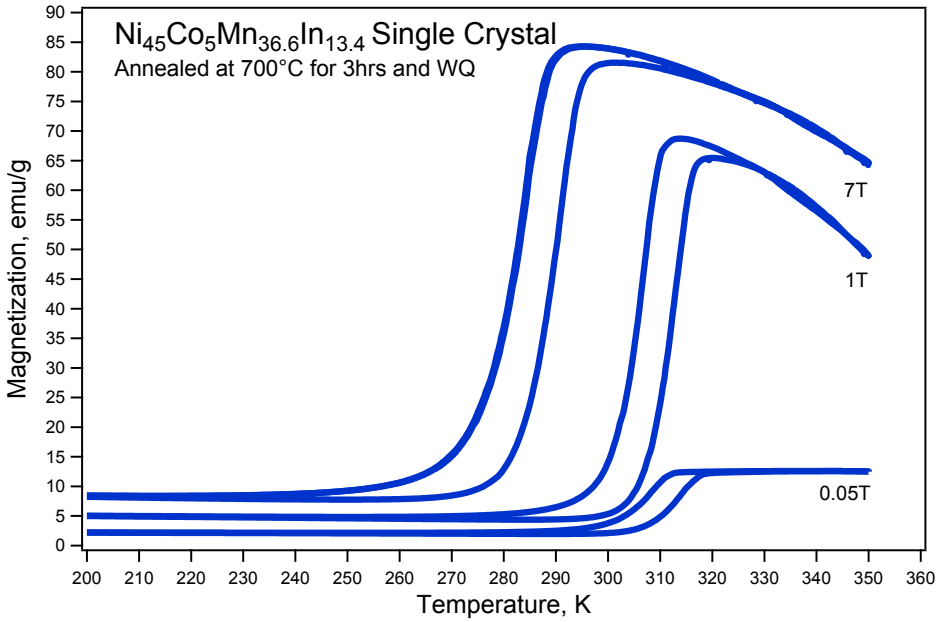

Figure 4-12) Thermomagnetization curves of $Ni_{45}Co_5Mn_{36.6}In_{13.4}$ single crystal annealed at 700°C. Measurements under 0.05T, 1T and 7T are indicated.

Figures 4-13 and 4-14 display the thermomagnetization curves of the current samples measured under the field of 0.05T and 7T, respectively. It is obvious from Figure 4-13 that the MT temperatures of all the samples except A-4 can be detected as demonstrated in Figure 2-10 on page 27. MT temperatures tend to increase by increasing annealing temperature, while there is not a regular trend in M_{sat}. Increasing trend of MT temperatures in the field of 7T by annealing temperature is shown in Figure 4-14, but there is again no indication of MT in the sample A-4.

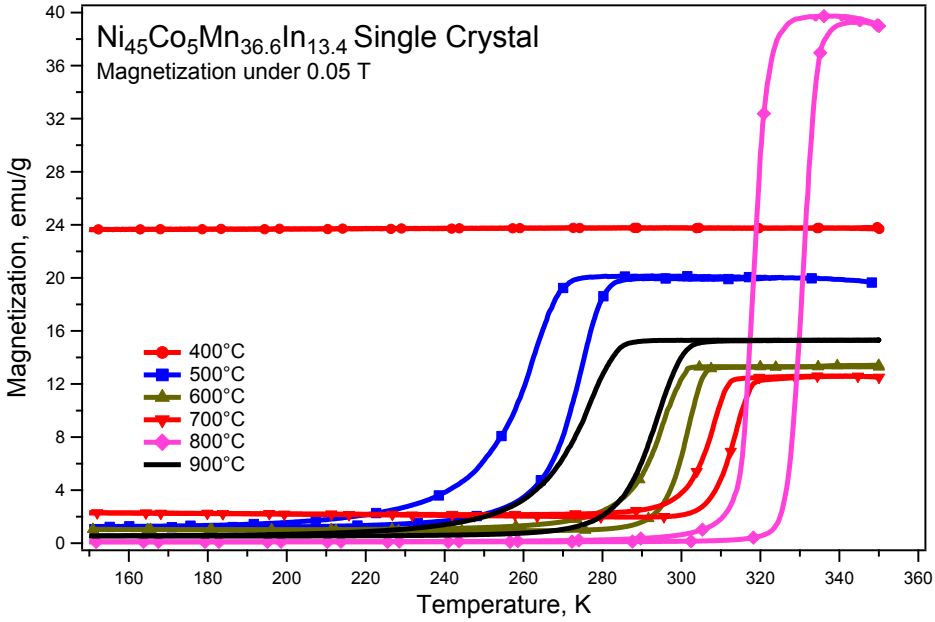

Figure 4-13) Thermomagnetization curves of $Ni_{45}Co_5Mn_{36.6}In_{13.4}$ single crystals annealed at temperatures of 400°C, 500°C, 600°C, 700°C, 800°C and 900°C. Measurements under 0.05T are indicated.

It is seen from the thermomagnetization measurements that the samples A-6 through A-9 successfully show metamagnetic phase transition. It is worth discussing the interruptions to MT in the samples A-4 and A-5. Matrix conditions and magnetic properties of an alloy are strongly dependent on how it was processed; annealing can lead to the changes in the microstructure or the crystal structure [74]. Hence, two possible reasons underlying the abnormal behavior of these two samples are: the presence of second phase precipitates in the matrix, and atomic order-disorder transformation during annealing. Annealed samples have been intended to conduct transmission electron microscopy (TEM) experiments to detect the possible formation of second phase precipitates in each sample matrix. However, no results have been received

so far since the brittleness problem made the sample preparation troublesome. More attempts are being made to overcome this issue for further analysis.

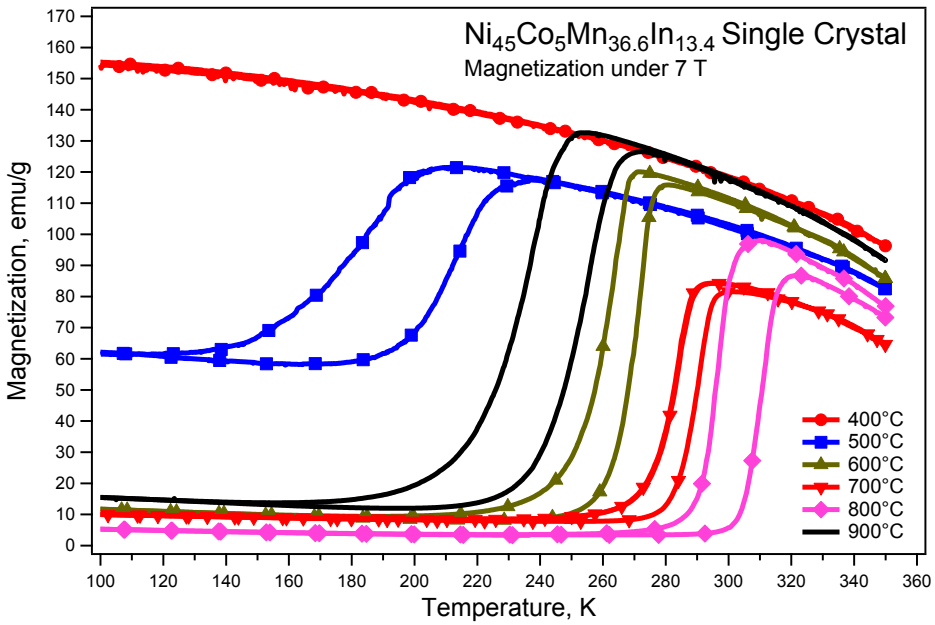

Figure 4-14) Thermomagnetization curves of $Ni_{45}Co_5Mn_{36.6}In_{13.4}$ single crystals annealed at temperatures of 400°C, 500°C, 600°C, 700°C, 800°C and 900°C. Measurements under 7T are indicated.

XRD experiments were conducted to determine whether there is an order-disorder transformation. Figure 4-15 shows the XRD patterns of the samples A-4 and A-9. Detected intensity peaks of the sample A-9 is correspondent to the calculated diffraction patterns of the ordered $L2_1$ structure. Since no peak was detected except (022) reflection, atomic ordering in the sample A-4 could not be determined. Although XRD experiments are still in progress, it can be estimated from the current results that the samples A-6 through A-9 have ordered $L2_1$ structure. Meanwhile, atomic ordering of the sample A-4 does not correspond to any defined atomic structure of Ni-Mn-based

MMSMAs in their austenite phase. The atomic structure of the sample A-5 possibly does not have a high degree of order as in the sample A-6 through A-9. We claim that the annealing temperature of 500°C may change the order of the sample A-5 to a low degree: B_2 structure, or coexistence of B_2 and $L2_1$ structures provided there is a heterogeneous stoichiometry. It is also claimed that increasing annealing time, e.g. 6 hours, may change the degree of order in the samples A-4 and A-5, and the interruptions to MT in these samples may be prevented. More accurate information about the atomic order of this sample will be attained after the XRD experiments.

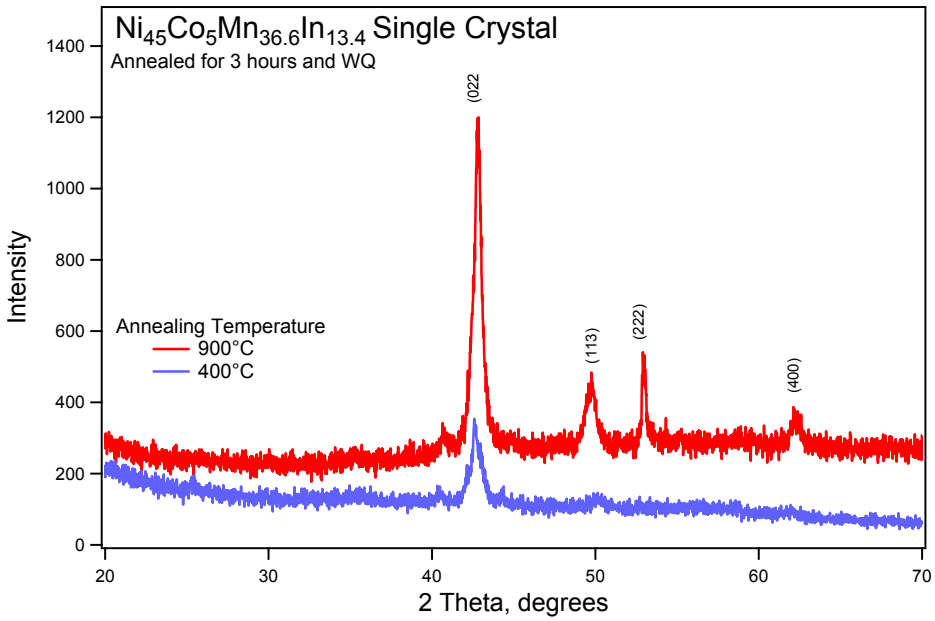

Figure 4-15) X-Ray Diffraction pattern of $Ni_{45}Co_5Mn_{36.6}In_{13.4}$ single crystal: the figure shows the results obtained from the samples which were annealed at 400°C and 900°C.

Figure 4-16 shows the M_s temperatures of the annealed samples as a function of magnetic field which all data points were extracted from the thermomagnetization

curves. Slopes of the linear fits, $m=dM_s/dH$, indicate the magnetic field dependence of the M_s temperatures for each sample. Annealing temperature does have an inverse relationship with dM_s/dH, except the sample A-9. dM_s/dH of -5.5K/T obtained from the sample A-9 is very small compared to $Ni_{45}Co_5Mn_{36.5}In_{13.5}$ single crystal processed at the same conditions where dM_s/dH is -12.6K/T reported by Karaca et. al [5]. Similarly, it is shown in Figure 4-6 that the In-13.5 sample has a larger drop in the M_s temperature by increasing magnetic field than that of In-13.4 sample. The maximum dM_s/dH of about -9.9K/T was achieved in the sample A-5 which is comparable to -12.6K/T in Reference 5.

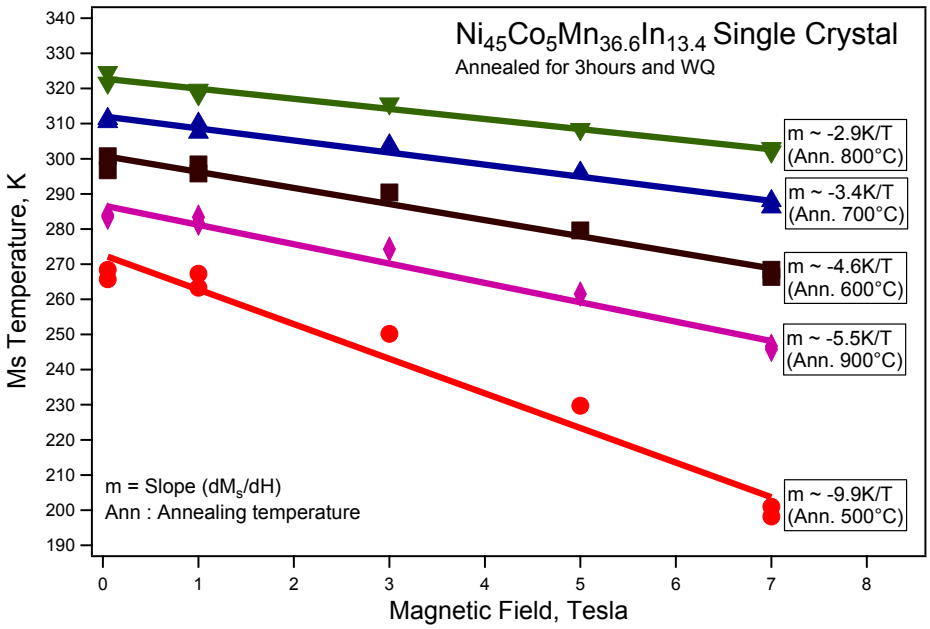

Figure 4-16) M_s temperatures of $Ni_{45}Co_5Mn_{36.6}In_{13.4}$ single crystals as a function of magnetic field. Annealing temperatures are shown in the figure.

Figure 4-17 indicates the variation in the M_s as a function of the annealing temperature in the fields of 0.05T and 7T. M_s in both 0.05T and 7T curves increase with the annealing temperature, and reach a maximum at 740°C. It can be claimed that

annealing at temperatures between 720°C and 800°C maximizes the temperature at which MT starts. Both the curves were extrapolated to the leftwards and MT did not occur at 400°C.

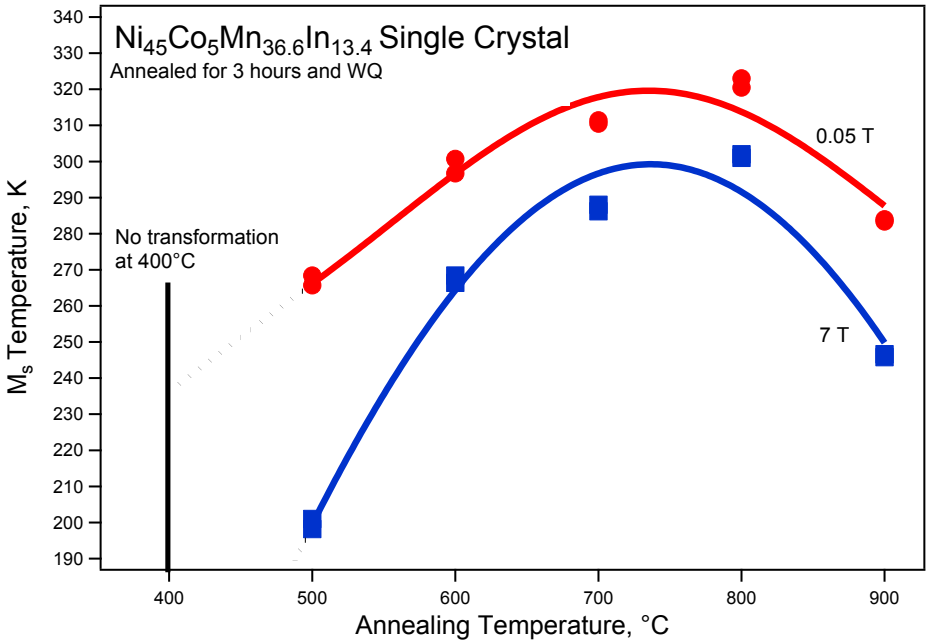

Figure 4-17) Martensitic transformation start temperatures of $Ni_{45}Co_5Mn_{36.6}In_{13.4}$ single crystals as a function of annealing temperature.

Single crystal $Ni_{45}Co_5Mn_{36.6}In_{13.4}$ samples were annealing at different temperatures, and MT and metamagnetic shape memory behavior were examined. It was confirmed that annealing has a significant influence on the MT temperatures. A small change in the processing of the alloy considerably changed the MT temperatures and M_{sat} values. Consequently, $Ni_{45}Co_5Mn_{36.6}In_{13.4}$ single crystals are prominent alloys that can be utilized in applications in a wide operating temperature range. However, brittleness is a real issue that needs to be solved. It can be pronounced that this problem

may be overcome by changing the cooling rate after annealing. In section 4.3, the homogenized samples will be cooled at different media and the results will be discussed.

5. MAGNETO-THERMO-MECHANICAL ANALYSIS AND MAGNETOCALORIC EFFECT IN Ni-Co-Mn-Sn POLYCRYSTALLINE ALLOYS

Ni-Co-Mn-Sn MMSMAs in polycrystalline form are investigated in this section. Several features of this alloy system which are similar to the other Ni-Mn-based alloys such as magnetic properties and MT [9, 20, 75-78], magnetocaloric effect [62, 79-81] and KA behavior of MT [65] have been reported. Although several attempts have been made to examine the magnetic properties of Ni-Co-Mn-Sn alloy system, there is not a detailed study on the thermomechanical properties coupled with the magnetism that have been reported up to date, except Ito et. at [82]. Ito et. al investigated the mechanical and shape memory properties of polycrystalline $Ni_{43}Co_7Mn_{39}Sn_{11}$ alloy fabricated by pressureless sintering. With enhanced ductility, improved fracture strain and magnetic shape memory effect this composition of Ni-Co-Mn-Sn alloy system has been found highly interesting for further research. Additionally, applicability, convenience and low cost of this fabrication technique gave us more motivation. Magnetic and thermomechcanical response of pressureless sintered $Ni_{43}Co_7Mn_{39}Sn_{11}$ polycrstalline alloys are studied in Section 5.1.

5.1 Magneto-Thermo-Mechanical Characterization of Polycrystalline $Ni_{43}Co_7Mn_{39}Sn_{11}$ Magnetic Shape Memory Alloys

Figure 5-1a shows the room temperature optical image of the $Ni_{43}Co_7Mn_{39}Sn_{11}$ polycrystalline alloy which was sintered for two days. The image shows porous regions

(dark spots mainly at triple junctions), twinned martensite grains and austenite grains. The volume fraction of the pores of the present alloy was determined to be about 6.5%. Ito et.al reported that the pores help to improve ductility and fracture strain in these alloys [82]. Pore shape is also an important factor for improved ductility. Ito et.al verified that the pressureless sintered polycrystalline $Ni_{43}Co_7Mn_{39}Sn_{11}$alloys sintered for six days in Figure 5-1b include more spherical pores that weaken the stress concentrations at the grain boundaries, than those sintered for shorter time periods [82]. Existence of more spherical pores is evident in the figure.

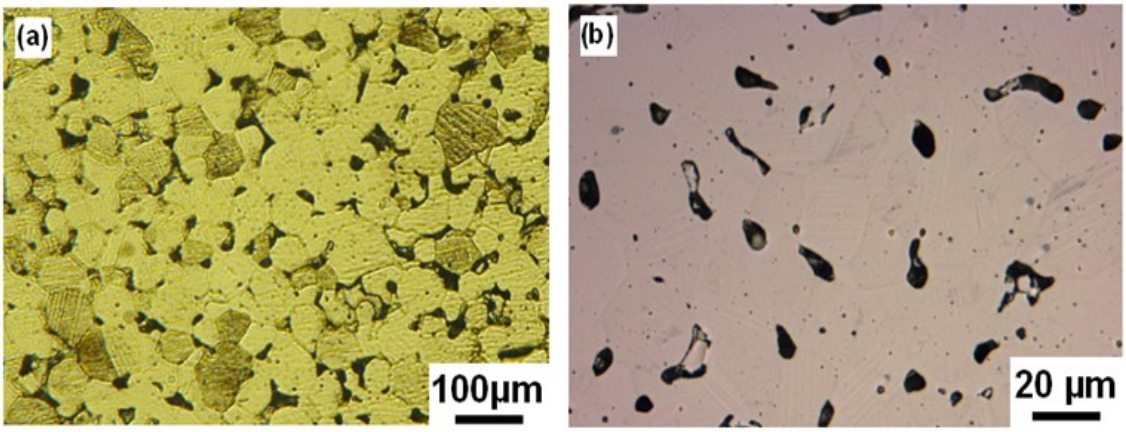

Figure 5-1) Room temperature optical images of $Ni_{43}Co_7Mn_{39}Sn_{11}$ polycrystalline alloys sintered at 900°C for a) 2 days and b) 6 days, and they were quenched in iced water [82].

As a first stage to analyze the magneto-thermo-mechanical response of the present samples, isobaric thermal cycling experiments were conducted. Figure 5-2 demonstrates the strain vs. temperature response of the 6-day sintered sample under various compressive stress levels. In these tests, the specimens were heated up to 413K to obtain the austenite phase and compressive stress was applied in austenite. Then the

samples were thermally cycled between 413 and 233K. Starting with 10 MPa, the compressive stress level was increased with an increment of 25MPa after each thermal cycle, up to 175MPa. The thermal cycles that were performed under 75MPa, 150MPa are not shown in the figure to avoid a complicated image. Since the transformation strain almost saturated at 175MPa (Figure 5-2), we did not want to fail the samples by increasing the stress level to conduct further experiments. The amount of compressive strain during cooling increases due to the martensitic phase transformation as the stress is leveled up. The higher the stress is applied, the higher strain is obtained. Figure 5-2 depicts the maximum strain is as high as 3.6% (3.2% is the recoverable transformation strain) which is the highest strain level reported so far in polycrystalline metamagnetic shape memory alloys (MMSMAs),except NiCoMnAl polycrystals that were fabricated by conventional ingot metallurgy where ε_{tr} is 3.53% under 175MPa [83]. This very high level of transformation strain can be originated from the texture of the samples since it is not expected to reach this strain level in a randomly oriented polycrystalline Ni-Mn-X(Sn,In,Sb) or Ni-Co-Mn-X alloys from our past experiences. It can be stated that there is a preferred orientation of grains in the present alloy rather than having a random orientation.

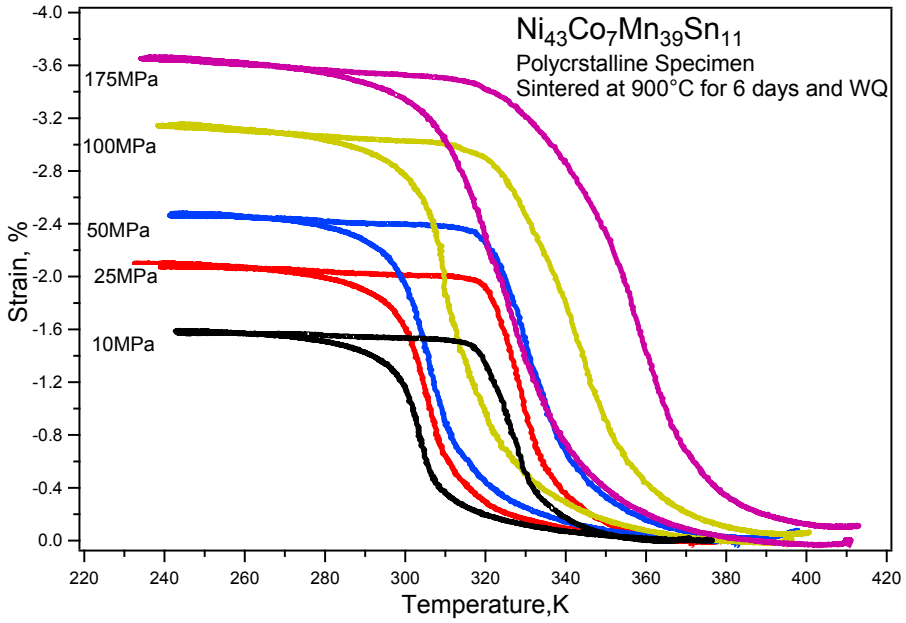

Figure 5-2) Constant stress cooling-heating response of the $Ni_{43}Co_7Mn_{39}Sn_{11}$ polycrystalline alloy which was sintered for 6 days across temperature interval through the martensitic transformation.

The four characteristic temperature of the MT were determined from the thermal cycling curves as shown in Figure 5-3. Recoverable transformation strain (ε_{tr}), irrecoverable strain (ε_{irr}), and temperature hysteresis (T_{hys}) are also defined in this curve. It is shown that there is a measurable irrecoverable strain in the heating-cooling cycles under 75MPa and over. ε_{irr} is determined at A_f+30K as shown in Figure 5-3. Figure 5-3 also shows how A_s, A_f, M_s, M_f, T_{hys}, ε_{tr} and ε_{irr} were determined from the constant stress heating-cooling experiments.

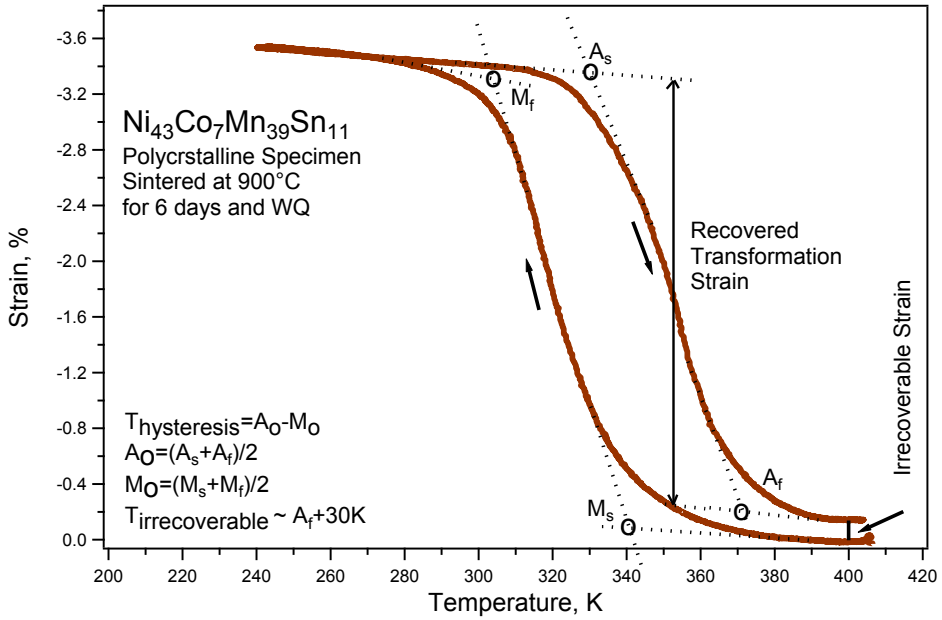

Figure 5-3) Illustrates how relevant transformation temperatures, hysteresis and strain levels were determined on a representative constant stress (150MPa) heating-cooling experiment.

ε_{tr}, ε_{irr}, and T_{hys} values of the 6-day sintered sample at different stress levels were plotted, and the general trends of each of these parameters were shown by least square fits in Figure 5-4. It is apparent that the ε_{tr} and ε_{irr} are directly related to the applied stress. ε_{tr} increases with the increasing stress and almost reaches the saturation value at high stress levels. Two data points for ε_{tr} are marked by the arrows in Figure 5-4 were obtained from the experiments under 10MPa and 50MPa after a series of tests to 175MPa. These measurements led to higher ε_{tr} due to the training effect. Since ε_{irr} is almost zero under 10MPa and 50MPa, the effect of training on ε_{irr} was not possible to determine. T_{hys} increases with applied stress similar to ε_{tr}. T_{hys} also increases with stress in Ni-Co-Mn-Al polycrystalline alloys at much larger values [84]. The increase in T_{hys} is typical for SMAs with microstructures (crystal structure, crystallographic

orientation/texture) which are prone to plastic dissipation mechanisms [5]. In a similar material, Ni-Co-Mn-In in single crystalline form oriented along the (100) direction, Karaca et.al [5] observed a reduction in T_{hys} with stress, although orientations like (123) demonstrated an opposite behavior. This may indicate that the present alloy may have a texture differing from perfect (100) texture. The two arrows on the thermal hysteresis plot point out positive influence of training on T_{hys}.

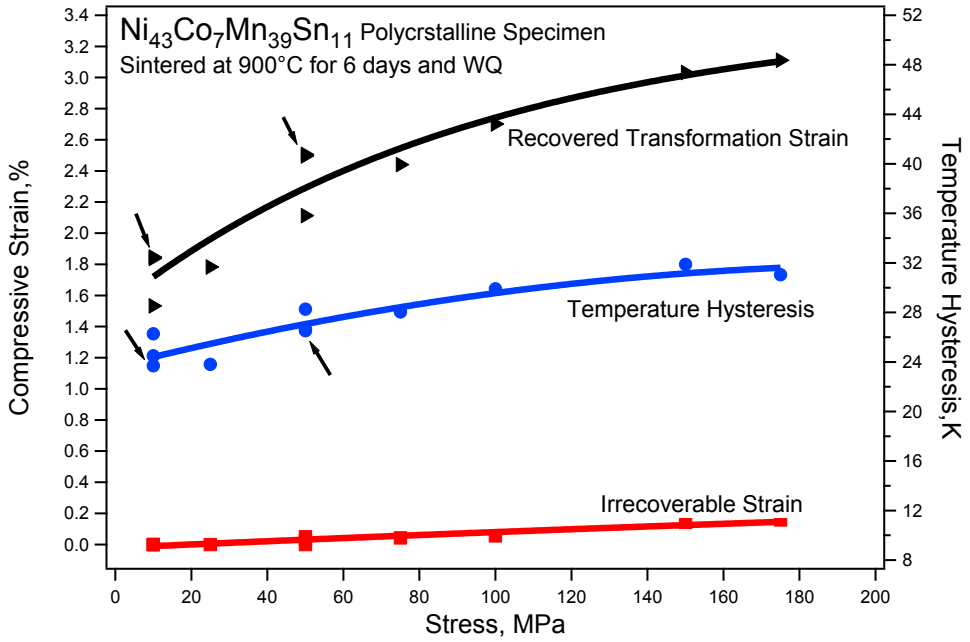

Figure 5-4) Recovered transformation strain and the irrecoverable strain levels for $Ni_{43}Co_7Mn_{39}Sn_{11}$ polycrystalline alloy as a function of compressive stress. Temperature hysteresis values that were determined from the constant stress heating-cooling experiments are also shown as a function of stress.

Figure 5-5 shows cooling-heating cycles of the 2-day sintered sample under various compressive stress levels from 10MPa to 100MPa. It was aimed to conduct the thermal cycling experiments of this sample under the same stress levels as those in

Figure 5-2. However, we did not go further 100MPa due to the possibility of crack formation during the experiment. The methods in Figure 5-3 were employed to determine the MT temperatures, ε_{tr}, ε_{irr}, and T_{hys} of the 2-day sintered sample. In this sample, ε_{tr} at 100MPa was found to be small compared to the ε_{tr} determined from the 6-day sample under the same stress level. However, T_{hys} of the 2-day sample for each stress level was measured to be lower than that of the 6-day sample.

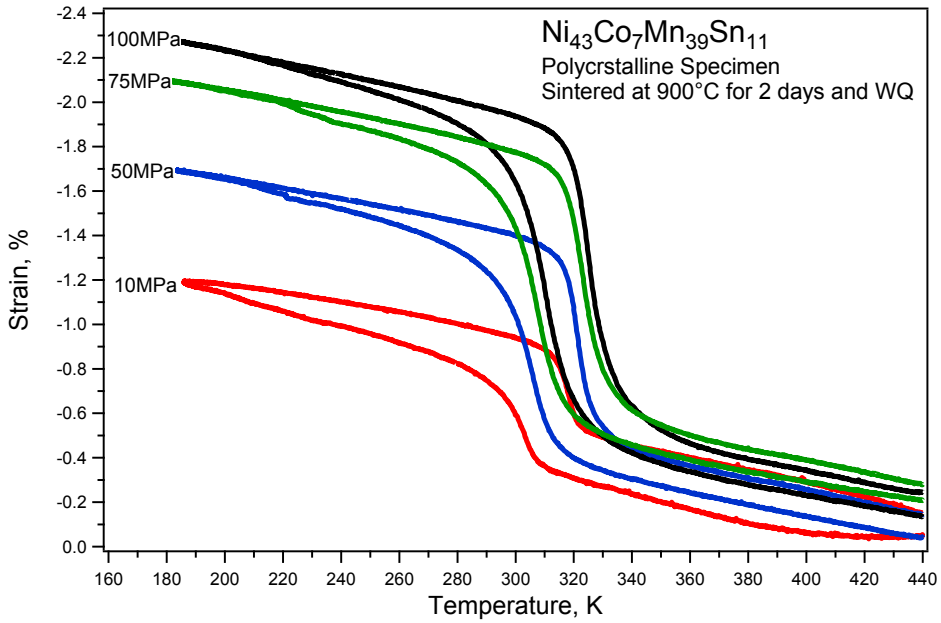

Figure 5-5) Constant stress cooling-heating response of the $Ni_{43}Co_7Mn_{39}Sn_{11}$ polycrystalline alloy which was sintered for 2 days across temperature interval through the martensitic transformation.

ε_{tr} and ε_{irr}, obtained from the thermal cycling experiments of 2- and 6-day sintered samples are compared in Figures 5-6. It is seen from this figure that ε_{tr} increases by stress for both samples while ε_{tr} is enhanced in the 6-day sintered sample by about 1% for each stress level. On the other hand, ε_{irr} in the samples show different behaviors:

ε_{irr} of the 6-day sintered sample increases when the applied stress is more than 50MPa, while it is almost constant up to 100MPa in the 2-day sintered sample. This constant ε_{irr} can be claimed as a weird behavior that is attributed to an error occurred during the experiment.

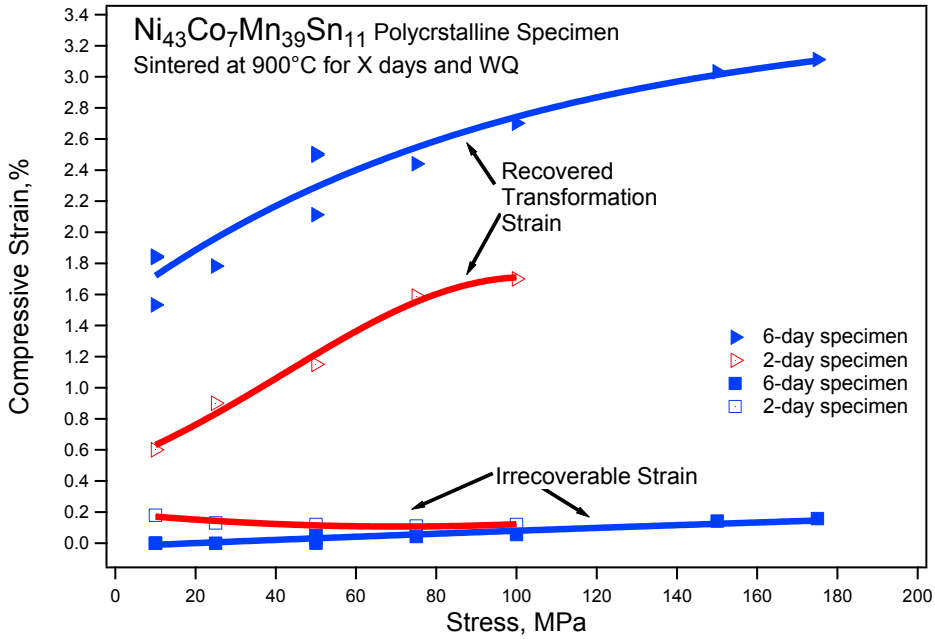

Figure 5-6) Recovered transformation strain and the irrecoverable strain levels for $Ni_{43}Co_7Mn_{39}Sn_{11}$ polycrystalline alloy for both 2- and 6-day sintered samples as a function of compressive stress.

Figure 5-7 indicates the difference between the T_{hys} of the 2- and 6-day sintered samples that were extracted from the thermal cycling tests in the Figures 5-5 and 5-2, respectively. The trends are shown by the least square fits: T_{hys} of the 2- day sintered sample is decreasing by stress whereas an adverse effect is seen in the 6-day sintered sample. Also, the difference between the T_{hys} values of the samples further increases for each consecutive stress level. Decreasing trend in the T_{hys} of the 2-day sintered sample

with respect to stress is similar to that of Ni-Co-Mn-In single crystal [5]. But, the T_{hys} values obtained from the current sample are much less than the values obtained from the Ni-Co-Mn-In single crystal for the corresponding stress values, e.g. 16K for the current sample under 100MPa while it is about 70K in the Ni-Co-Mn-In sample in Ref.5.

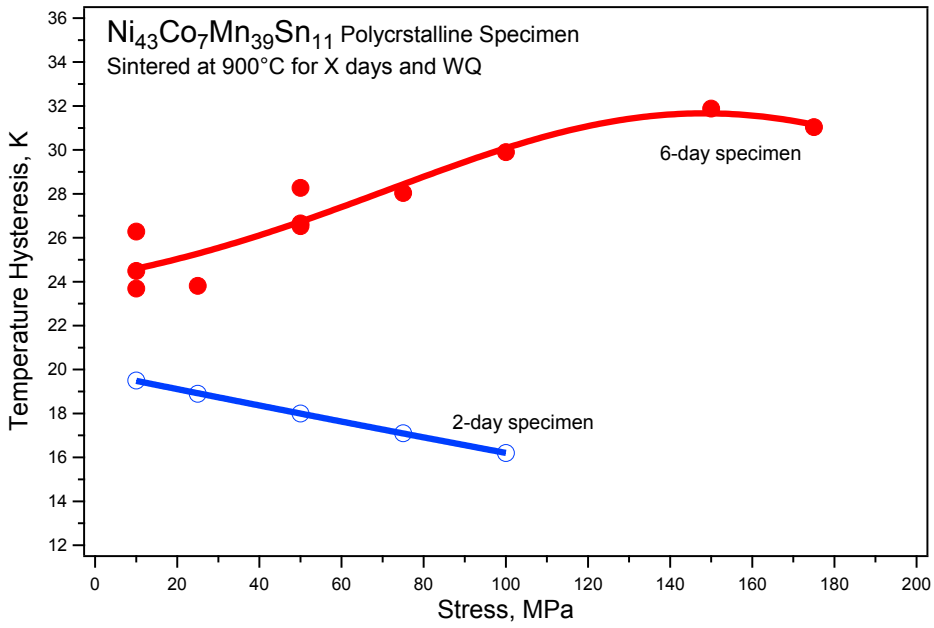

Figure 5-7) Temperature hysteresis values that were determined from the constant stress heating-cooling experiments for 2- and 6-day sintered samples as a function of stress.

Second stage of magneto-thermo-mechanical characterization was superelasticity experiments. Figure 5-8 and 5-9 depict the superelastic response of $Ni_{43}Co_7Mn_{39}Sn_{11}$ polycrystalline specimens which were sintered for 6- and 2-day, respectively. Operating temperature of the tests was set by 343K that is just above the A_f temperature. As shown in Figure 5-8, the 6-day sintered specimen was loaded up to reach 3% strain and unloaded. The specimen had been undergone to 1% and 2% strain loadings prior to the 3% loading experiments, but they are not shown here. 3% loading experiment was

repeated four times to confirm the stability of the superelastic response and to find out the strength level that can be achieved. The specimen showed minor reduction in the strength level. The superelastic responses of the second, third, and the fourth cycles were almost the same, and the curves showed minor differences. Consequently, the sample showed almost perfect superelastic (SE) response with a fully recovered strain in all the experiments. NiCoMnAl polycrystals [83] and the present alloy are the only examples of nearly perfect superelastic response which have been reported so far in polycrystalline MMSMAs. The critical Stress, σ_c for the onset of stress-induced martensitic transformation is found to be around 120MPa in Figure 5-8.

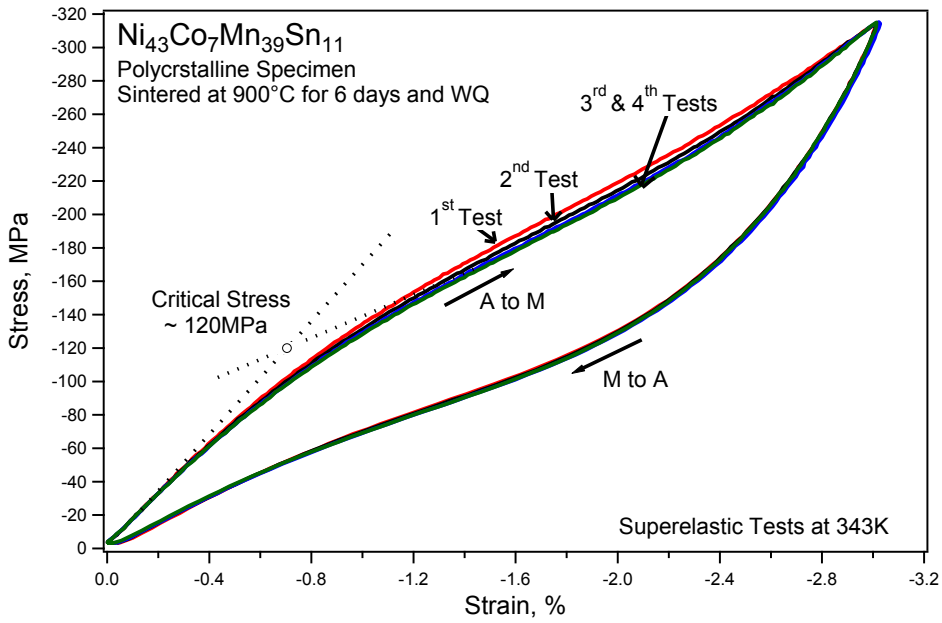

Figure 5-8) Superelastic tests of 6-day sintered $Ni_{43}Co_7Mn_{39}Sn_{11}$ polycrystalline alloy up to a strain level of 3% at 343K.

Despite the perfect SE in the 6-day sintered sample without ε_{irr}, the 2-day sintered sample did not show the same behavior as shown in Figure 5-9. At first glance, the specimen was loaded up to 1% strain and was unloaded. Then, the strain level was increased to 2% which resulted in ε_{irr} at the end of the test. The specimen was heated up to 423K and cooled back down to 343K for recovery. 2% loading-unloading cycle was again performed to possibly eliminate the ε_{irr}, but the result did not change. The heating-cooling process was performed before each test. At the final step, the specimen was loaded up to a 3% strain and unloaded. The specimen was broken during the second attempt of loading of 3% strain. Consequently, SE was not obtained from the 2-day sintered specimen.

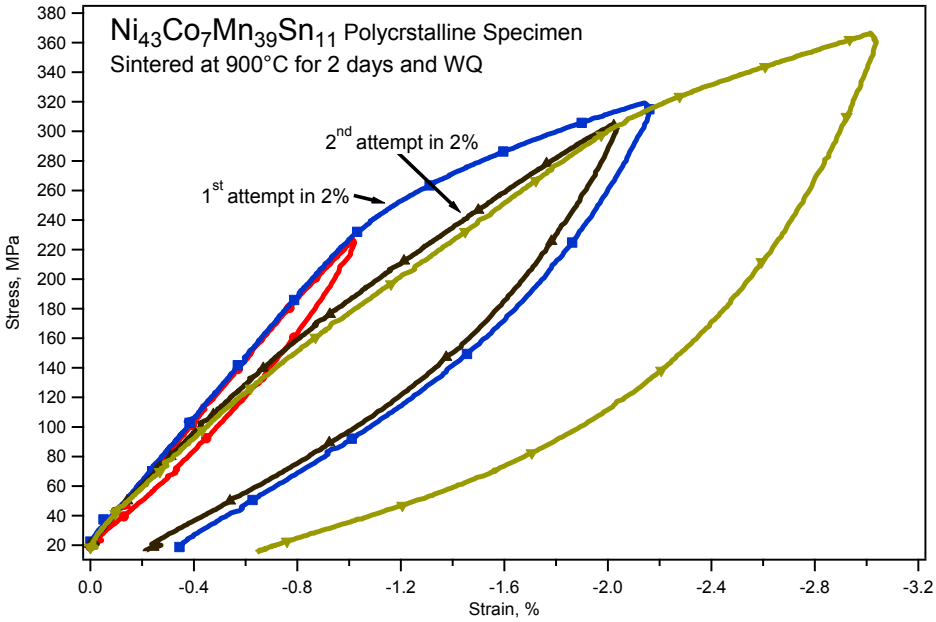

Figure 5-9) Superelastic tests of 2-day sintered $Ni_{43}Co_7Mn_{39}Sn_{11}$ polycrystalline alloy with the strain levels of 1%, 2% and 3% at 343K.

Third stage of the magneto-thermo-mechanical characterization was the magnetization response. The 6-day sintered sample was selected for magnetization measurements since it gave better mechanical test results and more reliable for further research. Figure 5-10 shows the thermo-magnetization curves of the 6-day sintered sample at the magnetic fields of 0.05T and 7T, which were selected from the results at 0.05T, 1T, 3T, 5Tand 7T. Similar to the single $Ni_{45}Co_5Mn_{36.6}In_{13.4}$ discussed in the previous section, and the other MMSMAs, metamagnetic phase transformation occurs from ferromagnetic austenite to paramagnetic martensite as seen in the figures. Also, the application of magnetic field reduced the transformation temperatures.

The forward and the reverse martensitic transformation temperatures are determined from the thermomagnetization curve as illustrated for the 0.05T curve in Figure 5-10. The transformation temperatures determined under zero stress are M_s = 313K, M_f = 295K, A_s= 316K and A_f = 328K. The magnetic field dependence of the M_s and A_s temperatures are given in Figure 5-11. They linearly decrease with the applied magnetic field. The linear fits are almost parallel to each other and the slope ($\Delta T/\Delta H$) was found to be about -4.4K/Tesla**,** which is comparable to those of the arc-melted [9] and spark plasma sintered [75] $Ni_{43}Co_7Mn_{39}Sn_{11}$ polycrystalline alloys where the slopes are around -4K/Tesla, and -5K/Tesla respectively. Also, saturation magnetization level of the present alloy is similar to the ones that were arc-melted and spark plasma sintered polycrystalline alloys [9, 75].

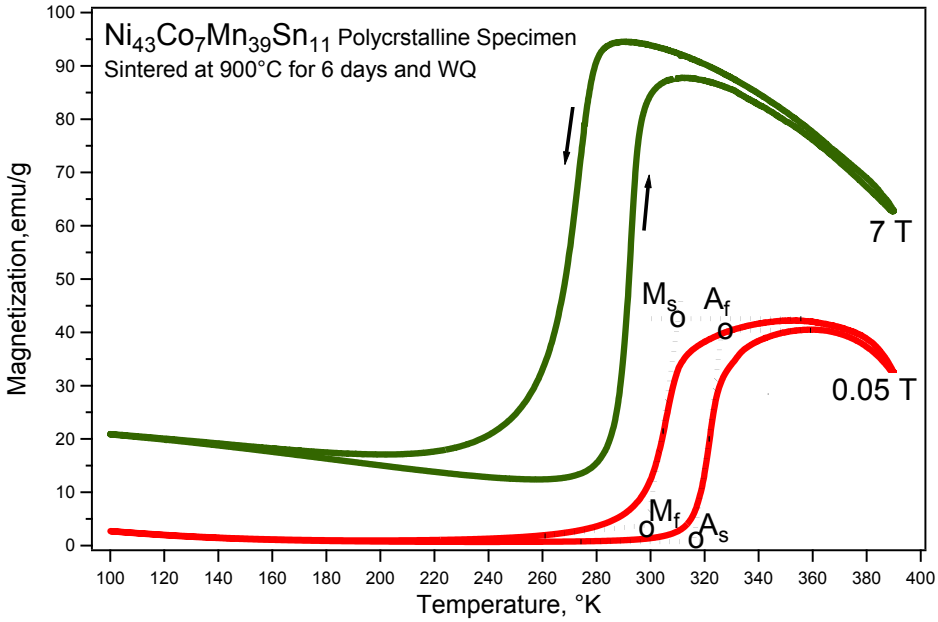

Figure 5-10) Thermomagnetization curves of 6-day sintered $Ni_{43}Co_7Mn_{39}Sn_{11}$ polycrystalline alloy under magnetic fields of 0.05T and 7T. Martensitic transformation temperatures are determined from the magnetization curves as shown for the response under 0.05T.

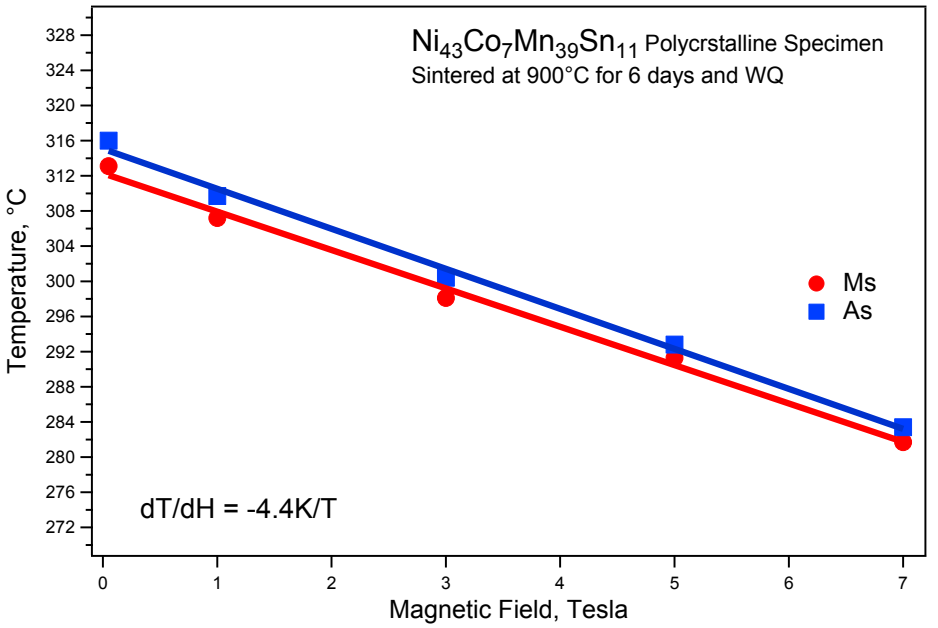

Figure 5-11) Indicates the forward and reverse transformation start temperatures of 6-day sintered $Ni_{43}Co_7Mn_{39}Sn_{11}$ polycrystalline alloy as a function of magnetic field which were extracted from the thermomagnetization curves. Data are linearly fitted.

Transformation temperatures obtained from the thermal cycling under stress and the thermomagnetization measurements of the 6-day sintered sample are plotted in the compressive stress vs. transformation temperatures phase diagram in Figure 5-12. Critical stress that was obtained from the superelastic test was also added. It is shown in the Figure 5-12 that there is more than one point for each transformation temperature plotted for the stress levels of 10MPa and 50MPa. These are the values obtained from the experiments conducted after the set of experiments shown in Figure 5-2 on page 57, which confirm the influence of training. The slopes of the linear fits in Figure 5-12 indicate the change in the stress required for the onset of martensitic transformation per unit temperature change. For the forward transformation to begin 4.7MPa compressive stress is required to increase the M_s Temperature by one degree.

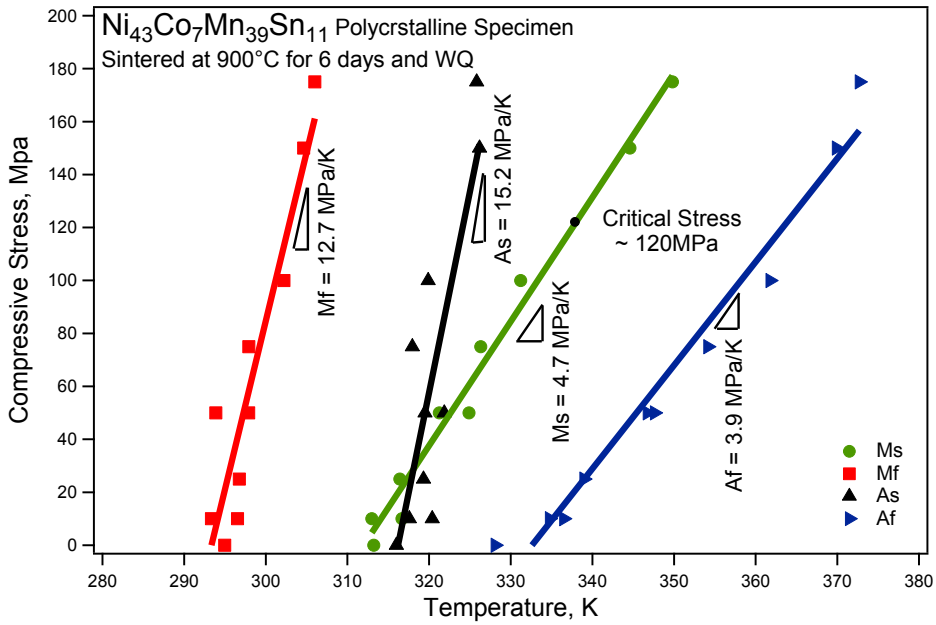

Figure 5-12) Compressive stress vs. Transformation temperatures phase diagram of 6-day sintered $Ni_{43}Co_7Mn_{39}Sn_{11}$ polycrystalline alloy.

It is indicated in Figure 5-12 that the linear fits all the transformation temperatures are not parallel to each other. This can be attributed to the changes in stored elastic strain energy and dissipated energy with increasing stress. It can be stated that these changes arise from the shape changes in the strain vs. temperature curves at each stress level in Figure 5-2, from which the data points to generate the phase diagram were extracted. Atli et al. [84] reported that the slope of the strain vs. temperature response during martensitic transformation (both forward and reverse directions) is influenced by the stored elastic strain energy under each stress level. There is an inverse relationship between the stored elastic strain energy and the slopes of the thermal cycling curves. Figure 5-2 shows a gradual decrease in the slope of each curve as the stress level increases. Consequently the differences between forward and reverse start and finish temperatures, Ms-Mf and Af-As increases at higher stress levels as shown in Figure 5-12. Moreover, the linear fits of As and Ms intersect approximately at 318K at 40MPa. This is similar to the polycrystalline NiCoMnAl shape memory alloys where the intersection occurs at 380K under 125MPa [84]. Karaca et al., on the other hand showed a different behavior for the NiCoMnIn single crystals that all linear fits to the transformation temperatures stay parallel to each other [5]. This intersection of the linear fits of As and Ms originates from the fact that the stored elastic strain energy during forward transformation reaches a sufficient value to initiate the reverse transformation at a temperature that is equal to or lower than Ms [84].

Figure 5-13 shows the MT start temperatures (A_s and M_s) of the 2- and 6-day sintered specimens in the phase diagram. Compared to the slopes of the linear fits, Ms of

the 2-day sintered specimen – about 6.6MPa/K - is greater than that of 6-day sintered one. For the slopes of the fits of the A_s temperatures, 6-day sintered specimen is bigger. Least square lines of the 2-day specimen intersect at a temperature and a compressive stress of about 320K and 90MPa, respectively. Thermal cycling experiments should be performed to obtain a more explicit view, but it is not possible at this point since the specimen was broken during testing.

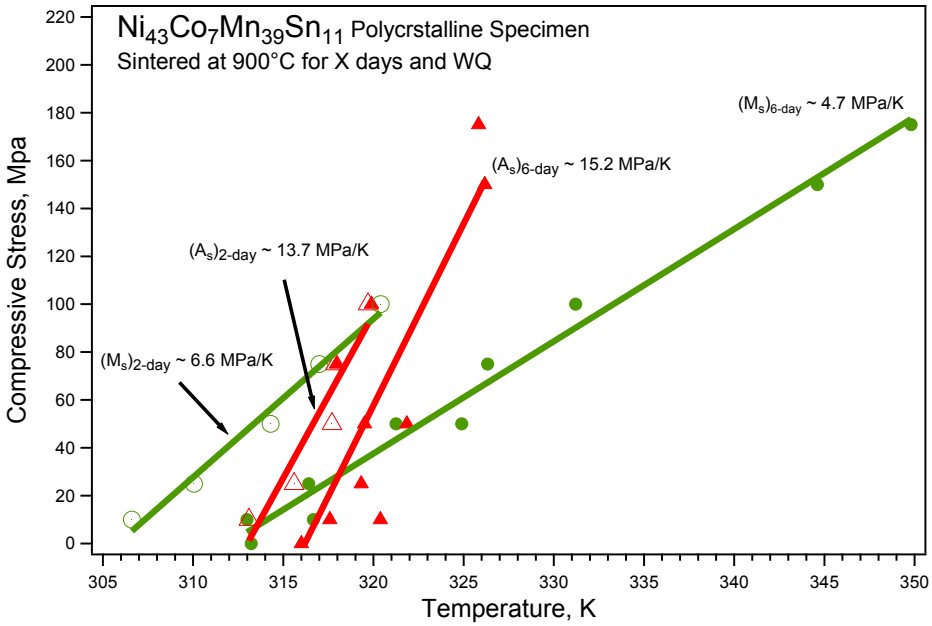

Figure 5-13) Compressive stress vs. forward transformation temperatures phase diagram of the 2- and 6-day sintered $Ni_{43}Co_7Mn_{39}Sn_{11}$ polycrystalline alloys; data of the 2-day sintered sample were extracted from the thermal cycling tests in Figure 2-5 on page 16.

Magnetostress is an important parameter which indicates the variation in the required stress level for the onset of martensitic transformation per unit change in the magnetic field. It is determined from the following relation [5]:

$$\frac{d\sigma}{dH} = \frac{dT}{dH}\frac{d\sigma}{dT} \tag{5.1}$$

where σ is the stress level required for the onset of the phase transformation, and H is the applied magnetic field to the specimen. The ($\partial T/\partial H$) of -4.4KT^{-1} and ($\partial\sigma/\partial T$) of 4.7$MPaK^{-1}$ can be determined from the slopes of M_s linear fits of the transformation temperature vs. magnetic field plot in the Figure 5-11, and the compressive stress vs. transformation temperature phase diagram in Figure 5-12, respectively. From these values, ($\partial\sigma/\partial H$) can be estimated to be approximately 21$MPaT^{-1}$ while it is about 19$MPaT^{-1}$ in NiCoMnAl polycrystalline alloys [83]. Despite being a polycrystalline material, the magnetostress achieved in the present alloy is quite comparable to 26$MPaT^{-1}$ obtained from NiCoMnIn single crystals along (100) orientation [5], and significantly higher than 5.7MPa achieved in NiMnGa single crystals [3]. Therefore, pressureless sintered NiCoMnSn polycrystalline alloys are promising candidates to be used as magnetic actuators due to low cost, ductility, capability to induce large MFIS, showing FIPT, and high level of magnetostress.

Magnetization vs. temperature response of the pressureless sintered $Ni_{43}Co_7Mn_{39}Sn_{11}$ polycrystalline alloy under different field levels in Figure 5-10 indicate that metamagnetic shape memory effect can be achieved during the reverse transformation. Figure 5-14 depicts the magnetic field induced strain vs. magnetic field curve (MFIS) at 319K. Prior to the experiment in Figure 5-14, the specimen was heated from room temperature to 353K to obtain a fully austenite phase under a compressive

stress level as low as 3.6 MPa to keep the specimen fixed in the test frame. Then, the stress level was increased to 10 MPa and the specimen was thermally cycled between 353K and 253K (Figure 5-15). The forward transformation was completed when the specimen was cooled down to 253K, and it was heated up to 319K near the onset of reverse transformation in Figure 5-2. Finally, magnetic field of 1.6T was applied perpendicular to the direction of compression, and then removed while the temperature was kept constant as shown in the inset in Figure 5-15. Figure 5-14 demonstrates that the magnetic field induced strain (MFIS) due to field induced phase transformation (FIPT) is approximately 0.6% achieved under 1.6T field. Application of magnetic field followed by heating the sample led to obtain MFIS levels which are comparable to the field induced shape recovery experiments performed by Kainuma et.al [9] and Ito. et. al [75]. In these experiments, both Ito et.al and Kainuma et.al applied 8T magnetic field to the predeformed samples in a direction parallel to the compression axis without preheating. Kainuma et.al confirmed 1% recovery strain in their arc-melted $Ni_{43}Co_{7}Mn_{39}Sn_{11}$ polycrystalline samples, whereas Ito et.al obtained only 0.56% recovery for their spark plasma sintered $Ni_{43}Co_{7}Mn_{39}Sn_{11}$ polycrystalline alloys. It is apparent that preheating the samples worked as an auxiliary mechanism to the magnetic field, and lowered the required field level for MFIS in our experiments. Therefore, our experimental method can be utilized as a way to induce shape recovery strains at low magnetic field levels.

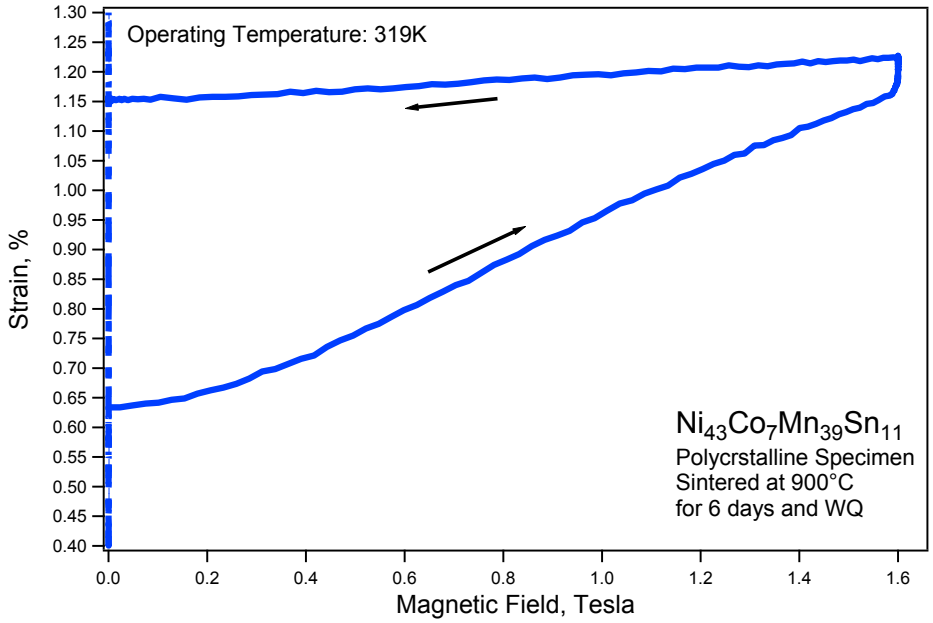

Figure 5-14) Magnetic field induced strain of the 6-day sintered sample was measured as a function of magnetic field from 0 to 1.6 Tesla at 319K.

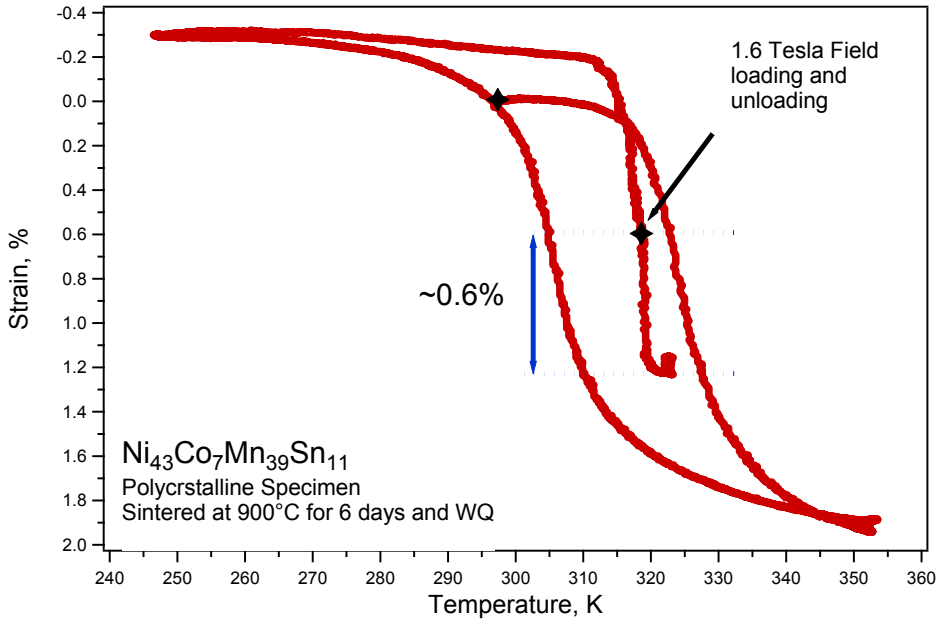

Figure 5-15) Shows the thermal cycling experiment of the 6-day sintered sample under 10MPa where heating was interrupted at 319K which is just below the onset of reverse martensitic transformation. Magnetic field of 1.6T was loaded at this temperature.

Table 5-1 summarizes the specimens on which experiments are conducted. Alloy composition of the specimens, their processing, and what kind of experiments they were performed are displayed in this table. First two specimens were investigated in this section and the remaining four - $Ni_{43}Co_4Mn_{42}Sn_{11}$ bulks specimens and ribbons -will be examined in the following section.

Table 5-1) Processing chart of Ni-Co-Mn-Sn polycrystalline alloys.

Specimen ID	Process	Tests			
		Thermal Cycling	Superelasticity	Magnetization	Magnetocaloric
$Ni_{43}Co_7Mn_{39}Sn_{11}$	Bulk - Sintered at 900°C for 6 days and WQ	DONE	DONE	DONE	
$Ni_{43}Co_7Mn_{39}Sn_{11}$	Bulk - Sintered at 900°C for 2 days and WQ	DONE	DONE		
$Ni_{43}Co_4Mn_{42}Sn_{11}$	Bulk - Induction melted			DONE	
$Ni_{43}Co_4Mn_{42}Sn_{11}$	Bulk - Annealed at 900°C for 1 day and WQ			DONE	
$Ni_{43}Co_4Mn_{42}Sn_{11}$	Ribbon - As-spun			DONE	
$Ni_{43}Co_4Mn_{42}Sn_{11}$	Ribbon - Annealed at 900°C for 2 hours and			DONE	DONE

5.2 Magnetic Characterization and Magnetocaloric Effect in Polycrystalline $Ni_{43}Co_4Mn_{42}Sn_{11}$ Bulk Alloys and Ribbons

Magnetic characterization of $Ni_{43}Co_4Mn_{42}Sn_{11}$ polycrystalline alloys in bulk form and ribbons is performed. Differing from most alloys in bulk form, ribbons can easily be magnetized with the application of very low magnetic field strengths. Magnetization response of the bulk and ribbon specimens is compared. Figure 5-16 depicts the

thermomagnetization curves of an induction melted bulk specimen, and a bulk specimen which was annealed at 900°C for 1 day, in the field of 0.05T. It is obvious from Figure 5-16 that magnetization response of the current material is considerably influenced by annealing. The induction melted bulk specimen does not seem to exhibit a good metamagnetic phase transition while the annealed one transforms into martensite with a low magnetization level from the ferromagnetic austenite phase. The austenite phase of the annealed specimen is ferromagnetic for a short temperature interval, and T_c is determined as about 365K by heating.

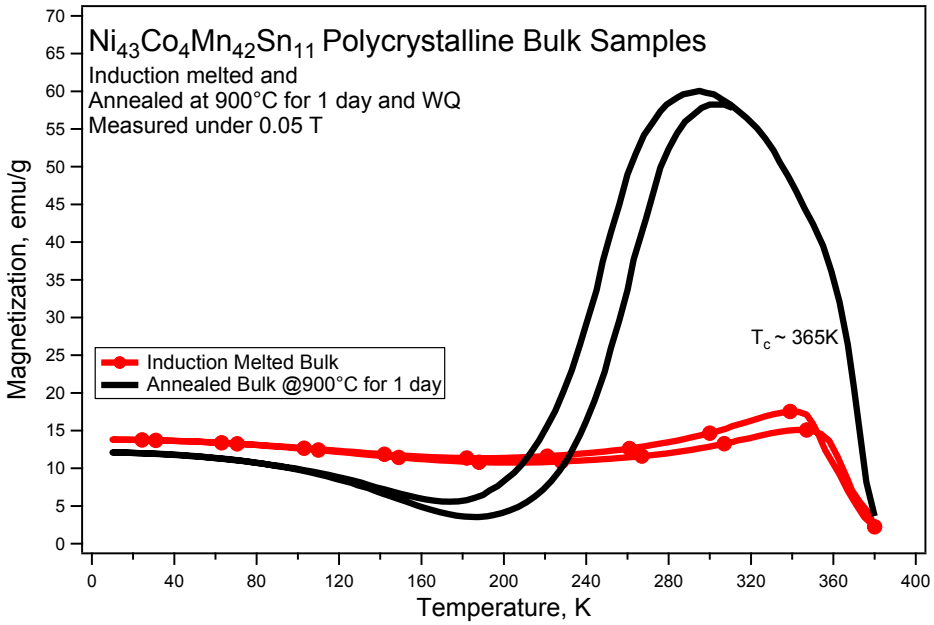

Figure 5-16) Thermomagnetization curves of $Ni_{43}Co_4Mn_{42}Sn_{11}$ polycrystalline bulk samples which were arc-melted and annealed at 900°C for 1 day, and water quenched. Magnetization measurements were performed under 0.05T.

Figure 5-17 depicts the magnetization response of the $Ni_{43}Co_4Mn_{42}Sn_{11}$ polycrystalline ribbons in the field of 0.05T. It is shown that both as-spun and the annealed ribbons show very good metamagnetic shape memory behavior with a sharp transition behavior between the austenite and martensite phases. It can be recalled from the Eq. 2.2 that the amount of ΔS_m which quantifies the magnetocaloric effect (MCE) is directly proportional to the slope of the thermomagnetization curve during MT. Thus, the magnetization response of the $Ni_{43}Co_4Mn_{42}Sn_{11}$ ribbons would rather be selected for the study of MCE than the bulk specimens. Once the as-spun and the annealed ribbons whose magnetization curves are shown in Figure 5-17 are compared, it is stated that the annealed ribbon has an improved magnetic shape memory properties such as higher magnetization in austenite, higher ΔM across MT, and lower T_{hys}. The M_s, M_f A_s and A_f temperatures are approximately 213K, 202K, 225K and 230K, respectively. T_c was determined to be about 340K. The MT temperatures play a significant role in determining the temperatures at which isothermal magnetization of the materials are measured.

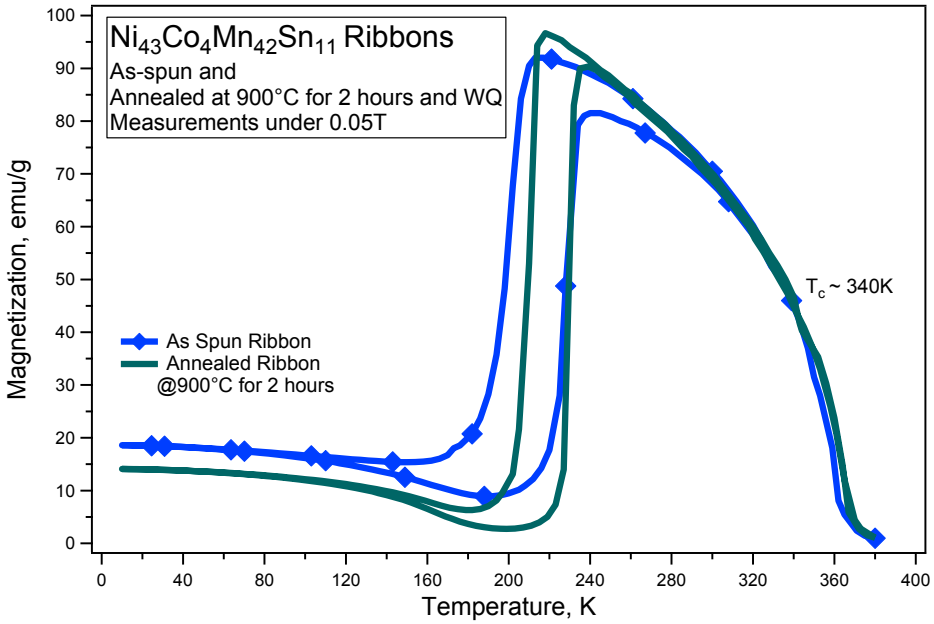

Figure 5-17) Thermomagnetization curves of $Ni_{43}Co_4Mn_{42}Sn_{11}$ polycrystalline ribbons which were as-spun and annealed at 900°C for 2 hours, and water quenched. Magnetization measurements were performed under 0.05T.

Figure 5-18 shows the 0.05T and 7T thermomagnetization curves of the $Ni_{43}Co_4Mn_{42}Sn_{11}$ polycrystalline ribbons which was annealed at 900°C for 2 hours and quenched in iced water. It is clearly seen that the application of 7T magnetic field did not lead to a large change in the magnetization, even reduced ΔM. A magnetic field of 7T decreased the MT temperatures as expected. However, the specimen did not completely transform to martensite up on cooling which is a sign of KA at high magnetic fields.

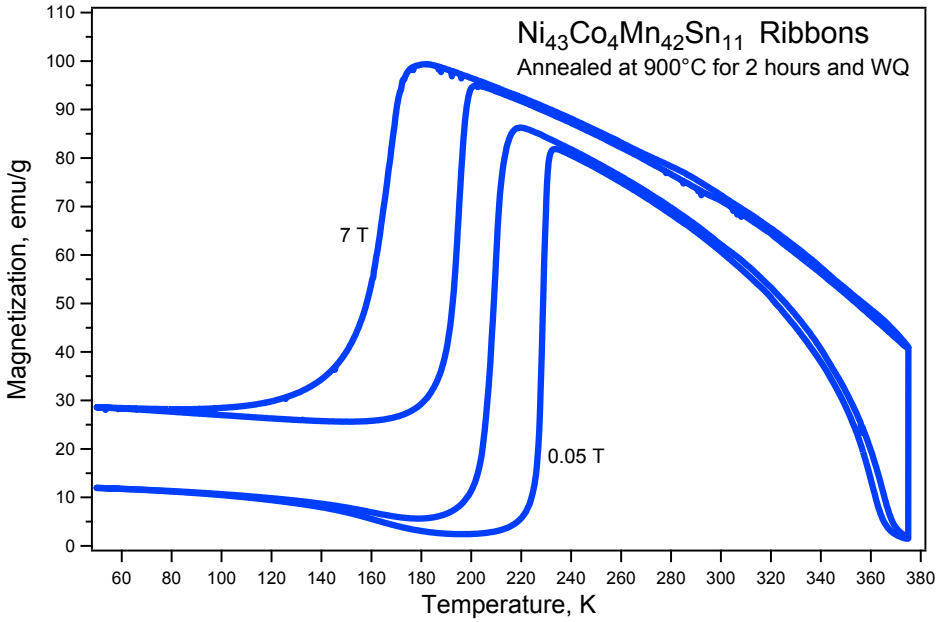

Figure 5-18) Thermomagnetization curves of $Ni_{43}Co_4Mn_{42}Sn_{11}$ polycrystalline ribbons annealed at 900°C for 2 hours, and water quenched. Magnetization measurements were performed under 0.05T and 7T.

Figure 5-19 demonstrates the isothermal magnetization curves $Ni_{43}Co_4Mn_{42}Sn_{11}$ polycrystalline ribbons up on loading of magnetic field of 7T and unloading. The temperatures at which the measurements were performed are based on the MT temperatures determined from Figure 5-17. The specimen was cooled down to 100K to obtain a fully martensite phase, followed by heating up to 180K where the specimen was still martensite. The first magnetization measurement was performed at 180K. Then temperature was set to 185K and magnetization of the specimen was measured one more time. Next measurement temperature was 189K. Magnetization measurement with a loading-unloading cycle of a magnetic field up to 7T was repeated starting at 189K, which is a close temperature value to the MT region, and increasing the operating

temperature with an increment of 3K. This type of heating is called the continuous heating. When the temperature value of 231K, which is just above the A_f temperature, incremental cycles of magnetization measurements were finished. The same magnetization measurement was performed at the temperatures 235K and 240K to confirm the magnetization response in the austenite phase.

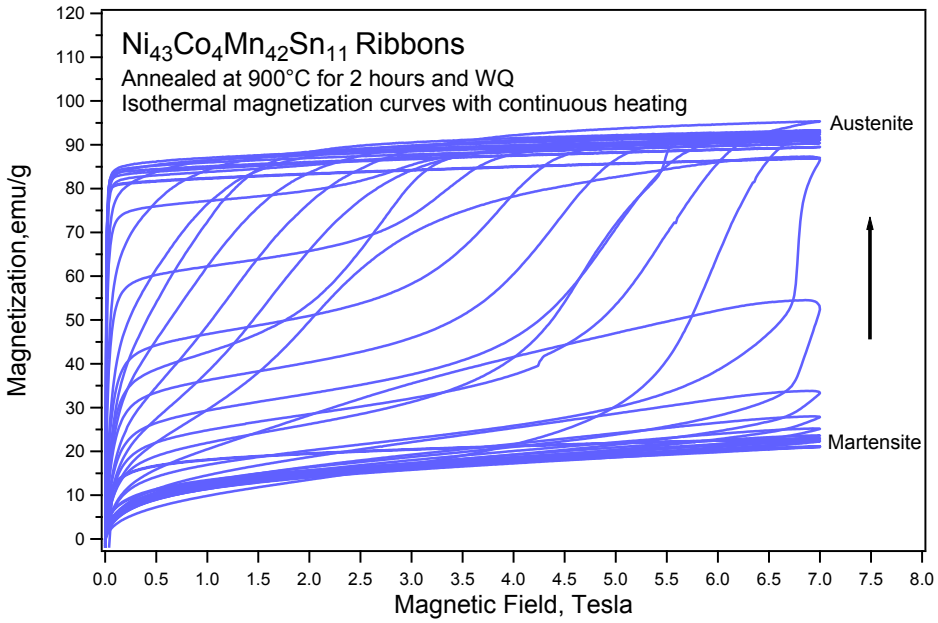

Figure 5-19) Isothermal magnetization curves of $Ni_{43}Co_4Mn_{42}Sn_{11}$ polycrystalline ribbons annealed at 900°C for 2 hours, and water quenched. Ribbons were tested by continuous heating.

It is obvious from Figure 5-19 that the magnetization levels of the measurements below 190K are low and no magnetization hysteresis is observed since the specimen is in martensite phase. When the operating temperature is in the MT range the measurements show magnetization hysteresis during unloading the magnetic field. When

the testing temperature reaches up to a level beyond the A_f temperature, again no hysteresis is observed from the magnetization curves because the specimen is fully austenite. The magnetization curves which were measured in an incremental temperature range are significant in determining the ΔS_m.

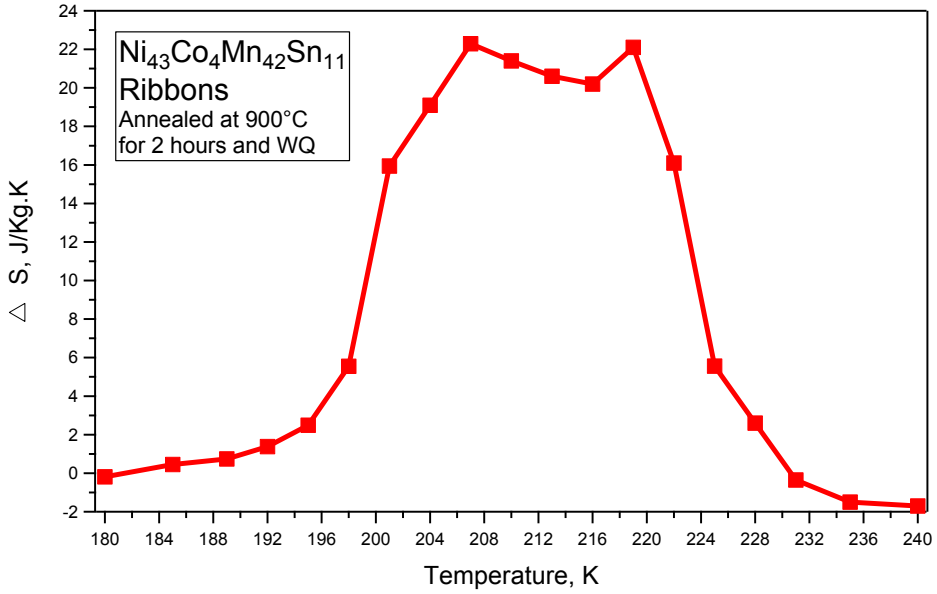

Figure 5-20) Magnetic entropy change of the annealed $Ni_{43}Co_4Mn_{42}Sn_{11}$ polycrystalline ribbons as a function of temperature.

Figure 5-20 displays the ΔS_m values of annealed $Ni_{43}Co_4Mn_{42}Sn_{11}$ polycrystalline ribbon as a function of operating temperature which all the ΔS_m values were calculated from the magnetization curves in Figure 5-19 by using Eq. 2.3 on page23. It can be concluded from Eq. 2.3 that the ΔS_m is related to area between the two incremental magnetization curves within the range of the applied magnetic fields. This area is very small when the specimen is in either austenite or martensite phases since there are tiny

changes in the levels of M_{sat} as a consequence of the magnetization measurements. However, the M_{sat} is very sensitive to temperature changes across MT, which in turn drastically increases the difference between the areas of the magnetization curves within small temperature variations. The maximum ΔS_m obtained from the current specimen is about 22 J kg^{-1} K^{-1} at 219K in the field of 7T. This value can be compared to $Ni_{43}Co_5Mn_{41}Sn_{11}$, $Ni_{42.7}Co_{5.2}Mn_{40.8}Sn_{11.3}$, $Ni_{48}Mn_{39}In_{13}$, and $Ni_{47}Mn_{40}In_{13}$ ribbons with maximum ΔS_m values of 10 J kg^{-1} K^{-1} at room temperature in the field of 10kOe [61], 33 J kg^{-1} K^{-1} at 269K in the field of 10kOe [79], 30 J kg^{-1} K^{-1} at 272K in the field of 5T [85], and 30 J kg^{-1} K^{-1} at room temperature in the field of 5T [86], respectively. The maximum ΔS_m obtained from the current specimen is lower than the annealed $Ni_{42.7}Co_{5.2}Mn_{40.8}Sn_{11.3}$ ribbon that was annealed at 850°C for 10 minutes and quenched in iced water [79]. The reason for getting a higher maximum for ΔS_m is it's being more sensitive to MT – metmagnetic phase transition with a very sharp curve. However, the maximum ΔS_m can be obtained from this specimen at only one temperature point (Figure 5 in Ref. 79). ΔS_m values at different temperatures even near the point where the maximum is obtained are very low. On the other hand, Figure 5-20 clearly shows that the maximum ΔS_m, and ΔS_m levels close to the maximum can be attained from the specimen in the current study. The temperature interval, in which high amounts of ΔS_m were observed is about 20K, may consequently increase the reliability of the material.

6. MAGNETIC PROPERTIES AND MAGNETOCALORIC EFFECT IN Fe-Mn-Ga METAMAGNETIC SHAPE MEMORY ALLOYS

Fe-Mn-Ga polycrystalline MMSMAs are discussed in this section. The distinguishing feature of Fe-Mn-Ga alloy system from the Ni-Co-Mn-X (X=In, Sn) MMSMAs mentioned in the previous sections is the magnetization levels during MT. Since the austenite is paramagnetic and martensite is ferromagnetic in these alloys [21], magnetic field application favors the highly magnetized martensite and the MT temperatures increase. Since mechanical stress also increases the MT temperatures, application of a magnetic field and stress can be employed in Fe-Mn-Ga alloys as auxiliary driving mechanisms for phase transformation. This will let to reduce the level of the magnetic fields and compensate the remaining force the mechanical stress in applications which low magnetic fields are required.

Following section will include the microstructure, magnetization and magnetocaloric measurements of $Fe_{44}Mn_{25.2}Ga_{30.8}$ polycrystalline alloys. Attempts of heat treatment and processing, and magnetization response of various Fe-Mn-Ga alloys will be discussed in the subsequent section.

6.1 Magnetocaloric Effect in $Fe_{44}Mn_{25.2}Ga_{30.8}$ Polycrystalline Alloys

Figure 6-1 shows the thermomagnetization curves of $Fe_{44}Mn_{25.2}Ga_{30.8}$ polycrystalline alloy in the fields of 0.05T and 7T that are selected from the measurements in 0.05T, 1T, 3T, 5T and 7T. The arc-melted specimens were heat treated at 1000°C for 1 day and quenched in iced water. Magnetization measurements in the

figure confirm the characteristic of MT in this alloy where paramagnetic austenite transforms to ferromagnetic martensite.

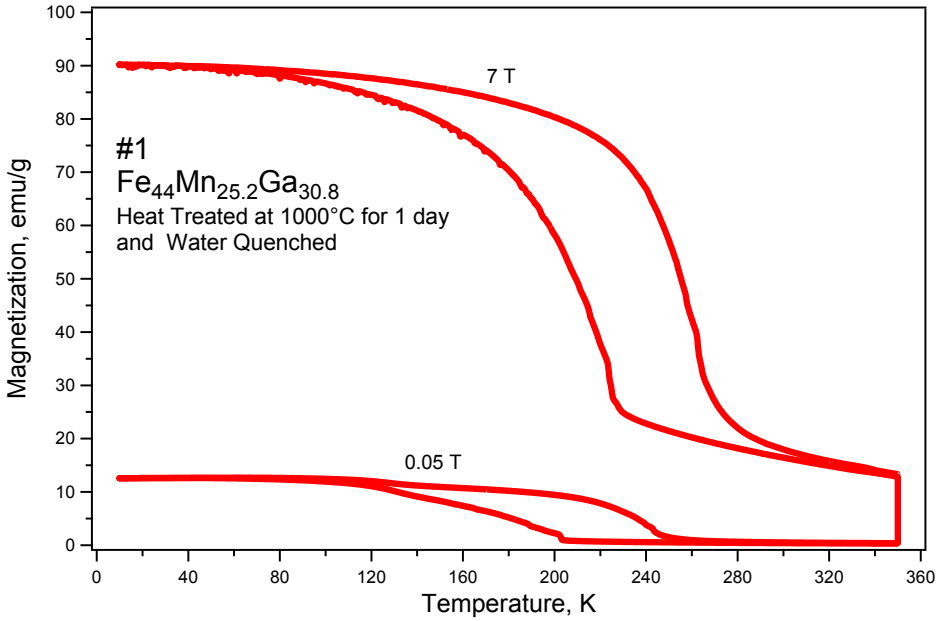

Figure 6-1) Thermomagnetization curves of $Fe_{44}Mn_{25.2}Ga_{30.8}$ polycrystalline alloy in the fields of 0.05T and 7T.

Magnetic field dependence of MT temperatures of polycrystalline $Fe_{44}Mn_{25.2}Ga_{30.8}$ alloy which were determined from the thermomagnetization curves is depicted in Figure 6-2. All data points were linearly fitted. It is seen that the MT temperatures increase by an application of magnetic field. There is no huge variation in the slopes of the linear fits, and the slope of the linear fit of the M_s – dM_s/dH - is given by 3.54K/T. This means that the application of a 1T magnetic field increases the M_s by about 3.5K. dMs/dH of the current sample is comparable to those of the single crystal $Ni_{45}Co_5Mn_{36.6}In_{13.4}$ and 6-day sintered polycrystalline $Ni_{43}Co_7Mn_{39}Sn_{11}$ alloys in the

previous sections which are -5.5K/T and -4.4K/T, respectively. dMs/dH can be increased by further alloying, or with a better heat treatment.

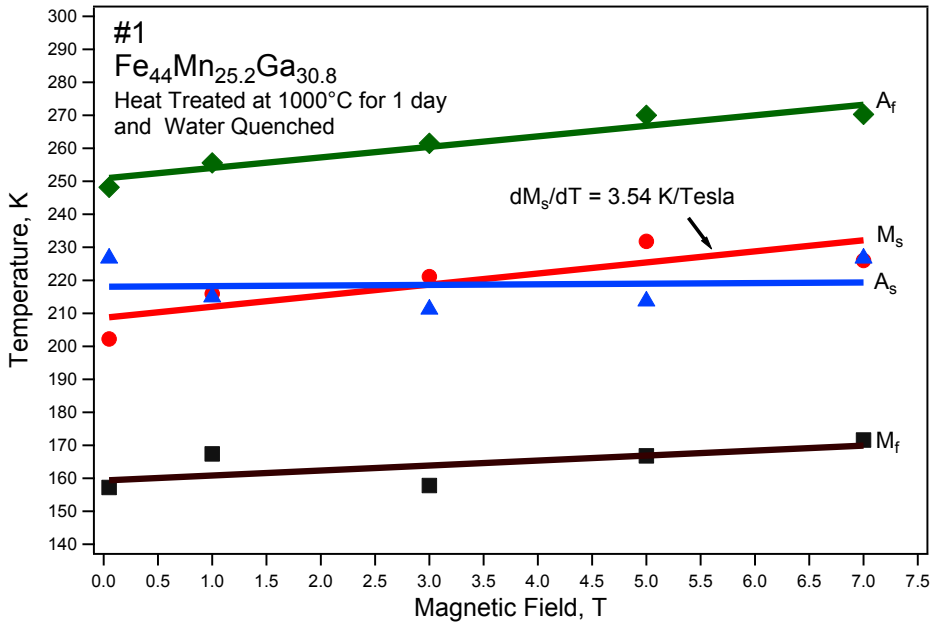

Figure 6-2) Magnetic field dependence of the MT Temperatures of $Fe_{44}Mn_{25.2}Ga_{30.8}$ polycrystalline alloy.

Figure 6-3a displays the room temperature optical image of the $Fe_{44}Mn_{25.2}Ga_{30.8}$ polycrystalline sample. It is obvious from the image that second phase precipitates are existent on the sample. To be able to detect the difference between the matrix of the sample and the second phases, BSE images were taken and compositional analysis was performed. Figure 6-3b shows one of the BSE image obtained where the second phases are clearly seen. It was verified by the compositional analysis that, the atomic percentages of the elements constituting the matrix and the second phases are different: The average composition of the second phase precipitates is $Fe_{43.6}Mn_{24.93}Ga_{31.5}$ (at %)

while the matrix composition is $Fe_{44}Mn_{25.2}Ga_{30.8}$ (at %) as denoted above. The matrix composition of the current sample was placed on the ternary phase diagram in Figure 6-23 on page 105, denoted by #1. It is apparent that the sample is in the borderline that defines the region of compositions showing MT. The average composition of the second phase precipitates is close to the borderline.

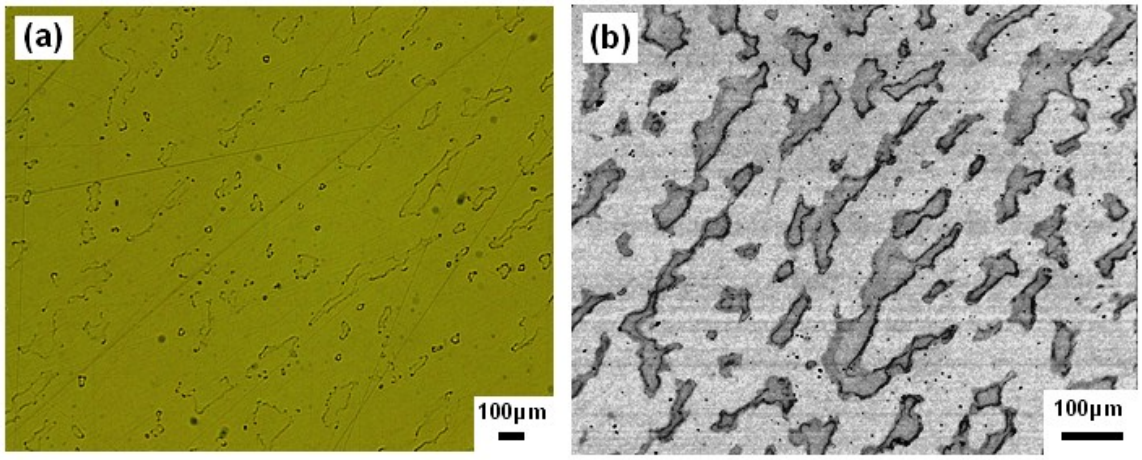

Figure 6-3) (a) Room temperature optical and (b) Backscattered electron (BSE) of $Fe_{44}Mn_{25.2}Ga_{30.8}$ polycrystalline alloy heat treated at 1000°C for 1 day and Water Quenched.

Figure 6-4 indicates the thermomagnetization curves of the current sample measured in two different Squid magnetometers. Since we experienced technical difficulties in the instrument, another instrument was utilized for further magnetization measurements. In Figure 6-4, 7T thermomagnetization curves of the first measurement performed in the previous instrument (Figure 6-1) and the new instrument are compared. Magnetization curve in the new magnetometer resulted in less M_{sat} and less steep MT,

which is attributed to a more difficult phase transition. Another reason for this problem is the sample`s being highly corrosive which makes the sample preparation troublesome.

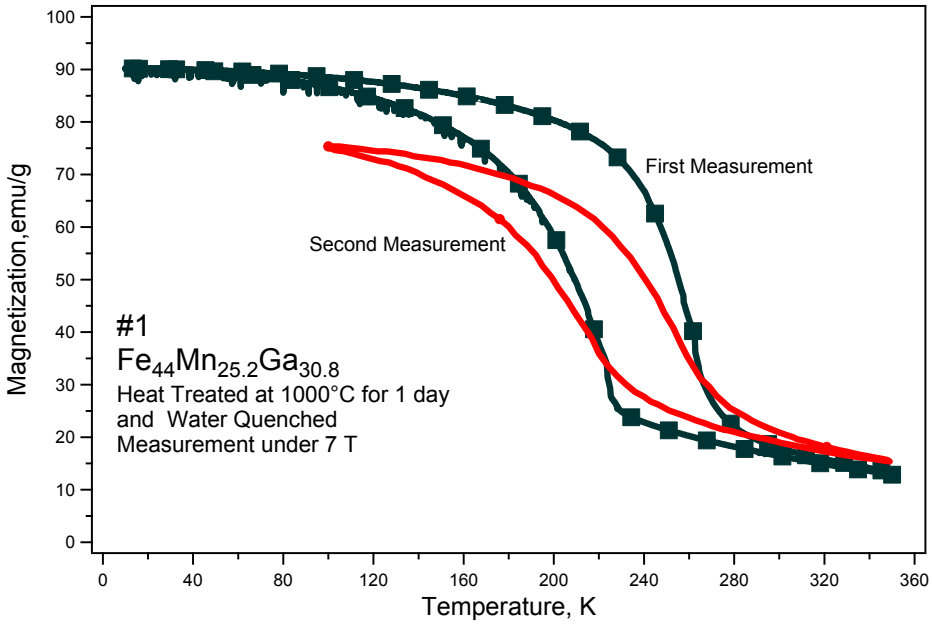

Figure 6-4) Thermomagnetization curves of $Fe_{44}Mn_{25.2}Ga_{30.8}$ polycrystalline alloy in the fields 7T in two different instruments.

Thermomagnetization measurements were done to quantify the MCE in the $Fe_{44}Mn_{25.2}Ga_{30.8}$ polycrystalline sample which is depicted in Figure 6-5. A magnetic field of 0.05T was applied to the sample in austenite and one cooling-heating cycle through MT was completed. Then, the same cycles were completed under the magnetic fields starting from 0.5T up to 7T with an increment of 0.5T. The classic method to measure the MCE is obtaining isothermal magnetization curves at incremental points within a temperature range. However, instrumental restrictions forced us to test the magnetization response as a function of temperature and generate a magnetization plot as a function

magnetic field by extracting data from Figure 6-5. Figure 6-6 shows the magnetization response in a field range from 0 to 7T at increasing temperature with an increment of 3K. The measurements at operating temperatures between 112K and 157K, and between 325K and 349K, showed no magnetization hysteresis since the material was fully martensite and austenite, respectively. However, hysteresis was observed at intermediate temperatures such as between 214K and 250K because the material was undergoing MT.

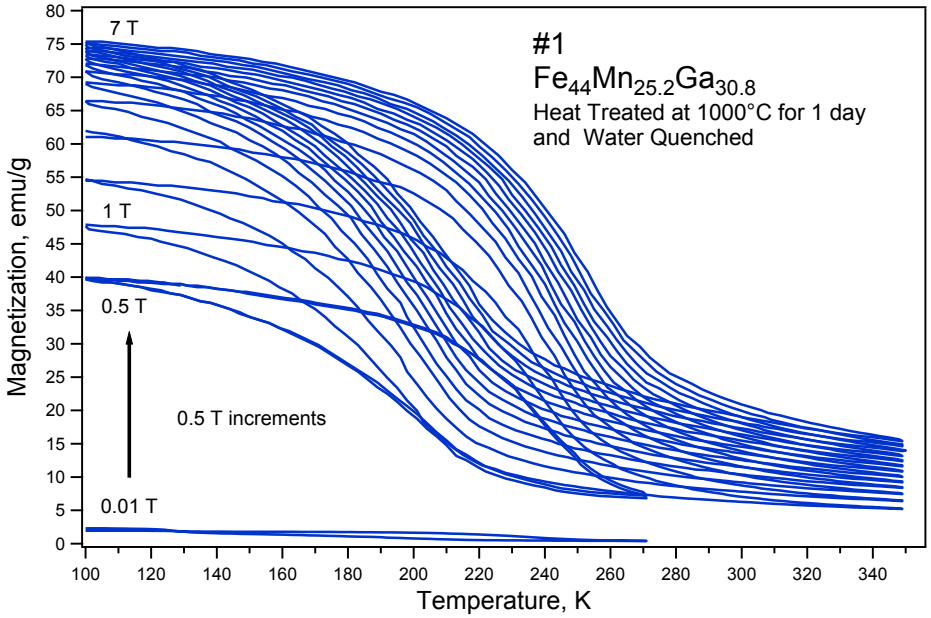

Figure 6-5) Thermomagnetization curves of $Fe_{44}Mn_{25.2}Ga_{30.8}$ polycrystalline alloy in the fields starting with 0.05T and increasing the level up to 7T with an increment of 0.5T.

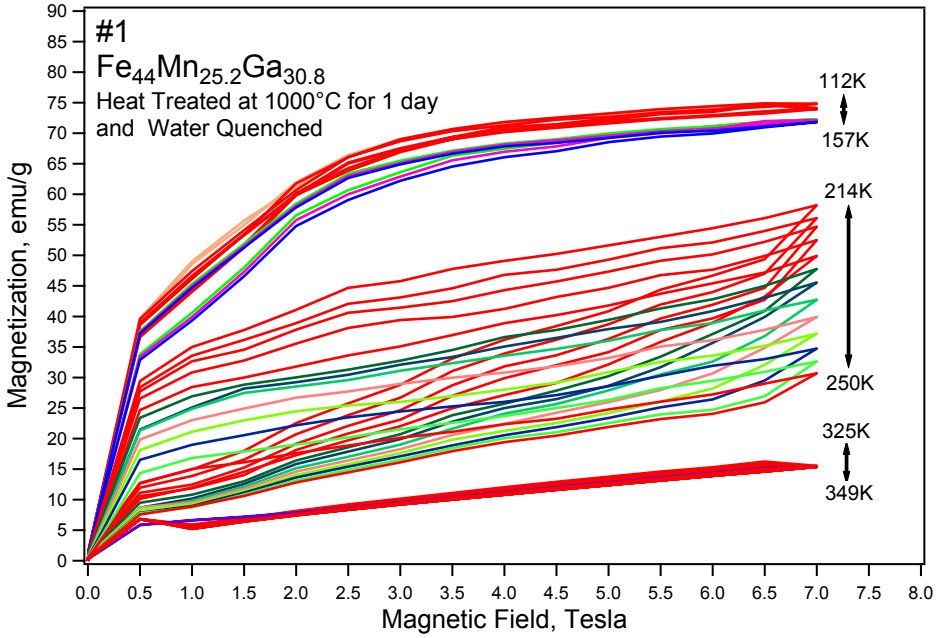

Figure 6-6) Isothermal magnetization curves of $Fe_{44}Mn_{25.2}Ga_{30.8}$ polycrystalline alloy up to 7T which the data points were extracted from the incremental thermomagnetization curves in Figure 6-4.

Figure 6-7 demonstrates the ΔS_m of $Fe_{44}Mn_{25.2}Ga_{30.8}$ polycrystalline sample a function of operating temperature which all the ΔS_m values were calculated from the magnetization curves in Figure 6-6 using the same method as in Section 5.2. A least squares fitting curve was also plotted to observe the general trend in the ΔS_m levels by temperature. It is shown that a maximum ΔS_m of approximately 6.7 J kg^{-1} K^{-1} is attained at 223K, which is low compared to the several MSMAs at where the maximum ΔS_m of more than 20 J kg^{-1} K^{-1} was observed (see Section 5.2) This low maximum ΔS_m observed from the current sample is due to the instrumental restrictions, less steep MT behavior, and the alloy`s corrosive character. Higher maximum levels of ΔS_m would be obtained provided the magnetization response in Figure 6-1, or a better one was attained.

Heat treatment temperature of the $Fe_{44}Mn_{25.2}Ga_{30.8}$ polycrystalline alloy was increased to 1050°C to remove the second phase precipitates observed in the previous case shown in Figure 6-3b. The processing time was again 1 day and the sample was water quenched at the end of heat treatment. Surprisingly, the heat treated sample at 1050°C did not exhibit MT which may be because of local melting during the heat treatment, and changes in the composition which led the alloy to be out of the range of MT as shown in Figure 6-23. The challenges during preparation and the analysis of the Fe-Mn-Ga alloy at this composition such as extreme corrosiveness and complexity of determining the true processing condition to obtain single phase samples, led us search for new compositions of Fe-Mn-Ga alloys. The following section will include the microstructure analysis and magnetization response of several Fe-Mn-Ga alloys.

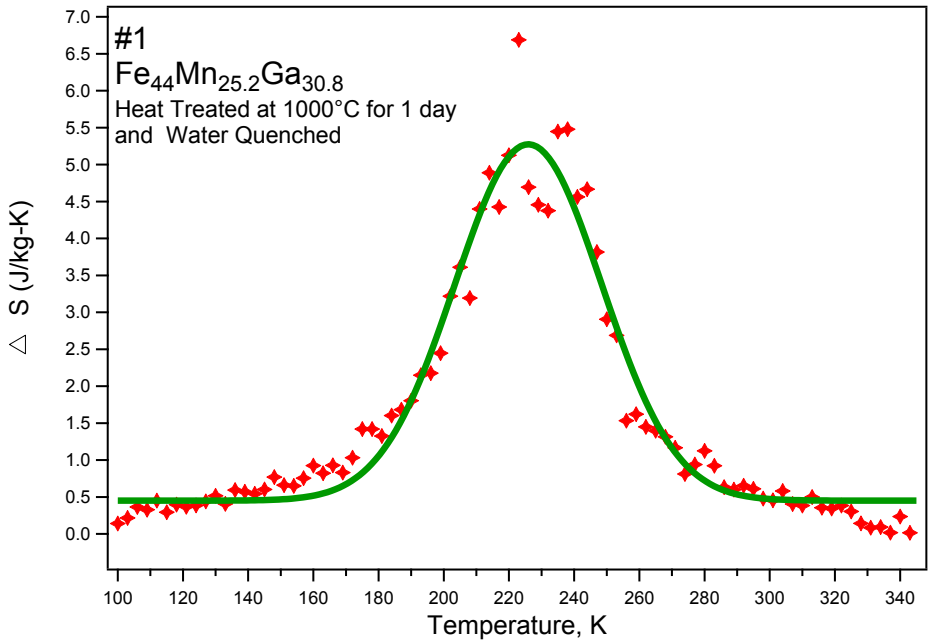

Figure 6-7) Magnetic entropy change in $Fe_{44}Mn_{25.2}Ga_{30.8}$ polycrystalline alloy as a function of temperature.

6.2 Systematic Heat Treatment Study and Magnetic Characterization of Fe-Mn-Ga Polycrystalline Alloys

Several Fe-Mn-Ga alloys are investigated in this section with systematic heat treatments to be able to determine the most plausible processing condition for enhanced magnetization response. Then, the Fe-Mn-Ga alloy composition with the highest MCE is aimed to be detected. Each sample is denoted by numbers instead of indices for the sake of simplicity. All the alloys in this study were water quenched (WQ) followed by the heat treatments at specified temperatures and durations, and the specified compositions are the matrix compositions. The sample that was analyzed in the previous section is the sample #1, as indicated in Figure 6-1 through Figure 6-7. Out of fifteen different alloys, MT was observed in the samples denoted by #7 and #9-14, whose results are included here.

Figure 6-8 shows the magnetization response of polycrystalline $Fe_{41.5}Mn_{28.2}Ga_{30.3}$ (#7) alloy in the temperature range from 50K to350K, in the fields of 0.05T and 7T. It was heat treated at 1050°C for 1 day but no MT was observed. Figure 6-9a displays the BSE image of the 1-day heat treated sample. Existence of second phase precipitates are clear from the image which is the possible reason for the absence of the phase transition. Subsequently, the sample #7 was heat treated at the same temperature for 1 week with the purpose of eliminating the precipitate formation. It is shown in the BSE image in Figure 6-9b that the precipitates completely disappeared and the sample is in the single phase. The single phase sample exhibit a phase transformation with T_{hys} of about 90K, which is quite a large value.

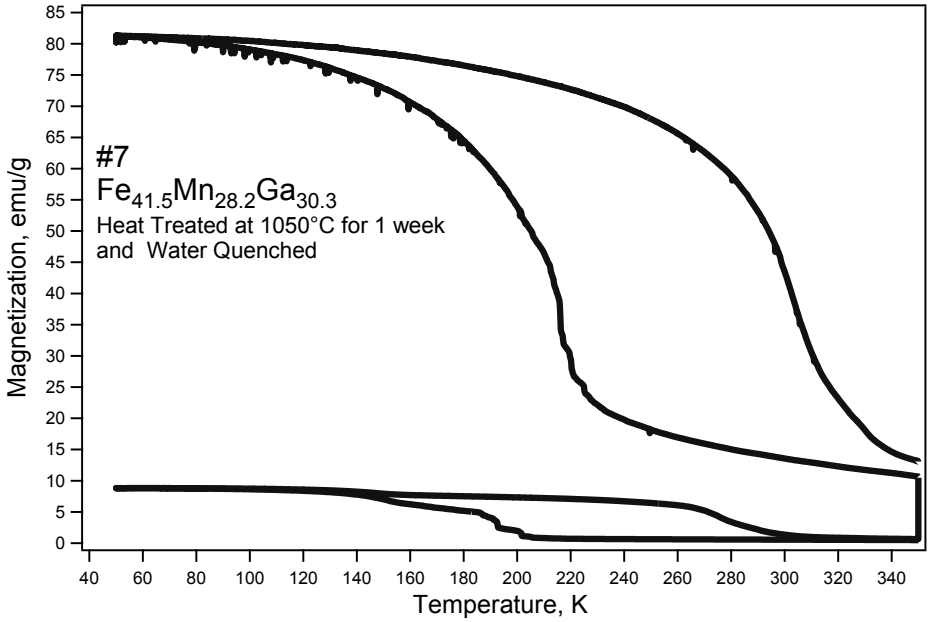

Figure 6-8) Thermomagnetization curves of $Fe_{41.5}Mn_{28.2}Ga_{30.3}$ (#7) polycrystalline alloy in the fields of 0.05T and 7T.

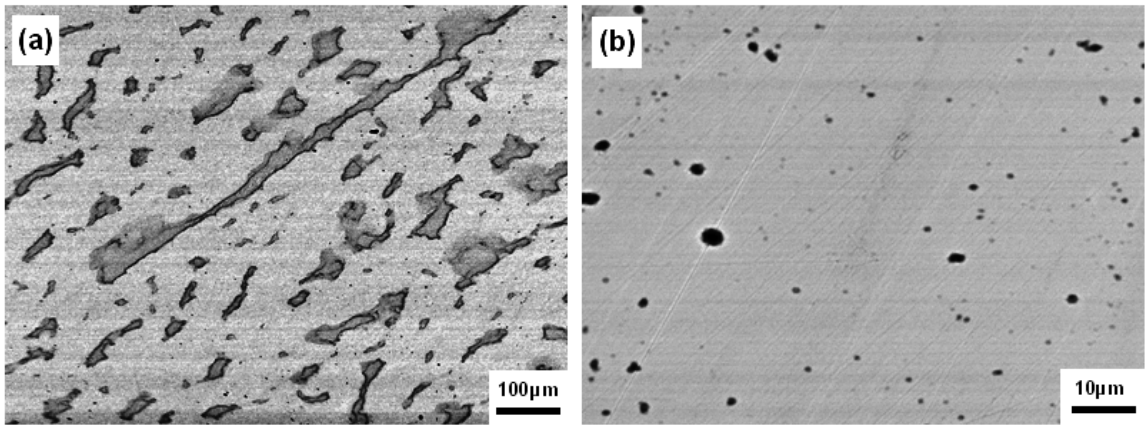

Figure 6-9) BSE images of the sample #7 that was heat treated at (a) 1000°C for 1 day and Water Quenched (b) 1050°C for 1 week and Water Quenched.

Figure 6-10 indicates the 0.05T and 7T thermomagnetization curves of $Fe_{42.2}Mn_{28.3}Ga_{29.5}$ (#9) single crystal. OM image of the as-received sample verifies the presence of dendrites as shown in Figure 6-11a, from which no MT was observed. After

heat treatment at 1050°C for 1 week, the phase transition from paramagnetic austenite to ferromagnetic martensite in Figure 6-10 was observed. Similar to the sample #7, the T_{hys} is considerably large and the slope of the thermomagnetization curve across MT is not very steep.

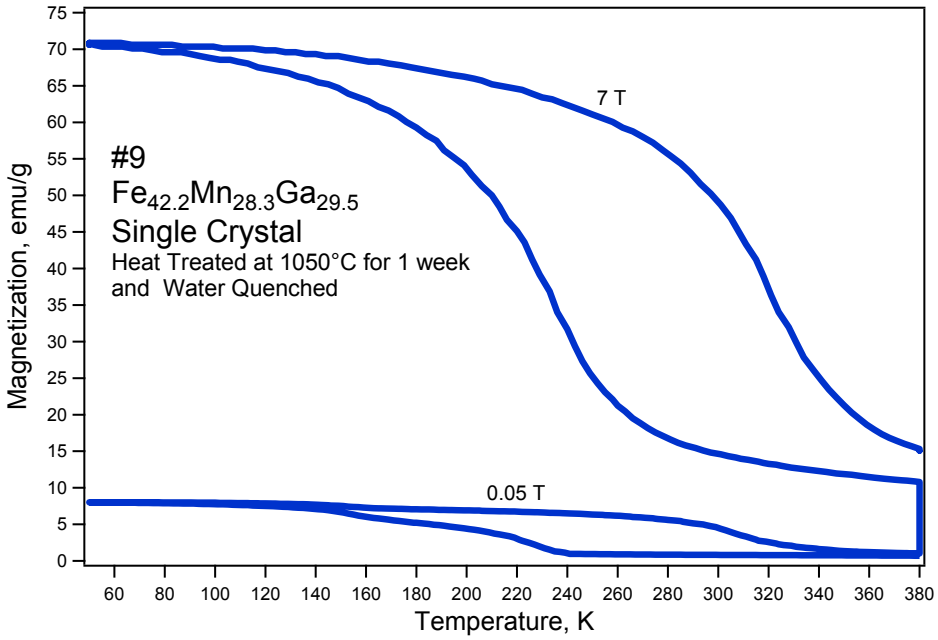

Figure 6-10) Thermomagnetization curves of single crystal $Fe_{42.2}Mn_{28.3}Ga_{29.5}$ (#9) alloy in the fields of 0.05T and 7T.

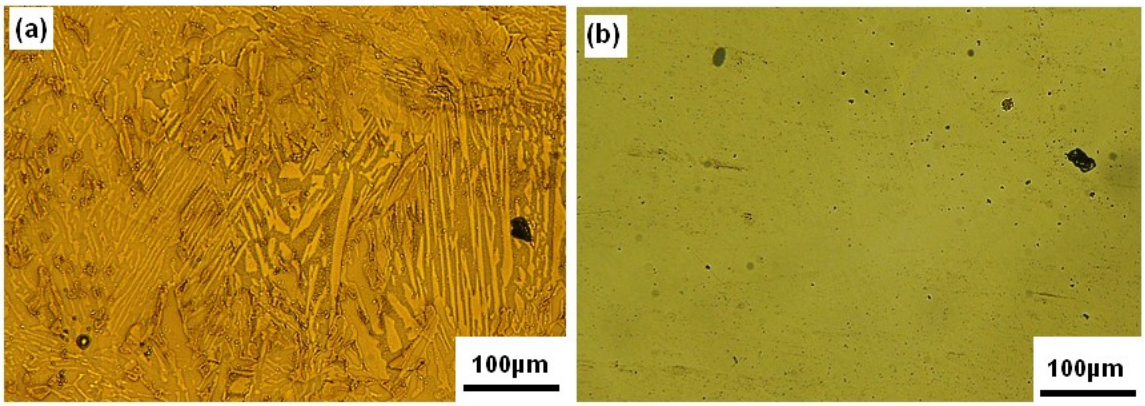

Figure 6-11) Optical images of sample #9 (a) as received and (b) heat treated at 1050°C for 1 week and Water Quenched.

Figure 6-12 depicts the magnetization curves of polycrystalline $Fe_{46.9}Mn_{23.7}Ga_{29.4}$ (#10) alloy as a function of temperature. The heat treatment condition for the alloy in the figure is 1050°C for 1 day. Two different specimens were prepared and tested for magnetization response. There is a tremendous change in the MT temperatures even though the processing condition of the specimens is the same. The specimen represented by the blue curve in Figure 6-12 exhibits a sharper phase transition behavior with higher MT temperatures, a sign of a higher MCE. Figure 6-12a displays the BSE image of the 1-day heat treated alloy. It is apparent that there is a preferred texture orientation of the precipitates observed in all grains. This improved texture which is present in the alloy is the possible reason for the smooth MT behavior. The difference in the MT temperatures and the slope of the curves across the phase transformation between two samples is due to the volume fraction of the second phase precipitates. The average composition of the precipitates is $Fe_{46.8}Mn_{23.7}Ga_{29.5}$ (at %)

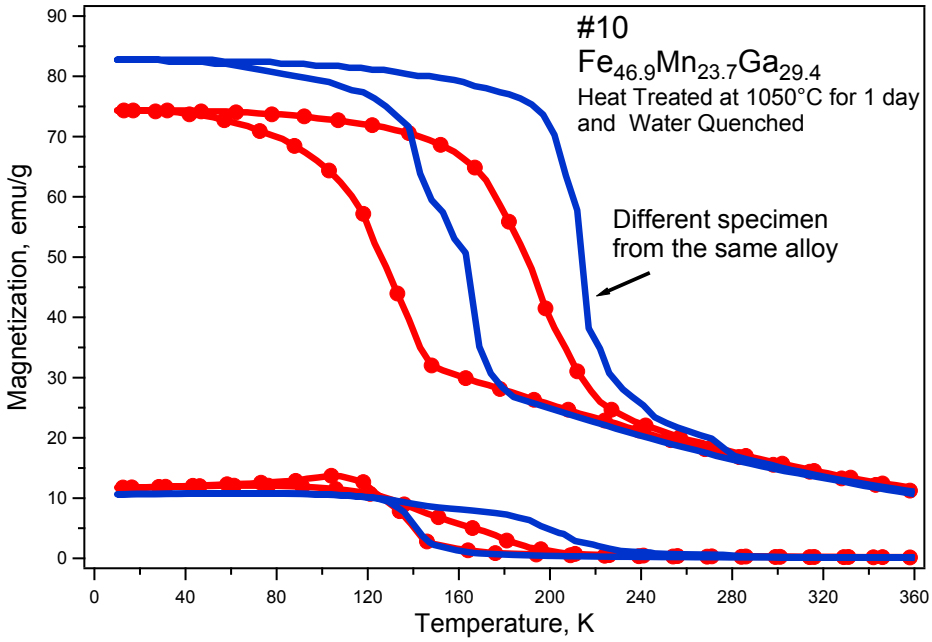

Figure 6-12) Thermomagnetization curves of $Fe_{46.9}Mn_{23.7}Ga_{29.4}$ (#10) polycrystalline alloy heat treated at 1050°C for 1 day and water quenched, in the fields of 0.05T and 7T. Two different specimens were tested.

Figure 6-13b displays the BSE image obtained from the sample #10 that was heat treated for 1 week at 1050°C. It is clear from the image that the second phases were completely removed. However, the 1-week heat treated sample did not show MT behavior because the results of compositional analysis showed that the samples were contaminated with Si during heat treatment due to melting of the quartz tube. In fact, a smooth transformation characteristic is expected from the single phase of the sample #10.

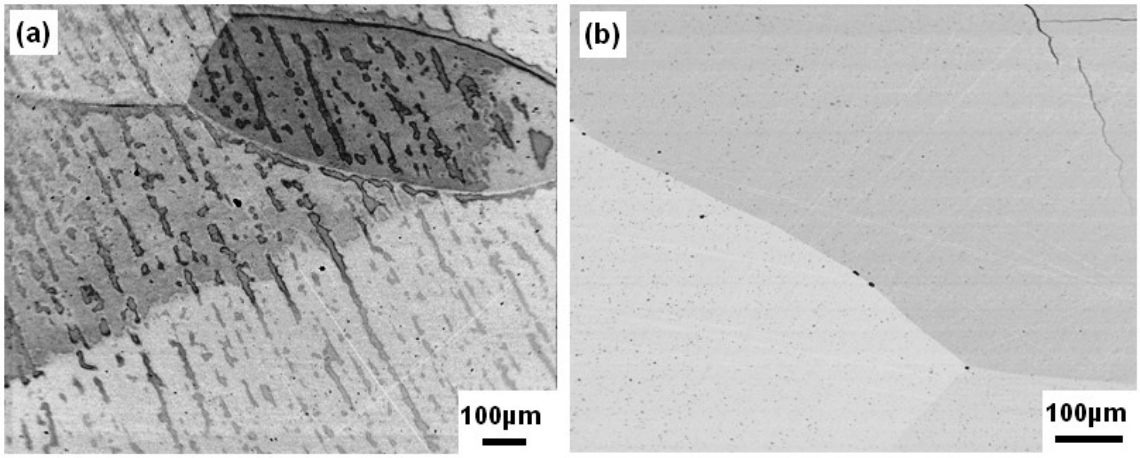

Figure 6-13) BSE images of sample #10 which was heat treated at (a) 1050°C for 1 day and Water Quenched and (b) 1050°C for 1 week and Water Quenched.

Figure 6-14 shows the thermomagnetization curves of polycrystalline $Fe_{47.6}Mn_{23.1}Ga_{29.3}$ (#11) alloy with the 1-day heat treatment at 1050°C under the applied fields of 0.05T and 7T. Similar to the sample #10, sample #11 exhibits MT behavior with 1day heat treatment. However, M_{sat} in the sample #11 is a bit lower than the composition of the sample #10 whose magnetization curve is demonstrated by the blue curve in Figure 6-12. The M_s, M_f, A_s and A_f temperatures in the field of 7T are 165K, 123K, 189K and 229K, respectively.

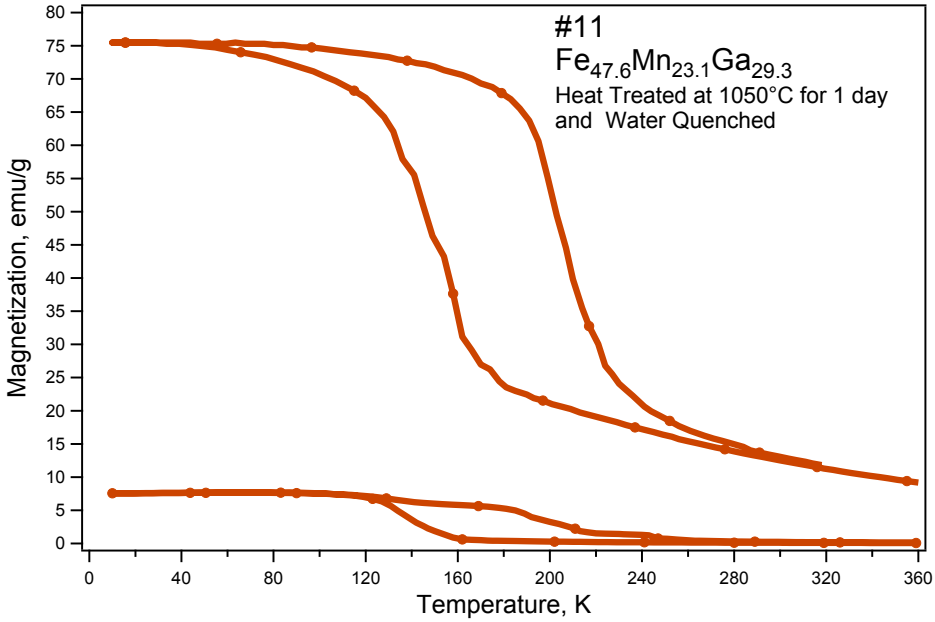

Figure 6-14) Thermomagnetization curves of $Fe_{47.6}Mn_{23.1}Ga_{29.3}$ (#11) polycrystalline alloy in the fields of 0.05T and 7T.

The magnetization responses of the sample #11 after 1-day and 1-week heat treatments at 1050°C under 0.05T and 7T were plotted in Figure 6-15. 1-day heat treated sample is denoted by a scattered plot whereas the 1-week heat treated one is shown by a solid curve. Magnetization curves under the field of 7T almost overlap while the 1-week heat treated sample shows higher M_s and M_{sat} under a 7T magnetic field. However, the curves under the field of 0.05T are considerably different from each other. The metamagnetic phase transition from paramagnetic austenite to ferromagnetic martensite is not clearly indicated in the 1-week heat treated sample, whereas the 1-day heat treated sample exhibits this characteristic behavior.

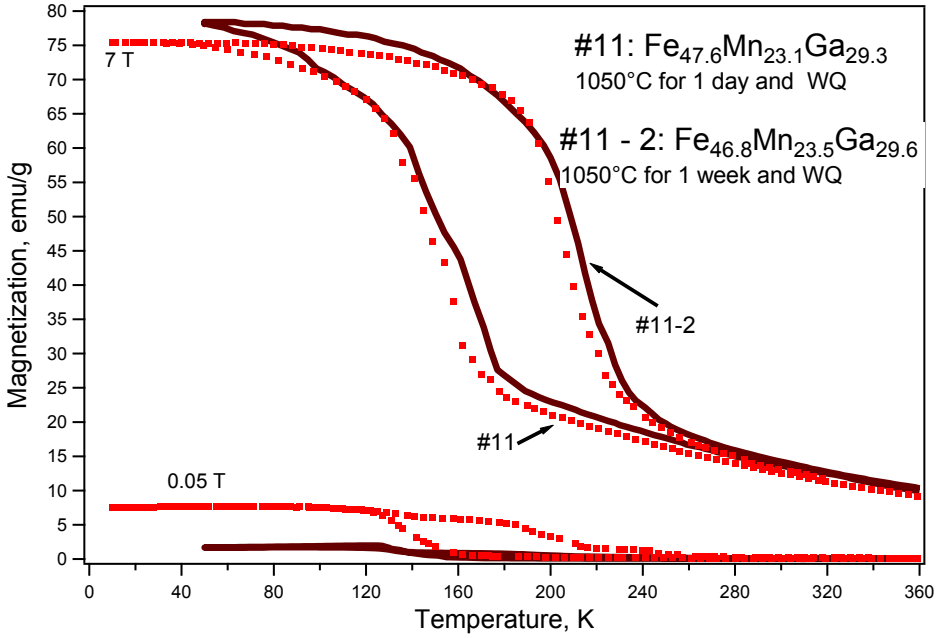

Figure 6-15) Comparison of the thermomagnetization curves of $Fe_{47.6}Mn_{23.1}Ga_{29.3}$ (#11) and $Fe_{46.8}Mn_{23.5}Ga_{29.6}$ (#11-2) polycrystalline alloy in the fields of 0.05T and 7T.

BSE images of the samples #11 and #11-2 are shown in Figures 6-16a and 6-16b, respectively. Similar to the sample #10, 1 day heat treatment of the sample #11 led to a favorably oriented texture structure of the second phases. The average composition of the second phases in this sample is $Fe_{47.4}Mn_{22.9}Ga_{29.7}$ (at %). On the other hand, all the second phases were removed by 1-week heat treatment. Si contamination was observed as a result of the compositional analysis like in the sample #10, but this did not affect the MT character of the sample since the concentration of Si on the sample surface was at trace element level.

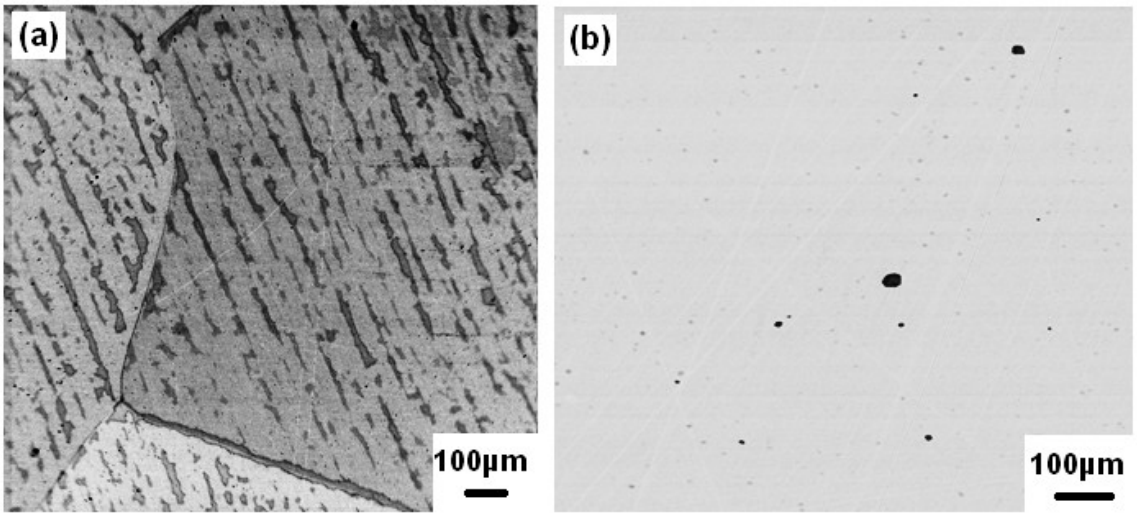

Figure 6-16) BSE images of the samples #11 and #11-2 heat treated at (a) 1050°C for 1 day and water quenched and (b) 1050°C for 1 week and water quenched, respectively.

A similar story to the samples #10 and #11 can be explained for polycrystalline $Fe_{45.9}Mn_{23.4}Ga_{30.7}$ (#12) alloy which the thermomagnetization curves in the fields of 0.05T and 7T are shown in Figure 6-17. The first attempt heat treatment was at 1050°C for 1 day similar to the previous samples. The magnetization response of the sample #12 is close to the magnetization responses obtained from the samples #10 and #11 with a larger T_{hys}. BSE images of the sample #12 are shown in Figure 6-18. The image in Figures 6-18a and 6-18b represent the 1-day and 1-week heat treated samples, respectively. The favorably oriented precipitates are seen in Figure 6-18a like those in the sample #10 as shown in Figure 6-13a and the sample #11 as in Figure 6-16a. However, the orientation of the texture is blurry in Figure 6-18a. The average second phase composition was determined to be $Fe_{45.7}Mn_{23.3}Ga_{31}$ (at %). The precipitates were removed after 1-week heat treatment at 1050°C as indicated in Figure 6-18b. However,

the Si contamination at this processing condition was the problem similar to the samples #10, which prevented MT behavior.

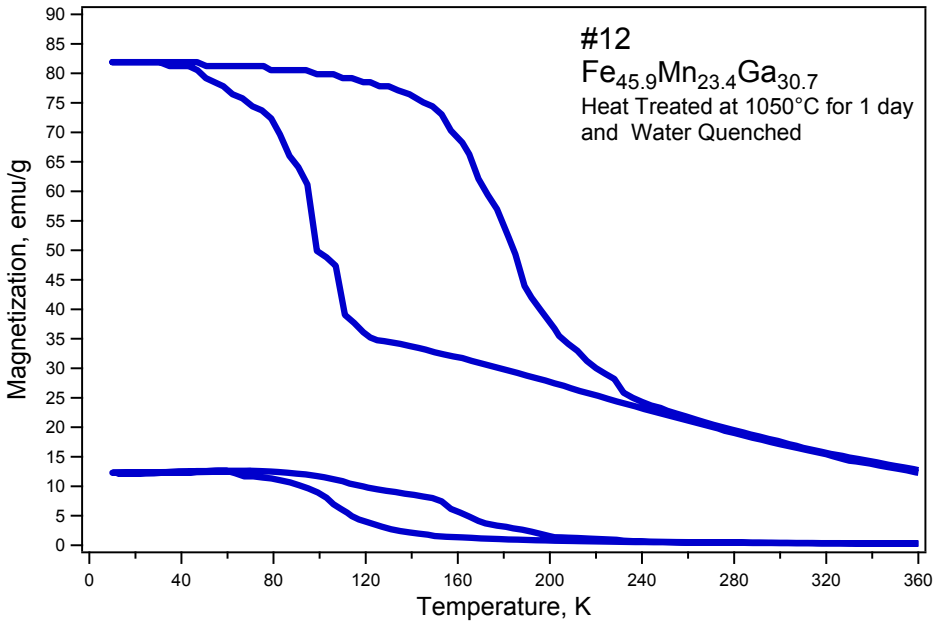

Figure 6-17) Thermomagnetization curves of $Fe_{45.9}Mn_{23.4}Ga_{30.7}$ (#12) polycrystalline alloy in the fields of 0.05T and 7T. The alloy was heat treated at 1050°C for 1 day and water quenched.

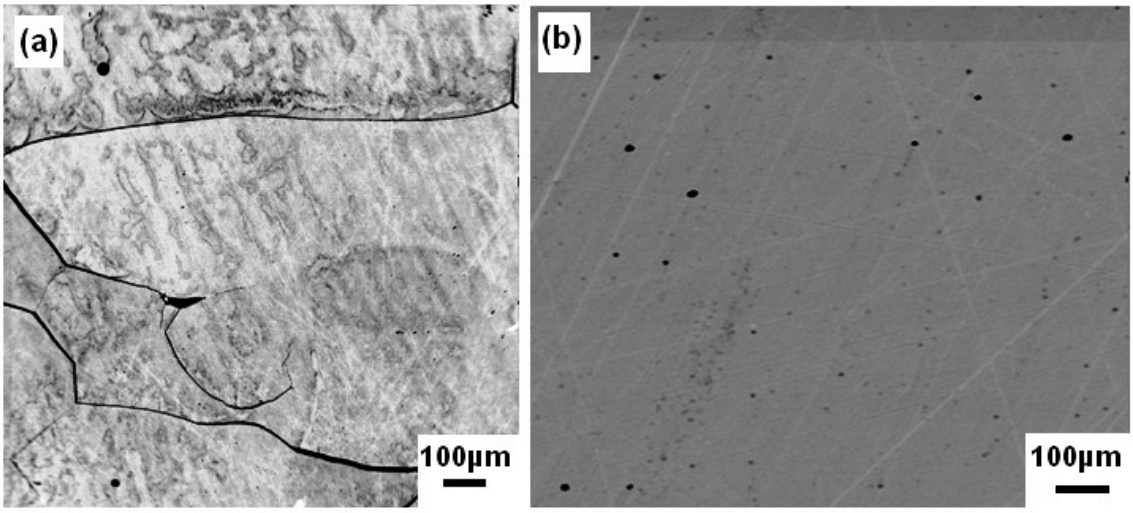

Figure 6-18) BSE images of the sample #12 heat treated at (a) 1050°C for 1 day and water quenched and (b) 1050°C for 1 week and water quenched.

Figure 6-19 shows the MT temperatures of $Fe_{41.7}Mn_{28.6}Ga_{29.6}$ (#13) polycrystalline alloy heat treated at 1050°C for 1 week with a DSC curve. Thermomagnetization curves did not give a smooth response since the maximum temperature is limited to 400K and the A_f of the sample was high. Two cooling-heating cycles were completed for stabilization and a better determination of MT temperatures. M_s, M_f, A_s and A_f were detected as 300K, 243K, 305K and 339K, respectively, and T_{hys} is about 50K. According to the determined MT temperatures, austenite and martensite phases must be coexistent at room temperature. The optical images in Figure 6-20 were taken from the sample #13 that was heat treated at 1050°C for 1 week. Figure 6-20a shows the mixture of the transforming phases with martensite twins at different grains. Once it is looked at a more magnified optical image of the same sample as shown in Figure 6-20b, the presence of the twins are apparent. It can be stated from both images

that the sample is single phase, and the circular regions represent the areas at which local melting occurred rather than precipitate formation.

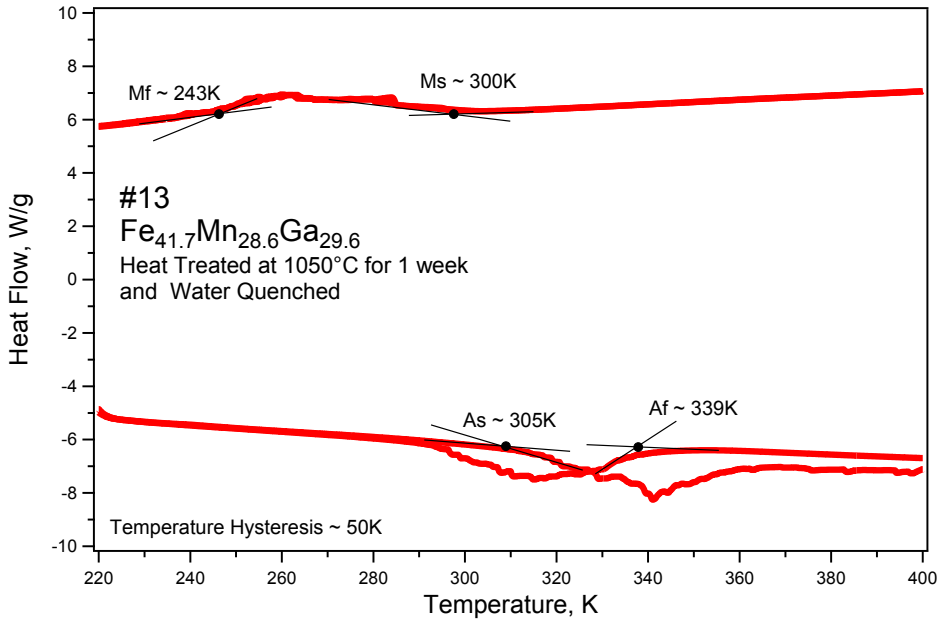

Figure 6-19) DSC measurements of $Fe_{41.7}Mn_{28.6}Ga_{29.6}$ (#13) polycrystalline alloy with a cooling-heating rate of 10 K min^{-1}.

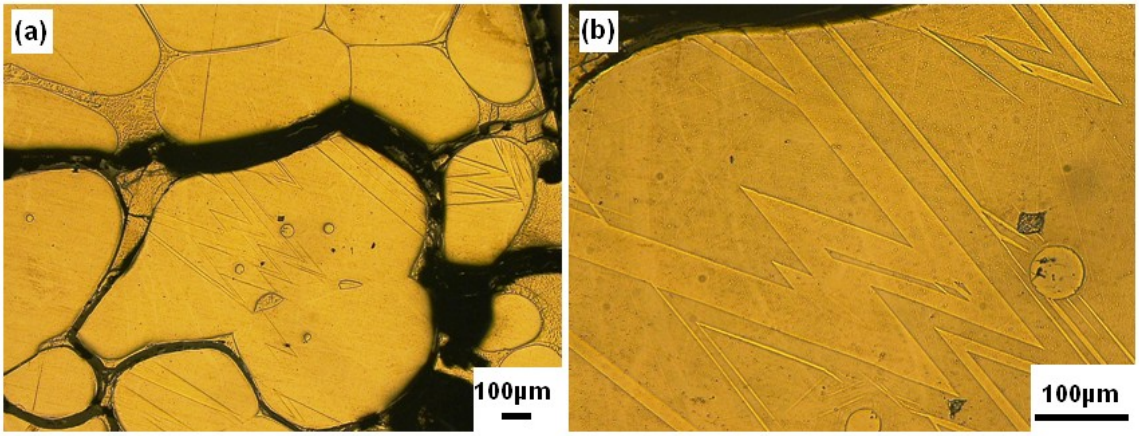

Figure 6-20) Room temperature optical images of $Fe_{41.7}Mn_{28.6}Ga_{29.6}$ (#13) polycrystalline alloy heat treated at 1050°C for 1 week and water quenched. Images (a) and (b) were taken from different regions.

Figure 6-21 shows the heat flow vs. temperature curves of polycrystalline $Fe_{39.1}Mn_{31.4}Ga_{29.5}$ (#14) alloy that was heat treated at 1050°C for 1 week. Similar to the sample #13, two cooling-heating cycles were completed to detect the MT temperatures. M_s, M_f, A_s and A_f were detected as 530K, 482K, 490K and 538K, respectively, with a very low T_{hys} of approximately 8K. It is concluded from those temperature values that the sample is fully martensite at room temperature, and a good high temperature SMA can be obtained from this composition of polycrystalline Fe-Mn-Ga alloys.

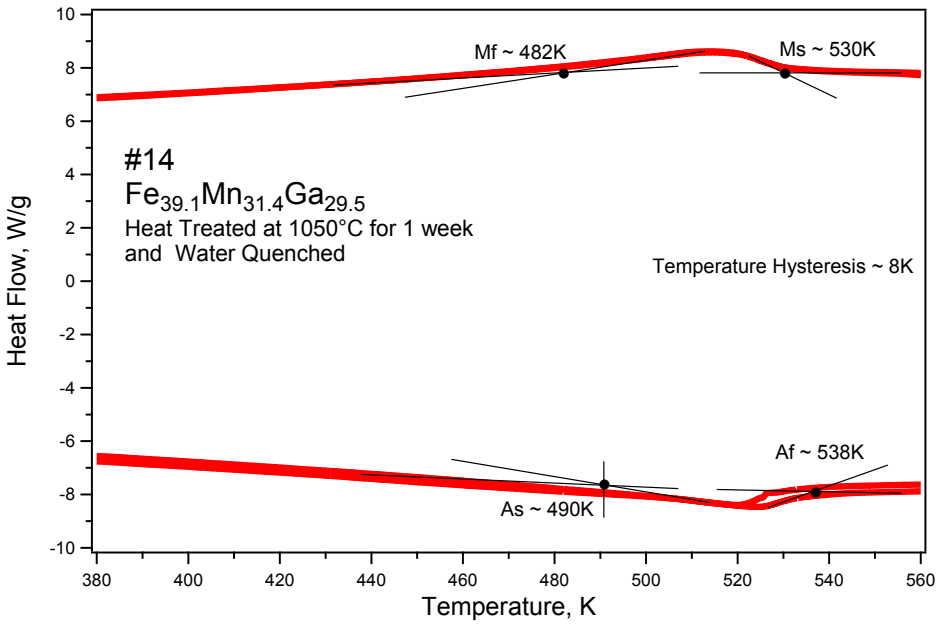

Figure 6-21) DSC measurements of $Fe_{39.1}Mn_{31.4}Ga_{29.5}$ (#14) polycrystalline alloy with a cooling-heating rate of 10 K min^{-1}.

Figure 6-22a is the room temperature optical image of the sample #14 where numerous martensite twins are present at different orientations. To be able to better

detect the martensite phase of the sample, BSE images were taken and one of those images is displayed in Figure 6-22b. It is more obvious from this image that the sample is martensite with different orientations at different crystals, which makes this sample available for the applications where SME is required at elevated temperatures.

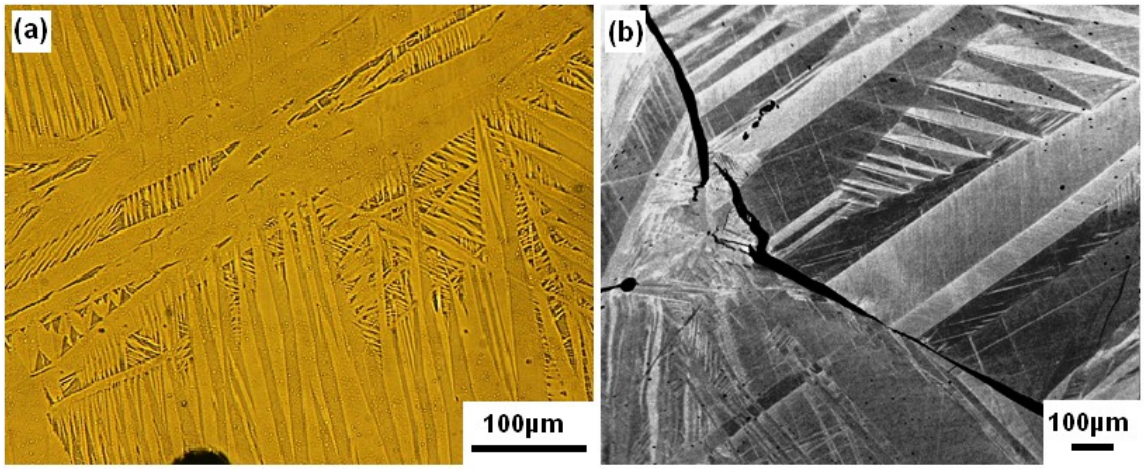

Figure 6-22) (a) Room temperature optical and (b) Backscattered electron (BSE) images of the sample #14 heat treated at 1050°C for 1 week and water quenched. The images were taken from different regions and at different magnifications.

The investigated polycrystalline Fe-Mn-Ga alloys in this section are listed in Table 6-1. The table begins with the sample notations, and also the nominal and real compositions of these samples are provided. The phase character of the samples at each processing condition were summarized with BSE and OM images, and shown in Table 6-1 too. Throughout the end of the investigation, it was concluded that the heat treatment temperature of 1050°C the ideal condition for all the samples to obtain MT and magnetic shape memory behavior. It is also understood that the heat treatment time of the alloys are either 1 day or 1 week depending on their compositions. Fe-rich alloys – #1 and #10-

12, where Fe compositions are greater than or close to 45 at% - exhibit transformation behavior via heat treatment for 1 day even if they are not single phase. The favorably oriented texture of the second phase precipitates is significant for MT and magnetic shape memory behavior. On the other hand 1-week heat treatment is required to obtain a single phase for all the samples.

Table 6-1) Processing chart of Fe-Mn-Ga alloys at various compositions

Alloy Notation	Element	Nominal Composition (at%)	Annealing	Real Composition (at%)	BSE	Optical Microscope	Squid	Description
1	Fe	43	1000°C - 1d	44/25.2/30.8	Matrix + 2nd phase	Matrix + 2nd phase	Transformation occurs	Arc-melted
	Mn	28						
	Ga	29						
7	Fe	42.5	1000°C - 1d	41.9/28.1/29.30	Matrix + 2nd phase	Matrix + 2nd phase	No transformation	
	Mn	28.5	1050°C - 1d	N/A	Matrix + 2nd phase	Matrix + 2nd phase		Purchased
	Ga	29	1080°C - 1d	N/A	Matrix + 2nd phase	Matrix + 2nd phase	No transformation	
			1050°C - 1w	41.5/28.2/30.3	Single Phase	Single Phase	Transformation	
9	Fe	42.5	As received	42.0/28.6/29.4	Matrix + 2nd phase	Matrix + 2nd phase	No transformation	Single
	Mn	28.5	1050°C - 1d	N/A	Matrix + 2nd phase	Matrix + 2nd phase	No transformation	
	Ga	29	1050°C - 1w	42.2/28.3/29.5	Single Phase	Single Phase	Transformation	crystal
10	Fe	48	1050°C - 1d	46.9/23.7/29.4	Dentritic Structure	Matrix + 2nd phase	Transformation	Arc-melted
	Mn	24	1050°C - 1w	46.3/23.3/30.3	Si Contamination	Single Phase	No transformation	
	Ga	28						
11	Fe	47	1050°C - 1d	47.6/23.1/29.3	Dentritic Structure	Matrix + 2nd phase	Transformation	Arc-melted
	Mn	25	1050°C - 1w	46.8/23.5/29.6	Si Contamination	Almost Single Phase		
	Ga	28						
12	Fe	45	1050°C - 1d	45.9/23.4/30.7	Dentritic Structure	Matrix + 2nd phase	Transformation	Arc-melted
	Mn	27	1050°C - 1w	45.4/24.9/29.7	Si Contamination	Single Phase	No transformation	
	Ga	28						
13	Fe	40	1050°C - 1w	41.7/28.6/29.6	Local melting	Martensite twins	DSC Result: Ms~27°C	Arc-melted
	Mn	30						
	Ga	30						
14	Fe	40	1050°C - 1w	39.1/31.4/29.5	Martensite twins	Martensite twins	DSC Result: High Temperature SMA: Ms~200°C	Arc-melted
	Mn	31						
	Ga	29						

6.3 Summary: Fe-Mn-Ga Ternary Phase Diagram

Fe-Mn-Ga samples that are investigated in the previous section were placed on the ternary phase diagram with respect to their compositions as shown in Figure 6-23. It was mentioned in Section 2.3 that the borderline surrounds the region in which the alloys with the compositions in this range exhibit magnetic shape memory properties. The investigated samples are shown with black solid circles in Figure 6-23 which all of them are located in the region of the point of interest, except the sample #14, which is a high temperature SMA. Polycrystalline $Fe_{43}Mn_{28}Ga_{29}$ alloy where MT and magnetic shape memory properties were first reported [21] is very close to the point where the sample #9 was placed. $Fe_{44}Mn_{28}Ga_{28}$ single crystal alloy [23] is shown by a dark blue square which is located on the bottom left border. The research on Fe-Mn-Ga, and our investigations confirm the existence of the borderline in Figure 6-23 as a constraint for desired material properties.

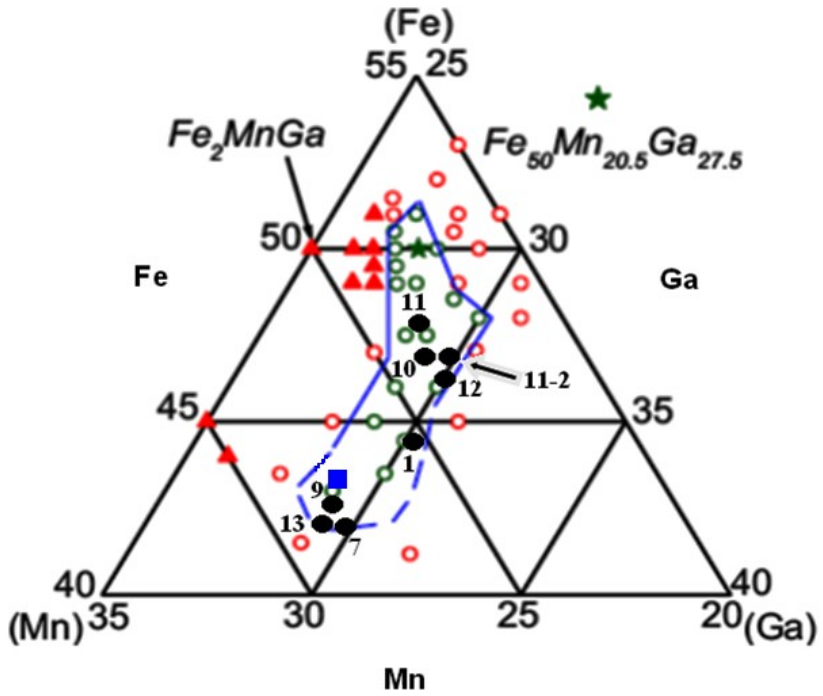

Figure 6-23) Phase diagram of Fe-Mn-Ga alloys investigated in the current study (Recall Figure 2-7 on page 20).

Among all the alloys examined in this section, the polycrystalline $Fe_{46.9}Mn_{23.7}Ga_{29.4}$ (#10) and $Fe_{47.6}Mn_{23.1}Ga_{29.3}$ (#11) alloys are the most promising candidates for magnetocaloric measurements due to a well-defined MT with metamagnetic shape memory properties as a consequence of thermomagnetization measurements. These alloys are located at the center of the region indicated in Figure 6-23. We can take advantage of relatively shorter heat treatment time -1 day – and the oriented texture of the precipitates to fabricate more alloys with similar compositions and conduct further research.

7. CONCLUSIONS

In the present study, single crystal $Ni_{45}Co_5Mn_{36.6}In_{13.4}$ (at %) alloys were homogenized at 900°C for 24 hours and quenched in iced water. Effect of changes in In content, annealing temperature, and cooling rate on magnetic properties and martensitic transformation were examined. The following conclusions are made after SQUID, XRD, and magneto-mechanical experiments:

1. Magnetization response of the samples single crystal $Ni_{45}Co_5Mn_{36.8-x}In_{13.2+x}$ (x=0, 0.2 and 0.3) were attained. It was verified that the M_s temperature decreases by increasing In concentration at the expense of Mn content. It was also shown that increasing In content increases M_{sat} and T_{hys}. Incomplete MT in the single crystal $Ni_{45}Co_5Mn_{36.5}In_{13.5}$ is associated with KA behavior.
2. Homogenized samples of single crystal $Ni_{45}Co_5Mn_{36.6}In_{13.4}$ were annealed at temperatures starting from 400°C up to 800°C with a 100°C increment, for 3 hours, and cooled through water quenching. It was confirmed that increasing annealing temperature ascends the MT temperatures. MT was not observed from the sample annealed at 400°C, while an incomplete phase transition occurred in the sample annealed at 500°C. Typical metamagnetic shape memory behavior was attained from the other samples. XRD experiments showed that the abnormal behaviors of the annealed samples at 400°C and 500°C are due to change in atomic ordering. Another possible reason is formation of second phase precipitates which hinders the phase

transition. Future TEM experiments and more detailed XRD experiments will help to understand the intrinsic reason for the abnormal behaviors.

3. Homogenized samples of single crystal $Ni_{45}Co_5Mn_{36.6}In_{13.4}$ were cooled through furnace cooling, water quenching and oil quenching. Furnace cooled sample showed KA arrest behavior and MT was thoroughly interrupted under the field of 5T. In addition, the lowest M_s temperature and the highest M_{sat} were obtained from the furnace cooled specimen.
4. Among the several samples that were processed at different conditions, the annealed sample at 600°C for 3 hours can selected for investigating magnetocaloric properties due to its sharp magnetization curve across martensitic transformation, low T_{hys}, and being available for room temperature applications.

Thermoelastic martensitic transformation, superelastic response and magnetic properties of bulk $Ni_{43}Co_7Mn_{39}Sn_{11}$ polycrystalline alloys sintered without pressure at 900°C for 2 and 6 days are investigated. Similar response was observed from both samples. The results attained from 6-day sintered sample are summarized here since it exhibits more improved properties than the 2-day sintered sample. Moreover, magnetization response and magnetocaloric effect were studied in polycrystalline $Ni_{43}Co_4Mn_{42}Sn_{11}$ ribbons and bulk specimens. It was concluded that:

1. The relatively less cost and the simplicity of pressureless sintering of $Ni_{43}Co_4Mn_{42}Sn_{11}$ powders can make these alloys a good alternative for practical applications. Optical images reveal the porous structure of the specimen which led to the improvement in the ductility as well as the fracture toughness. Isobaric heating-

cooling experiments show that the increasing stress leads to an increase in the recoverable transformation strain levels saturating at around 3.2%. Irrecoverable strain and the temperature hysteresis also increase with strain.

2. It was confirmed that the pressureless sintered polycrystalline NiCoMnSn samples demonstrate meta-magnetic shape memory effect with an MFIS level of about 0.6%. Furthermore, nearly perfect super-elastic response was verified in the present alloy. With small grain size and easy processing features, we can achieve strength levels as high as 320MPa.
3. Magnetization response of $Ni_{43}Co_4Mn_{42}Sn_{11}$ bulk samples and ribbons were compared and concluded that the ribbons are more suitable choice for MCE measurements due to high magnetization levels at low applied magnetic fields, sharp MT behavior, and a short annealing time.
4. As a result of isothermal magnetization measurements at incremental temperatures within MT region, and magnetic entropy calculations, a maximum ΔS_m of 22 J kg^{-1} K^{-1} at 219K up on application of a 7T field, were obtained from the annealed $Ni_{43}Co_4Mn_{42}Sn_{11}$ ribbons. Within a wide temperature range ΔS_m values near the maximum can be reached which increases the availability of the this alloy.

Magnetization response and MCE in $Fe_{44}Mn_{25.2}Ga_{30.8}$ polycrystalline alloy heat treated at 1000°C for 1 day and water quenched was examined. In addition, a systematic heat treatment study on Fe-Mn-Ga polycrystalline alloys at several compositions was performed, and magnetization and MT behavior were investigated.

1. A maximum ΔS_m near 6.7 J kg^{-1} K^{-1} was attained from the $Fe_{44}Mn_{25.2}Ga_{30.8}$ polycrystalline alloy at 223K in the field of 7T. This value is low compared to the values obtained from some other MMSMAs. ΔS_m can further be increased by new processing conditions. However, this composition of Fe-Mn-Ga alloys is highly corrosive that makes the sample preparation and receiving repeatable results difficult.
2. Among several heat treatment attempts of Fe-Mn-Ga alloys, it was decided that 1050°C is an appropriate temperature for processing. The heat treatment time was selected to be 1 week to eliminate the precipitate formation, and obtain single phase alloys. However, MT and magnetization response were observed in $Fe_{46.9}Mn_{23.7}Ga_{29.4}$, $Fe_{47.6}Mn_{23.1}Ga_{29.3,}$ and $Fe_{45.9}Mn_{23.4}Ga_{30.7}$ alloys by 1-day heat treatment. BSE images of the 1-day heat treated alloys show that there is an improved texture with preferred orientations. Similar properties would be expected after 1-week heat treatment too, but Si contamination during heat treatment prevented them from showing these properties.
3. Considering the magnetization response of the alloys in the present work, $Fe_{46.9}Mn_{23.7}Ga_{29.4}$ and $Fe_{47.6}Mn_{23.1}Ga_{29.3}$ can be chosen for MCE measurements because of having sufficiently high M_{sat}, sharp and smooth MT behavior and relatively low T_{hys}.

REFERENCES

[1] K. Ullakko, J. K. Huang, C. Kantner, R. C. O'Handley, and V. V. Kokorin, Appl. Phys. Lett. 69, 1966 (1996).

[2] H. E. Karaca, I. Karaman, B. Basaran, D. C. Lagoudas, Y. I. Chumlyakov, and H.J. Maier, Scripta Mater. 55, 803 (2006).

[3] H. E. Karaca, I. Karaman, B. Basaran, Y. I. Chumlyakov, and H. J. Maier, Acta Mater. 54, 233 (2006).

[4] H. E. Karaca, I. Karaman, B. Basaran, D. C. Lagoudas, Y. Chumlyakov, and H. J.Maier, Acta Mater. 55, 4253 (2007).

[5] H. E. Karaca, I. Karaman, B. Basaran, Y. Ren, Y. I. Chumlyakov, and H. Maier, Adv. Func. Mat. 19, 983 (2009).

[6] A. Sozinov, A.A. Likhachev, N. Lanska, and K.Ulakko, Appl. Phys. Lett. 80, 1746 (2002).

[7] J.H. Kim, F. Inaba, T. Fukuda, and T. Kakeshita, Acta Mater. 54, 493 (2006).

[8] X. Moya, L. Manosa, A. Planes, T. Krenke, M. Acet, and E.F., Wassermann, Mater. Sci.Eng. A 438, 911 (2006).

[9] R. Kainuma, Y. Imano, W. Ito, H. Morito, Y. Sutou, K. Oikawa, A. Fujita, K. Ishida, S. Okamoto, O. Kitakami, and T. Kanomata, Appl. Phys. Lett. 88, 192513 (2006).

[10] T. Krenke, E. Duman, M. Acet, E. F. Wassermann, X. Moya, L. Manosa, and A. Planes, Nat Mater. 4, 450 (2005).

[11] R. Kainuma, Y. Imano, W. Ito, Y. Sutou, H. Morito, S. Okamoto, O. Kitakami, K. Oikawa, A. Fujita, T. Kanomata, and K. Ishida, Nature 439, 957 (2006).

[12] R. Kainuma, K. Oikawa, W. Ito, Y. Sutou, T. Kanomata, and K. Ishida, J. Mater. Chem. 18, 1837 (2008).

[13] K. Oikawa, W. Ito, Y. Imano, Y. Sutou, R. Kainuma, K. Ishida, S. Okamoto, O. Kitakami, and T. Kanomata, Appl. Phys. Lett. 88, 122507 (2006).

[14] Z. D. Han, D. H. Wang, C. L. Zhang, S. L. Tang, B. X. Gu, and Y.W. Du, Appl. Phys. Lett. 89, 182507 (2006).

[15] K. Koyama, H. Okada, K. Watanabe, T. Kanomata, R. Kainuma, W. Ito, K. Oikawa, and K. Ishida, Appl. Phys. Lett. 89, 182510 (2006).

[16] S.Y. Yu, Z.H. Liu, G.D. Liu, J.L. Chen, Z.X. Cao, G.H. Wu, B. Zhang, and X.X. Zhang, Appl. Phys. Lett. 89, 162503 (2006).

[17] B. Zhang, X.X. Zhang, S.Y. Yu, J.L. Chen, Z.X. Cao, and G.H. Wu, Appl. Phys. Lett. 91, 012510 (2007).

[18] W. Ito, K. Ito, R.Y. Umetsu, R. Kainuma, K. Koyama, K. Watanabe, A. Fujita, K. Oikawa, K. Ishida, and T. Kanomata, Appl. Phys. Lett. 92, 021908 (2008).

[19] R. Kainuma, W. Ito, R.Y. Umetsu, K. Oikawa, and K. Ishida, Appl. Phys. Lett. 93, 091906 (2008).

[20] F. Chen, Y. X. Tong, B. Tian, Y. F. Zheng, and Y. Liu, Intermetallics 18, 188 (2010).

[21] T. Omori, K. Watanabe, R.Y. Umetsu, R. Kainuma, and K. Ishida, Appl. Phys. Lett. 95, 082508 (2009).

[22] W. Zhu, E.K. Liu, L. Feng, X.D. Tang, J.L. Chen, G.H. Wu, H.Y. Liu, F.B. Meng, and H.Z. Luo, Appl. Phys. Lett. 95, 222512 (2009).

[23] T. Omori, K. Watanabe, X. Xu, R.Y. Umetsu, R. Kainuma, and K. Ishida, Scripta. Mater. 64, 669 (2011).

[24] X. Xu, W. Ito, R.Y. Umetsu, R. Kainuma, and K. Ishida, Appl. Phys. Lett. 95, 181905 (2009).

[25] H. Sehitoglu, I. Karaman, R. Anderson , X. Zhang , K. Gall, H.J. Maier, and Y. Chumlyakov, Acta Mater. 48, 3311 (2000).

[26] I. Karaman, B. Basaran, H. E. Karaca, A. I. Karsilayan, and Y. I. Chumlyakov, Appl. Phys. Lett. 90, 172505 (2007).

[27] S.J. Murray, M. Marioni, S.M. Allen, R.C. O`Handley, and T.A. Lagrasso, Appl. Phys. Lett. 77, 886 (2000).

[28] T. Wada, Y. Liang, H. Kato, T. Tagawa, M. Taya, and T. Mori, Mater. Sci. Eng. A 361, 75 (2003).

[29] T. Sakomata, T. Fukuda, T. Kaeshita, T. Takeuchi, and K. Kishio, J. Appl. Phys. 93, 8647 (2003).

[30] T. Kakeshita, T. Takeuchi, T. Fukuda, M. Tsujiguchi, T. Saburi, R. Oshima, and S. Muto, Appl. Phys. Lett. 77, 1502 (2000).

[31] K. Oikawa, T. Ota, T. Ohmori, Y. Tanaka, H. Morito, A. Fujita, R. Kainuma, K. Fukamichi, and K. Ishida, Appl. Phys. Lett. 81, 5201 (2002).

[32] Y. Sutou, Y. Imano, N. Koeda, T. Omori, R. Kainuma, K. Ishida, and K. Oikawa, Appl. Phys. Lett. 85, 4358 (2004).

[33] Z. D. Han, D. H. Wang, C. L. Zhang, H. C. Xuan, B. X. Gu, and Y. W. Du, Appl. Phys. Lett. 90, 042507 (2007).

[34] H. C. Xuan, D. H. Wang, C. L. Zhang, Z. D. Han, B. X. Gu, and Y. W. Du, Appl. Phys. Lett. 92, 102503 (2008).

[35] S. Aksoy, T. Krenke, M. Acet, E. F. Wassermann, X. Moya, L. Mañosa, and A. Planes, Appl. Phys. Lett. 91, 241916 (2007).

[36] V. K. Sharma, M. K. Chattopadhyay, K. H. B. Shaeb, A. Chouhan, and S.B. Roy, Appl. Phys. Lett. 89, 222509 (2006).

[37] L. Mañosa, X. Moya, A. Planes, O. Gutfleisch, J. Lyubina, M. Barrio, J. L.Tamarit, S. Aksoy, and T. Krenke, M. Acet, Appl. Phys. Lett. 92, 012515 (2008).

[38] J. Liu, N. Scheerbaum, S. Weiß, and O. Gutfleisch, Appl. Phys. Lett. 95, 152503 (2009).

[39] V.K. Pecharsky, K.A. Gschneidner, Jr., A.O. Pecharsky, and A.M. Tishin, Phys. Rev. B 64, 144406 (2011).

[40] E. Warburg, Ann. Phys. Chem. 13, 141 (1881).

[41] V.K. Pecharsky, and K.A. Gschneidner, Phys. Rev. Lett. 78, 4494 (1997).

[42] A. Fujita, S. Fujieda, Y. Hasegawa, and K. Fukamichi, Phys. Rev. B 67, 104416 (2003).

[43] H. Wada, and Y. Tanabe, Appl. Phys. Lett. 79, 3302 (2001).

[44] O. Tegus, E. Brück, K.H.J. Buschow, and F.R. de Boer, Nature 415, 150 (2002).

[45] J.M.D. Coey, J. Magn. Magn. Mater. 248, 441 (2002).

[46] S.J. Lee, J.M. Kenkel, V.K. Pecharsky, and D.C. Jiles, J. Appl. Phys. 91, 8543 (2002).

[47] V.K. Pecharsky, and K.A. Gschneidner, Adv. Mater. 13, 683 (2001).

[48] O. Tegus, E. Bruck, L. Zhang, Dagula, K.H.J. Buschow, and F.R. de Boer, Physica B 319, 174 (2001).

[49] Y.Q. Zhang, and Z.D. Zhang, J. Alloy Comp. 365, 35 (2004).

[50] S.A. Nikitin, G. Myalikgulyev, A.M. Tishin, M.P. Annaorazov, K.A. Asatryan, and A.L. Tyurin, Phys. Lett. A 148, 363 (1990).

[51] J. Marcos, A. Planes, L. Manosa, F. Casanova, X. Batlle, and A. Labarta, Phys. Rev. B 66, 224413 (2002).

[52] J. Marcos, L. Manosa, A. Planes, F. Casanova, X. Batlle, and A. Labarta, Phys. Rev. B 68, 094401 (2003).

[53] L .Pareti, M. Solzi, F. Albertini, and A. Paoluzi, Eur. Phys. J. B 32, 303 (2003).

[54] A.K. Pathak, I. Dubenko, C. Pueblo, S. Stadler, and N. Ali, Appl. Phys. Lett. 96, 172503 (2010).

[55] A.K. Pathak, I. Dubenko, Y. Xiong, P.W. Adams, S. Stadler, and N. Ali, J. Appl. Phys. 109, 07A916 (2011).

[56] H.C. Xuan, Y.X. Zheng, S.C. Ma, Q.Q. Cao, Y. Zhao, Y. Yang, and H. Zhang, J. Appl. Phys. 108, 103920 (2010).

[57] M.K. Chattopadhyay, V.K. Sharma, and S.B. Roy, Appl. Phys. Lett. 92, 022503 (2008).

[58] X. Zhang, B. Zhang, S. Yu, Z. Liu, W. Xu, G. Liu, J. Chen, Z. Cao, and G. Wu, Phys. Rev. B 76, 132403 (2007).

[59] M. Khan, N. Ali, and S. Stadler, J. Appl. Phys. 102, 053919 (2007).

[60] S. Kustov, M.L. Corro, J. Pons, and E. Cesari, Appl. Phys. Lett. 94, 191901 (2009).

[61] Z.H. Liu, S. Aksoy, and M. Acet, J. Appl. Phys. 105, 033913 (2009).

[62] M.S. Can, X.H. Cheng, Z.C. Liang, W.L. Yu, C.Q. Qi, W.D. Hui, and D.Y. Wei, Chin. Phys. B 19, 117503 (2010).

[63] A. Fujita, S. Fujieda, Y. Hasegawa, and K. Fukamichi, Phys. Rev. B 67, 104416 (2003).

[64] X.A. Xu ; W. Ito, M. Tokunaga, R.Y. Umetsu, R. Kainuma, and K. Ishida, Mater.Trans. 51, 1357 (2010).

[65] R.Y. Umetsu, K. Ito, W. Ito, K. Koyama, T. Kanomata, K. Ishida, and R. Kainuma, J. Alloy Comp. 509, 1389 (2011).

[66] M.K. Chattopadhyay, S. B. Roy, and P. Chaddah, Phys.Rew.B 72, 180401(R) (2005).

[67] P.N. Segrè, V. Prasad, A.B. Schofield, and D.A. Weitz, Phys. Rev. Lett. 86, 6042 (2001).

[68] M. Hermes, and M. Dijkstra, Euro Phys. Lett. 89, 38005 (2010).

[69] R. Zhang, and K.S. Schweizer, Phys. Rev. E 83, 060502(R) (2011).

[70] X.A. Xu ; W. Ito, R.Y. Umetsu, K. Koyama, R. Kainuma, and K. Ishida, Mater.Trans. 51, 469 (2010).

[71] R.Y. Umetsu, W. Ito, K. Ito, K. Koyama, A. Fujita, K. Oikawa, T. Kanomata, R. Kainuma, and K. Ishida**,** Scripta Mater. 60, 25 (2009).

[72] V.K. Sharma, M.K. Chattopadhyay, and S. B. Roy, Phys. Rev. B 76, 140401 (2007).

[73] L. Chen, F.X. Hu, J. Wang, J. Shen, J.R. Sun, B.G. Shen, J.H. Yin, L.Q. Pan, and Z. Hunag, J. Appl. Phys. 109, 07A939 (2011).

[74] T. Miyamoto, W. Ito, R.Y. Umetsu, T. Kanomata, K. Ishida, and R. Kainuma, Mater. Trans. 52, 1836 (2011).

[75] K. Ito, W. Ito, R.Y. Umetsu, H. Kawaura, R. Kainuma, and K. Ishida, Scripta Mater. 61, 504 (2009).

[76] V. Srivastava, X. Chen, and R. James, Appl. Phys. Lett. 97, 014101 (2010).

[77] K. Ito, W. Ito, R.Y. Umetsu, M. Nagasako, R. Kainuma, A. Fujita, K. Oikawa, and K. Ishida, Mater. Trans. 49, 1915 (2008).

[78] W. Ito, X. Xu, R.Y. Umetsu, T. Kanomata, K. Ishida, and R. Kainuma, Appl. Phys. Lett. 97, 242512 (2010).

[79] S.C. Ma, Q.Q. Cao, H.C. Xuan, C.L. Zhang, L.J. Shen, D.H. Wang, and Y.W. Du, J. Alloy Comp. 509, 1111 (2011).

[80] S.C. Ma, H.C. Xuan, L.Y. Wang, Q.Q. Cao, D.H. Wang, and Y.W. Du, Appl. Phys. Lett. 97, 052506 (2010).

[81] V.V. Khovaylo, K.P. Skokov, O. Gutfleisch, H. Miki, R. Kainuma, and T. Kanomata, Appl. Phys. Lett. 97, 052503 (2010).

[82] K. Ito, W. Ito, R.Y. Umetsu, I. Karaman, K. Ishida, and R. Kainuma, Scripta Mater. 63, 1236 (2010).

[83] W. Ito, B. Basaran, R. Y. Umetsu, I. Karaman, R, Kainuma, and K. Ishida, Mater. Trans. 51, 525 (2010).

[84] K.C. Atli, I. Karaman, R.D. Noebe, A. Garg, Y.I. Chumlyakov, and I.V. Kireeva, Metall. Mater. Trans. A 41A, 2485 (2010).

[85] X.G Zhao, C.C. Hsieh, J.H. Lai, X.J. Cheng, W.C. Chang, W.B. Cui, W. Liu, and Z.D. Zhang, Scripta Mater. 63, 250 (2010).

[86] D.M. Kumar, N.V. R. Rao, M.M. Raja, D.V. S. Rao, M. Srinivas, S.E. Muthu, S. Arumugam, and K.G. Suresh, J Magn. Mag. Mater. 324, 26 (2012).

VITA

Name: Cengiz Yegin

Address: Texas A&M University Dept. Mech. Eng. 3123 TAMU College Station TX 77843-3123

Email: mostlordling@neo.tamu.edu

Education: B.S., Mechanical Engineering, Bogazici University, 2005

M.S., Materials Science and Engineering, Texas A&M University, 2012